AIR FILTRATION: PREDICTING AND IMPROVING INDOOR AIR QUALITY AND ENERGY PERFORMANCE

by

James Montgomery

B.A.Sc., The University of Waterloo, 2008
M.A.Sc., The University of British Columbia, 2010

A THESIS SUBMITTED IN PARTIAL FULFILLMENT OF
THE REQUIREMENTS FOR THE DEGREE OF

DOCTOR OF PHILOSOPHY

in

The Faculty of Graduate and Postdoctoral Studies

(Mechanical Engineering)

THE UNIVERSITY OF BRITISH COLUMBIA
(Vancouver)

July 2015

Abstract

Air filtration is used to reduce particle concentrations in the indoor environment to provide improved occupant health due to reduced exposure. Increased focus on occupant health in emerging design standards is leading to the installation of higher efficiency filtration systems. These systems generally have higher resistance to flow and therefore impose a greater energy penalty. Previous air filter models have used simplified assumptions with regards to the dynamics of filter operation, which have limited the potential to determine energy efficiency or optimization approaches to system design and operation. This dissertation focuses on developing an improved air filter model to investigate the potential for system modifications to reduce energy consumption and improve indoor air quality (IAQ) within commercial buildings.

A new air filter performance model was developed using generalizable results from ASHRAE Standard 52.2-2012 and validated against laboratory and real-world experiments. The results showed better agreement with laboratory tests than with real operation. The filter model was combined with existing indoor particle dynamics and epidemiological models to determine the impacts of changes to system operation through monetization of operation costs and health benefits. Laboratory experiments were performed to evaluate the role that particle properties and relative humidity play in determining the filter performance changes with the aim of better understanding the reasons for discrepancies in operation between laboratory and field filter tests.

Operation can now be optimized by accounting for dynamic characteristics of filter performance. Benefits of improved filtration efficiency were found to outweigh added costs. Adopting specific indoor particle concentration limits is recommended to replace existing specifications relying on filter efficiency. System designs can then be optimized to account for local particle concentration and energy costs. A number of system design changes have been highlighted that allow for simultaneous reduction in operation cost and indoor particle concentrations. Relative humidity has been identified as a critical parameter in filter performance and standardized tests should be modified to account for variability in relative humidity and particle characteristics typical of real operation to allow for improvements to future model predictions.

Preface

The identification and design of this research was performed by the author with the close guidance of Dr. Green and Dr. Rogak. Chapters 3-7 comprise work originally produced for publication in peer-reviewed journals and have received various contributions from co-authors.

Chapters 1 & 2 were written by the author with input and advice from Dr. Green and Dr. Rogak. The original review for this section was performed for the peer-reviewed publications associated with the following chapters.

Chapter 3 contains material from a published work. Montgomery, J. F., Green, S. I., Rogak, S. N., & Bartlett, K. (2012). Predicting the energy use and operation cost of HVAC air filters. Energy & Buildings, 47, 643–650. The author derived the model, developed and set-up the field experiment, performed calculations and analysis, and wrote the majority of the manuscript with the guidance of Dr. Green, Dr. Rogak, and Dr. Bartlett.

Chapter 4 contains material from a published work. Montgomery, J. F., Green, S. I., Rogak, S. N., & Bartlett, K. (2012). Predicting the energy use and operation cost of HVAC air filters. Energy & Buildings, 47, 643–650. The author performed all analyses and wrote the majority of the manuscript with the guidance of Dr. Green, Dr. Rogak, and Dr. Bartlett.

A version of Chapter 5 has been published. Montgomery, J. F., Reynolds, C. C. O., Rogak, S. N., & Green, S. I. (2015). Financial Implications of Modifications to Building Filtration Systems. Building and Environment, 85, 17–28. The author designed the research, performed all analysis and wrote the majority of the manuscript with the guidance of Dr. Green, Dr. Rogak, and Dr. Reynolds.

A version of Chapter 6 has been accepted for publication. Montgomery, J. F., Green, S. I. & Rogak, S. N., (2015). Impact of relative humidity on HVAC filters loaded with hygroscopic and non-hygroscopic particles. Aerosol Science and Technology. The author designed the experiment, conducted 50% of the experiments, performed all analysis and wrote the majority of the manuscript with the guidance of Dr. Green, and Dr. Rogak.

Chapter 7 has been written with the intention for submission to a peer-reviewed journal. The author identified the research program and modified existing experimental methods to suit the needs of this work. The author was responsible for conducting all of the tandem differential mobility analyzer experiments. The author and Dr. You conducted the microscopy experiments with the assistance of Dr. Saeid Kamal of the LASIR lab at UBC. The author wrote the majority of the manuscript with input from Dr. Green, Dr. Rogak, Dr. Bertram, and Dr. You.

Chapters 8 & 9 were written by the author with guidance from Dr. Green and Dr. Rogak. The conclusions and future work discussed therein are a result of conversation and collaboration with the colleagues listed above throughout the development of this dissertation.

Table of Contents

List of Tables

List of Figures

List of Symbols

$\$_E$	Electricity price	USD/kWh
$\$_F$	Filter purchase price	USD/filter
$\$_g$	Gas price	USD/kWh
$\$_i$	Monetary value of morbidity/mortality incident	USD/incident
$\$_L$	Filter installation price	USD/filter
α	Particle removal mechanisms	-
β	Particle introduction mechanisms	-
δ	Conversion factor for HDD/CDD calculations	0.02393 s·kWh/J/day
ε_0	Permitivitty of free space	8.84×10^{-12} F/m
ε_D	Single fiber efficiency due to diffusion	-
ε_G	Single fiber efficiency due to gravitational settling	-
ε_i	Size resolved filtration efficiency	-
ε_I	Single fiber efficiency due to impaction	-
ε_{OA}	Outdoor air filter efficiency	-
ε_{Qq}	Single fiber efficiency due to charged fiber and charged particle	-
ε_{0q}	Single fiber efficiency due to neutral fiber and charged particle	-
ε_{Q0}	Single fiber efficiency due to charged fiber and neutral particle	-
ε_R	Single fiber efficiency due to impaction	-
ε_{RA}	Return air filter efficiency	-
ε_{RCL}	Recirculation air filter efficiency	-
ε_{SA}	Supply air filter efficiency	-
ε_T	Total single fiber efficiency	-
η_f	Homogeneity Factor	-
η_{heat}	Efficiency of gas heating	-
η_o	Annual fraction of system operation time	-
η_s	Fan System efficiency	-
η_t	Fraction of year office is occupied	-
λ	Mean free path	m
λ_d	Particle deposition	s^{-1}
μ	Dynamic viscosity	Pa·s
ν	Solid volume fraction	-
ρ_{air}	Density of air	1.2 kg/m^3
ρ_p	Density of particle	kg/m^3

a	Filter constant	-
b	Filter constant	-
d	Filter constant	-
d_p	Particle diameter	m
d_f	Fiber diameter	m
e	Income elasticity	-
f	Fiber correction factor	-
f_{OA}	Fraction of outdoor air	-
$f(v)$	Hydrodynamic Factor	-
g	Gravitational acceleration on the Earth	9.81 m/s^2
g_i	Filter constant	-
k	Mixing factor	-
k_B	Boltzmann's constant	$1.38x10^{-23} m^2 kg \cdot s^{-2} K^{-1}$
$k_{i,j}$	Characteristic coefficient of collection	-
m	Dust mass	g
q	Particle charge	C
t	Time	s
x	Thickness	m
y_0	Annual baseline health endpoint occurrence	events/yr/person
y_i	Health endpoint	events/yr/person
A_{fl}	Floor loading	$\#/m^2$
A_i	Value of avoided morbidity/mortality endpoint	USD/yr
B_i	Morbidity/mortality effect estimate	$\mu g^{-1}/m^{-3}$
C_{cool}	Cost for cooling	USD/yr
C_A	Annual cost of filter operation	USD/yr
C_F	Annual cost of filter purchase	USD/yr
C_{heat}	Cost for heating	USD/yr
C_i	Size resolved particle concentration	g/m^3, $\#/m^3$
C_{IA}	Indoor particle concentration	$\#/m^3$
C_L	Annual cost of filter installation and disposal	USD/yr
C_n	Cunningham slip correction factor	-
C_{OA}	Oudoor particle concentration	$\#/m^3$
$C_{p,air}$	Specific heat capacity of air	1000 J kg^{-1} K^{-1}
CDD	Cooling Degree Days	day K yr^{-1}
COP	Coefficient of performance	-
D	Coefficient of diffusion	m^2 s^{-1}
D_p	Dielectric constant	-

D_i	Correction functions for filter efficiency	-
DHC	Dust holding capacity	g
E	Energy	J
E_{exp}	Experimental energy consumption	J
E_{the}	Theoretical energy consumption	J
G	Indoor particle generation	#/s
GNI	Gross national income	USD/person
HDD	Heating Degree Days	day K yr^{-1}
Kn	Knudsun Number	(-)
L_{fl}	Floor loading	$\#/m^3$
L_u	Upper limit of filter efficiency	(-)
M	Particle mobility	s kg^{-1}
N	Number of occupants	persons
N_{filter}	Number of filters	#
N_R	Interception parameter	-
N_{Qq}	Dimensionless capture parameter	-
N_{0q}	Dimensionless capture parameter	-
N_{Q0}	Dimensionless capture parameter	-
P	Pressure drop, flow resistance	Pa
P*	Normalized Pressure Drop	-
P_i	Initial flow resistance	Pa
P_{exp}	Experimental pressure drop	Pa
P_f	Final flow resistance	Pa
P_{Bldg}	Building penetration	-
P_{the}	Theoretical pressure drop	Pa
Pe	Peclet Number	-
PLI	Price Level Index	-
$PM_{2.5}$	Particulate matter ≤2.5μm	$\mu g/m^3$
PM_{10}	Particulate matter ≤10μm	$\mu g/m^3$
Q	Fiber charge per unit length	C/m
Q	Flow rate	m^3/s
Q_{design}	Design flow rate	m^3/s
Q_{Exf}	Exfiltration air flowrate	m^3/s
Q_{Exh}	Exhaust air flowrate	m^3/s
Q_{filter}	Flow rate per filter	m^3/s
Q_{Inf}	Infiltration air flowrate	m^3/s
Q_{OA}	Outdoor air flowrate	m^3/s
Q_{RA}	Return air flowrate	m^3/s
Q_{RCL}	Recirculation air flowrate	m^3/s

QF	Quality Factor	Pa^{-1}
R	Resuspension rate	s^{-1}
Re	Reynolds Number	-
S	Dimensionless fiber projected area	-
St	Stokes Number	-
T	Temperature	K
V	Velocity	m/s
V_B	Building volume	m^3
V_D	Velocity in duct	m/s
W	Power	W
W_{ave}	Average power	W
W_{exp}	Experimental power consumption	W
W_{the}	Theoretical power consumption	W

List of Abbreviations

ASHRAE – American Society of Heating, Refrigerating, and Air-Conditioning Engineers

BAS – Building Automation System

C-R – Change-Response

CAD – Canadian Dollars

CDD – Cooling Degree Day

COP – Coefficient of Performance

DHC – Dust Holding Capacity

DMA – Differential Mobility Analyzer

DRH – Deliquescence Relative Humidity

EA – Exhaust Air

Exf – Exfiltration

FoM – Figure of Merit

GF – Growth Factor

GNI – Gross National Income

HDD – Heating Degree Day

HEPA – High Efficiency Particle Air

HVAC – Heating, Ventilating, and Air-Conditioning

IAQ – Indoor Air Quality

Inf – Infiltration

kep – Key Energy Performance

LEED – Leadership in Energy and Environmental Design

LCC – Life Cycle Cost

MERV – Minimum Efficiency Reporting Value

OA – Outdoor Air

PLI – Price Level Index

PM – Particulate Matter

QF – Quality Factor

RA – Return Air

RCL – Recirculated Air

RH – Relative Humidity

SA – Supply Air

SEM – Scanning Electron Microscope

SMPS – Scanning Mobility Particle Sizer

TDMA – Tandem Differential Mobility Analyzer

UFP – Ultrafine Particles

USD – US Dollars

USEPA – United States Environmental Protection Agency

WHO – World Health Organization

YVR – Vancouver International Airport

List of Supplementary Materials

Acknowledgements

I owe a great debt of gratitude to everyone at UBC who has made this research possible. I would like to express my deepest appreciation to my supervisors Dr. Sheldon Green and Dr. Steve Rogak. Thank you for patience while I found my way, your belief in my potential, and your friendship while climbing. Thanks to my supervisory committee, Greg Johnson, Dr. Karen Bartlett, and Dr. Boris Stoeber for continued guidance. And to my many colleagues, I am grateful for the help, motivation, and support.

This research would not have been possible without the funding support of a number of organizations. In particular I would like to acknowledge the support of the Natural Sciences and Engineering Research Council of Canada (NSERC), the Sustainable Building Science Program (UBC), the American Society for Heating, Refrigerating, and Air-conditioning Engineers (ASHRAE), and the Transatlantic Partnership for Excellence in Engineering (TEE).

Finally, thank you to my friends and family for their continued support.

1 Introduction

1.1 Background and Motivation

Buildings account for 20%-40% of global energy consumption and represent a significant potential for efficiency improvements [1]. The heating, ventilating, and air-conditioning (HVAC) system is the dominant user of energy within a building accounting for approximately 50% of total energy consumption. In Canada, the energy consumption of commercial and institutional buildings accounts for 12% of the secondary energy use and 11% of national greenhouse gas emissions [2]. The energy consumption from specific components of the HVAC system can vary significantly based on specifics of location, design, and operation. The fan power, used to drive air through the system can account for up to ~1/3 of the energy consumption of the HVAC system [3]. The primary drivers of fan energy consumption are flow rate, fan system efficiency, and flow resistance. The flow rate and fan system efficiency are dictated primarily by system needs and equipment selection. The flow resistance is determined by design and component selection of equipment in the path of the airstream. In offices and large institutional buildings air filtration components impose an average flow resistance of ~400 Pa (including prefilters and primary filters) of the 1,000-1,500 Pa total static pressure (resistance) of the fan system. This contributes 25-40% to the overall fan energy consumption during building operation.

Recent advances in building design standards and rating systems, including ASHRAE guidelines, LEED and Living Building Challenge, have focused on reductions in building energy use and improvements in indoor air quality (IAQ). A major focus has been the control of particulate matter (PM) exposure within the built environment. Increased exposure to elevated particulate matter and other indoor pollutants has been linked to negative impacts such as lost productivity, increased absenteeism, and increased prevalence of respiratory illness and mortality [4,5]. Exposure to airborne particles can have detrimental health impacts for human populations [6-12] even for exposure to low concentrations [6,13]. Health impacts associated with exposure to particulate matter (PM) vary widely and include asthma [10], bronchitis [12], cardiovascular disorders [8], lung cancer [9], and premature mortality [6,7,11]. Early studies provided correlations between PM_{10} and health impacts. Recent investigations have shown that the impact is greater for $PM_{2.5}$ and some evidence is emerging that suggests that ultrafine particles (UFP) and the black carbon component of particulate matter have a greater impact on health than do larger particle size fractions [14-16].

A number of organizations have developed air quality guidelines. The World Health Organization (WHO) guidelines for annual average outdoor particle concentrations are 20 $\mu g/m^3$ for PM_{10} and 10 $\mu g/m^3$ for $PM_{2.5}$ [17]. The US Environmental Protection Agency (USEPA) sets similar limits for $PM_{2.5}$ at 12 $\mu g/m^3$. People spend approximately 90% of their time within the indoor environment [18] and as such indoor air quality is important to consider for human health, especially in vulnerable populations. Separate indoor air quality guidelines have not been developed and outdoor concentration limits are often used. Indoor particle concentrations are influenced by both indoor (cooking, smoking, particle re-suspension, cleaning activities, etc.) and outdoor (atmospheric, industrial, traffic, etc.) sources. The relative contribution of indoor and outdoor sources to indoor particle concentration is a strong function of building type, ventilation system, and particle size. The general trend is one of higher contributions from outdoor sources for small particles with contributions of over 50% for particles smaller than 1μm [19]. This necessitates particle reduction indoors, which can only be achieved through active control technology such as fibrous filters.

Air filters are an important active link between the air quality and energy consumption of an HVAC system. Filters remove particles to protect equipment and reduce exposure to building occupants. Reductions in energy consumption of air filtration technology without compromising particle removal performance have the potential for significant impacts to building energy efficiency and have not been the subject of sufficient investigation. Prior to implementing system changes a better understanding of energy consumption of air filters and an adequate means of quantifying and comparing energy efficiency is required.

1.2 Review of HVAC Application

Numerous factors affect the indoor environment and how it is perceived by occupants including temperature, humidity, air movement, biology, personal preference, and particle, biological and gaseous pollutants [20,21]. The goal of the HVAC system is to provide clean, conditioned air to the space to provide a healthy, comfortable environment [22]. There are a wide variety of system design types suitable to achieve these goals including variations in fans, duct layouts, heating and cooling mechanisms, and controls algorithms. A common design is to utilize one or more centralized air-handling units that force air through the distribution network into conditioned spaces. The air-handling unit controls the flow rate, fraction of outdoor versus return or recirculated air, and temperature and humidity of the airstream. It will also, generally contain particle and, possibly, gaseous phase filtration equipment [22].

The design of the HVAC system is subject to guidelines and constraints based on local standards and bylaws. In North America these are typically guidelines developed by ASHRAE and adopted in national, provincial/state, or local building codes. Similar standards are developed and adopted elsewhere such as the European Committee for Standardization. ASHRAE 62.1-2013 provides guidelines for the design of the air handling system to provide acceptable ventilation within the built environment to ensure proper air quality and contaminant control [23]. ASHRAE 55-2013 dictates the environmental characteristics to be met to ensure thermal comfort for the majority of occupants [24]. ASHRAE 90.1 provides design constraints to ensure system energy efficiency while meeting other design considerations [25]. These and other standards and guidelines must be considered for proper design and operation of the building system.

1.2.1 Filter Testing

The need to provide clean indoor air is set forth by ASHRAE 62.1 for gas and solid phase pollutants. Fibrous air filters are the most common control technology used to remove particles from the air stream in the HVAC system. The performance classification for fibrous air filters is described in ASHRAE 52.2 for North America and in EN779 in Europe [26]. Both standards outline methods to classify and compare performance based on the particle removal efficiency of the air filter. ASHRAE 52.2 describes the testing methodology to produce the required results for filter performance comparison. The main output from the test is to produce a Minimum Efficiency Reporting Value (MERV) for the filter. The MERV is determined by comparing the particle removal efficiency of filters in the size range 0.3-10μm for specific groupings: E1 from 0.3-1μm, E2 from 1-3μm, and E3 from 3-10μm. The tests described in ASHRAE 52.2 also compare filter flow performance. The relation between flow resistance and flow rate through a clean filter is provided as well as the relation between flow resistance and dust loading at a specified flow rate. The tests are performed with constant environmental conditions between given ranges of temperature and relative humidity. The dust for the loading test is specified as ASHRAE dust, which consists of a mixture of Arizona Road Dust, Carbon Black, and Cotton Linters. The test method provides an indication of how the air filter will perform but is limited in the potential for energy comparison as will be discussed later in this dissertation.

1.3 Review of Filtration Theory

HVAC air filtration is a dynamic process that varies with system parameters such as flow rate, particle size, and filter characteristics. The macroscale filter characteristics (flow resistance and filtration efficiency) that determine system cost and efficacy are related to the microscopic structure of the air filter (fiber properties, geometry, particle buildup, etc.). The presence of fibers in the air stream imposes drag forces resulting in a resistance to flow through the filter media. As air passes through the filter it transports aerosol particles within the fibrous bed. As a first approximation, if a particle comes in contact with a fiber it is considered to be captured, or filtered, by the filter (particle bounce or detachment is ignored). Filters operate based on distinct particle capture mechanisms. The main mechanical capture mechanisms relevant to HVAC filtration include diffusion, interception, impaction, and gravitational Settling [27]. In addition to mechanical capture mechanisms, particles can also be removed by electrostatic effects either through particle charging or electric charges present on the filter fibers. The flow resistance and particle capture efficiency of an air filter is affected by the aerosol particles and varies with filter loading.

1.3.1 Flow Resistance

The airflow and pressure drop (or flow resistance) through a fibrous filter can be approximated by theoretical modeling of the filter fibers. The filter is approximated as an array of parallel cylinders and the flow field through the array determined by assuming that flow can be approximated by Stokes flow (Re=0). Typical HVAC air filters operate with Reynolds numbers in the range of 0.002 to 2. The flow field is solved for repeating cells within the theoretical filter structure of a parallel or staggered array of cylinders (Figure 1.1 a & b, respectively). From the solution of the Stokes flow around the cylinder the drag force per unit length and thus the total pressure drop of the flow through the theoretical filter can be solved with the general form [27]:

$$P = \frac{16 v x \mu V}{d_f^2 f(v)} \qquad \text{Equation 1.1}$$

where P is the pressure drop (Pa); v is the solid volume fraction (-); x is the filter thickness (m); μ is the dynamic viscosity of air (Pa·s); V is the interstitial velocity (m/s), $V=V_0(1-\alpha)-1$; V_0 is the nominal filter face velocity (m/s); d_f is the fiber diameter (m); and $f(v)$ is the hydrodynamic factor (-).

Equation 1.1 is of a form similar to Darcy's Law and shows that the theoretical pressure drop of a filter is proportional to the flow rate of air through it [27]. Some investigations have shown that this relation can have good agreement with experimental results for filter media [27]. Other work on whole filter samples have shown that the dependence is non-linear and site compression of the media with increased pressure drop as a potential reason [28,29].

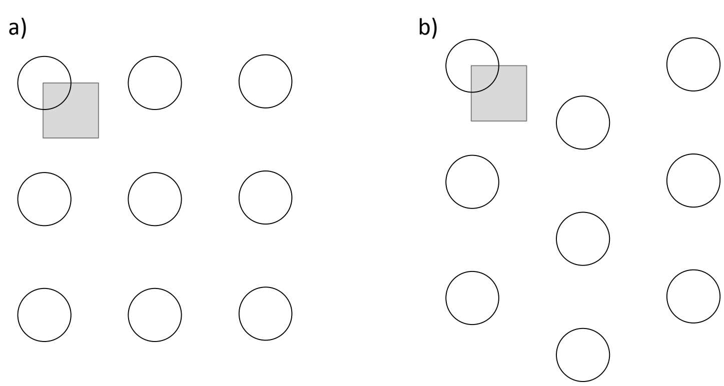

Figure 1.1: Idealized filter as arrays of parallel (a) or staggered (b) cylinders

The expression for the hydrodynamic factor differs depending on the assumed boundary conditions of the solution to flow around the filter fiber in each cell. The two most prominent theories are those of Happel [30] and Kuwabara [31] for which the hydrodynamic factor is, respectively:

$$f(v) = -\frac{1}{2}ln(v) - \frac{1}{2}\frac{(1-v^2)}{(1+v^2)} \qquad \text{Equation 1.2}$$

$$f(v) = -\frac{1}{2}ln(v) - 0.75 + v - \frac{v^2}{4} \qquad \text{Equation 1.3}$$

Initial comparisons with flow of a viscous liquid through an array of parallel cylinders showed good agreement with the theoretical expression developed by Kuwabara [32].

The derivation of the flow field and pressure drop through a parallel array of cylinders assumes that all cylinders are equally spaced and have equal diameters. Real filters differ from this simplified assumption by having a distribution of fiber diameters and by consisting of randomly oriented fibers. These differences have been accounted for through analytical and experimental comparisons. Numerous methods have been developed to account for varying levels of polydispersity of filter fibers through analytical [33-35], experimental [36,37], and numerical [38,39] investigations. The general consensus of the investigations is that fiber polydispersity can be accounted for using the standard filter pressure drop calculations assuming a weighted average of the fiber diameters.

Comparisons of pressure drop in real filters with theoretical models has shown significant variation in the level of agreement [27]. Reasons for this deviation include fiber polydispersity, gas slip on the fiber surface, fiber crossing, and filter compaction. The aerodynamic slip at the fiber surface can be accounted for using the cell model to provide a modified expression for filter pressure drop and hydrodynamic factor [36,40-42]. Further corrections are accounted for by including the homogeneity factor (η_f) defined as the ratio of theoretical pressure drop to actual pressure drop, which is typically between 1.13-2.25 [43]. The equations for pressure drop and hydrodynamic factor can be modified to account for these corrections and take the revised form:

$$P = \frac{16vx\mu V(1+1.966Kn)}{d_f^2 f(v)}$$ Equation 1.4

$$f(v) = -\tfrac{1}{2}ln(v) - 0.75 + v - \frac{v^2}{4} + 1.966Kn\left(-\tfrac{1}{2}ln(v) - 0.25 + v - \frac{v^2}{4}\right)$$

Equation 1.5

where Kn is the Knudsen number defined as $Kn=2\lambda/d_f$ (-); and λ is the mean free path of a gas molecule (65nm for air at STP).

1.3.2 Filtration Efficiency

The particle removal efficiency of a filter media is determined based on the capture efficiency of a single fiber, or ‘single fiber efficiency’. The single fiber efficiency is the ratio of the particles in the upstream parcel of air swept out by the fiber projected area removed by a real fiber divided by the total number of particles in that parcel of air [27]. By definition the single fiber efficiency can be greater than one if the fiber removes particles that are initially in the upstream area outside of the fiber projected area (e.g. removal by diffusion or electrostatic forces). The main particle removal mechanisms present in HVAC air filtration are gravitational settling, diffusion, interception, impaction, and electrostatic charge (Figure 1.2). The particle capture mechanisms typically act in concert though the particle removal is often dominated by one or more depending on particle size, shape, density, and charge.

The efficiency of the entire depth of filter media can then be determined based on the single fiber efficiency with the assumption that the air filter can be approximated by an array of parallel cylinders as described in Section 1.3.1 [27]:

$$\varepsilon_i = 1 - exp\left[\frac{4v\varepsilon_T x}{\pi(1-v)d_f}\right]$$ Equation 1.6

where ε_i is the filter efficiency (-); ε_T is the total single fiber efficiency (-) from all capture mechanisms; and the remaining variables are as described above.

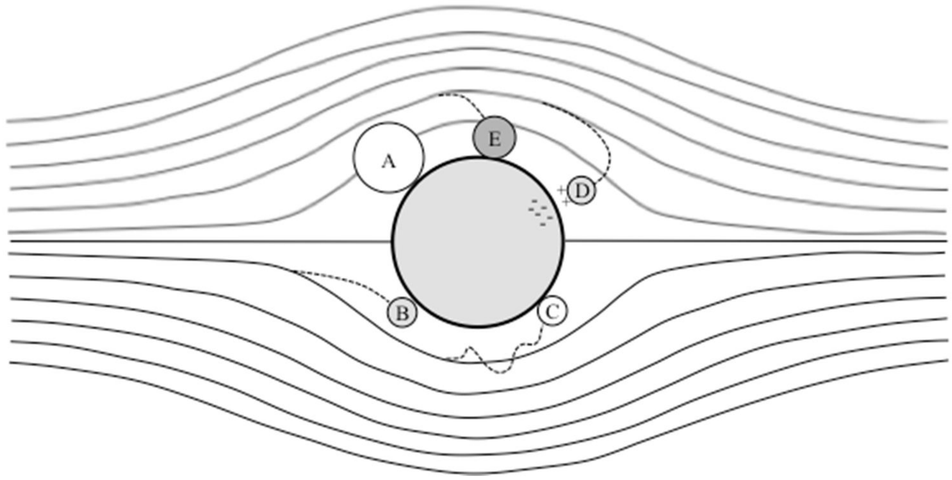

Figure 1.2: Air filter particle capture mechanisms; A) interception, B) impaction, C) diffusion, D) electrostatic attraction, E) gravitational settling.

1.3.2.1 Overall Efficiency

Rigorous analytical solutions have been developed for a number of capture mechanisms acting simultaneously on aerosol particles [44-46]. A complete description of all mechanisms cannot be solved analytically and the standard method is to combine the individual single fiber efficiency for each individual capture mechanism by assuming they act sequentially. The total single fiber efficiency, ε_T, can then be determined by:

$$\varepsilon_T = 1 - \prod_{i=1}^{n}(1 - \varepsilon_i) \quad \text{Equation 1.7}$$

where ε_i are the single fiber efficiency for each particle capture mechanism.

Capture by diffusion is dominant for small particles while interception and impaction are dominant in larger particles. Gravitational settling does not play an important role in typical HVAC filter applications. Electrostatic forces enhance collection efficiency for all particle sizes.

1.3.2.2 Gravitational Settling

Capture by gravitational settling is a result of the particles settling from the air stream due to gravitational forces. Gravitational settling is most easily visualized in still air as a particle depositing in the direction of the gravitational field and coming in to contact with the fiber surface. Gravitational settling also occurs within a moving airstream as it passes over a filter fiber and the single fiber efficiency can be derived analytically based on the ratio of the settling velocity of a particle to the free stream velocity as [44,47]:

$$\varepsilon_G = \frac{d_p^2 \rho_p g}{18\mu V} \quad \text{Equation 1.8}$$

where ε_G is the single fiber efficiency due to gravitational settling (-); d_p is the particle diameter (m); ρ_p is the particle density (kg/m^3); g is the gravitational acceleration on the Earth (9.81m/s^2); μ is the dynamic viscosity of air (Pa·s); and V is the free stream velocity (m/s).

1.3.2.3 Diffusion

Small particles in an air stream will exhibit a random displacement due to Brownian diffusion that will tend to increase the collection efficiency on a fiber surface. The collection efficiency as a result of Brownian diffusion is a function of the relative magnitude of particle motion due to diffusion and the free stream flow velocity. Single fiber efficiency can be determined analytically assuming the diffusion layer is small. The single fiber efficiency has been determined through a number of analytical [27,48-51] and experimental [46,52,53] methods with a consensus on the form:

$$\varepsilon_D = \frac{2.6}{\eta_f} f(v)^{-1/3} Pe^{-2/3} \quad \text{Equation 1.9}$$

$$Pe = \frac{V d_f}{D} \quad \text{Equation 1.10}$$

$$D = M k_B T \quad \text{Equation 1.11}$$

$$M = \frac{C_n}{3\pi\mu d_p} \quad \text{Equation 1.12}$$

$$C_n = 1 + \frac{2.492\lambda}{d_p} + \frac{0.84\lambda}{d_p} exp\left(-\frac{0.87 d_p}{2\lambda}\right) \quad \text{Equation 1.13}$$

where ε_D is the single fiber efficiency for capture by diffusion (-); η_f is the homogeneity factor (-); $f(v)$ is the hydrodynamic factor (-); Pe is the Peclet number (-); D is the coefficient of diffusion (m^2 s^{-1}); M is the particle mobility (s kg^{-1}); k_B is Boltzmann's constant (1.38x10^{-23}m^{2}kg s^{-2}K^{-1}); T is the gas temperature (K); C_n is the Cunningham slip correction factor (-); μ is the gas dynamic viscosity (Pa·s); d_p is the particle diameter (m); and λ is the mean free path of a gas molecule.

1.3.2.4 Interception

Particle capture by interception occurs when a particle following a streamline of the flow field around a filter fiber encounters the fiber surface. This is a passive operation that will occur if the streamline on which a particle is flowing passes within ½d_p of the fiber. The single fiber interception efficiency accounting for gas slip has been determined analytically and experimentally to have the form [27,42,54,55]:

$$\varepsilon_R = \frac{(1+N_R)}{2\eta_f f(v)}\left[(1+N_R)^{-2} + 2(1+1.996Kn)(1+N_R)ln(1+N_R) - 1\right]$$

Equation 1.14

$$N_R = \frac{d_p}{d_f}$$ Equation 1.15

where ε_R is the single fiber efficiency due to interception (-); N_R is the dimensionless interception parameter (-); and the remaining parameters are described above.

1.3.2.5 Impaction

Particles with a large Stokes number will tend to deviate from the streamlines around a filter fiber due to inertia. If this deviation results in the particle impacting on the fiber it is considered to be captured due to inertial impaction. The equation for single fiber efficiency due to impaction must be determined numerically and requires the simplifying assumption that no particle bounce occurs on impact [27]. As a result numerous computationally and empirically derived relations exist [47,56-60] that all provide the same general shape of the efficiency versus particle diameter curve. One of the empirically determined relations that has found use in HVAC filter analysis is [27]:

$$\varepsilon_I = \frac{St^3}{St^3 + 0.77St^2 + 0.22}$$ Equation 1.16

$$St = \frac{d_p^2 \rho_p V C_n}{18\mu d_f}$$ Equation 1.17

where ε_I is the single fiber collection efficiency by impaction (-); St is the Stokes number of the particle (-); d_p is the particle diameter (m); ρ_p is the particle density (kg/m3); V is the free stream velocity (m/s); C_n is the Cunningham slip correction coefficient (-); μ is the gas dynamic viscosity (Pa·s); and d_f is the fiber diameter (m).

1.3.2.6 Electrostatic Charge

Electrostatic charges present on the fibers or particles will enhance the collection efficiency of the filter media. The equations have been derived and experimentally validated through numerous studies [61-66]. All approaches require simplifying assumptions and are subject to a large amount of uncertainty. A summary of the single fiber collection efficiency of electrostatic capture mechanisms is provided by Brown [27].

For the case of uniformly charged fibers and charged particles the capture mechanism is characterized by coulombic forces. The single fiber efficiency can be determined by:

$$\varepsilon_{Qq} = \pi N_{Qq} \qquad \text{Equation 1.18}$$

$$N_{Qq} = \frac{Qq}{3\pi^2 \varepsilon_0 \mu d_p d_f V} \qquad \text{Equation 1.19}$$

where ε_{Qq} is the single fiber capture efficiency for the charged fiber and charged filter; N_{Qq} is the dimensionless capture parameter (-); Q is the fiber charge per unit length (C/m); q is the particle charge (C); ε_0 is the permittivity of free space (8.84×10^{-12} F/m); μ is the dynamic viscosity (Pa·s); d_p is the particle diameter (m); d_f is the fiber diameter (m); and V is the free stream velocity (m/s).

For the case of uniformly charged fibers and neutral particles the capture is enhanced by polarizing forces that cause the particles to drift towards the fiber. The single fiber efficiency can be determined by:

$$\varepsilon_{Q0} = \pi N_{Q0} \qquad \text{Equation 1.20}$$

$$N_{Q0} = \frac{Q^2 d_p^2}{3\pi^2 \varepsilon_0 \mu d_f^3 V}\left(\frac{D_p - 1}{D_p + 2}\right) \qquad \text{Equation 1.21}$$

where N_{Q0} is the dimensionless capture parameter (-); and D_p is the dielectric constant of the particle (-).

For the case of neutral fibers and charged particles the capture is enhanced by image forces. The single fiber efficiency can be determined by:

$$\varepsilon_{0q} = \frac{2}{f(v)^{1/2}} N_{0q}^{\ 1/2} \qquad \text{Equation 1.22}$$

$$N_{0q} = \frac{q^2}{12\pi^2 \varepsilon_0 \mu d_p d_f^3 V}\left(\frac{D_p - 1}{D_p + 1}\right) \qquad \text{Equation 1.23}$$

where N_{0q} is the dimensionless capture parameter (-).

More complex models have been produced for non-uniformly charged fibers and cases of highly charged particles. Alternative theoretical and empirical formulations exist for each scenario with no generally agreed upon solution for practical development.

1.4 Dissertation Objectives and Organization

The primary goal of this dissertation is to improve the understanding of air filter energy use and impact on indoor air quality. This is achieved through development and validation of an air filter model, exploration of the model uses, and experiments to further advance our understanding of filter dynamics. The research goal is approached from both a macroscale perspective to improve modeling and performance of full-scale air-handling systems and microscale experimental investigations to provide deeper insight into the role of operation parameters on filter performance. The work provides insight into the role that filter selection plays in building performance and how existing design standards and testing methods can be improved. The work is separated into five research chapters each designed to address specific gaps in the literature leading to the overall goal. The chapters are presented chronologically as performed throughout the course of the author's doctoral degree. Conclusions drawn at the end of each research chapter pertain to the work contained in that chapter. Conclusions from the dissertation as a whole are provided in Chapter 8 and account for lessons learned throughout the degree.

Chapter 2 summarizes a literature review of studies relevant to the current dissertation to provide context for the subsequent research chapters.

Chapter 3 describes the derivation of a new model to predict the energy use and operation cost of an air filter. The model was developed to use information available from existing standardized air filter tests so as to be readily useful to building operators and designers. The model improves upon previous efforts by including the dynamic attributes of air filter operation such as flow rate, filtration efficiency, and flow resistance. The outcome of the newly developed model is to allow for prediction of energy consumption while accounting for variation in system flow, particle concentration, and loading conditions. This will allow comparisons of the impact of filter selection, system operation, and local conditions on energy and cost.

Chapter 4 presents a case study detailing the immediate practical uses of the air filter energy model for comparing energy efficiency and operation cost between numerous alternative filter solutions at the Vancouver International Airport. The annual operation cost of different air filters specified to meet air cleaning requirements at the airport are determined based on local electricity prices and air pollution measurements. A comparison of the newly developed model with previous methods was undertaken to highlight increased functionality of the new method. The work highlights the potential of the new model for decision-making purposes and explores the impact of different operating conditions and filter characteristics on the cost of filter operation. The results provide details of the actual life cycle cost of operating air filters and an improved understanding of the range of costs for a specified filter performance.

Chapter 5 investigates the impact of modified ventilation and filtration systems to inform building designers, operators, and policy makers of relative effectiveness and costs. Indoor aerosol dynamics, filter cost, and epidemiological models were combined to compare size-resolved indoor particle concentrations, operation costs, and monetized health benefits from reduced occupant exposure within an office building. Comparisons were performed to develop an understanding of the relative magnitude of costs and benefits of system and filter choices. Comparisons were made for a number of cities to examine the impact of variation in local air quality, electricity prices, and economic conditions. The addition of health endpoints improves the strength of filter modelling by capturing the importance of occupants to a whole building analysis. The results represent the first instance of a specific study to determine how changes to air filtration systems impact energy, cost and health, thus providing the required context and tools for future policy analysis.

Chapter 6 describes an experimental investigation of the impact of relative humidity on loaded HVAC air filters. Flat sheets of commercial filter media were loaded with hygroscopic, non-hygroscopic, or a mixture of particles, in a laboratory apparatus and exposed to changes in relative humidity. The goal of the study was to assess the potential impact of relative humidity on filter performance and to determine if it was a potential reason for discrepancies in performance between standardized tests and real operation. The work builds upon previous studies of HEPA filter response to relative humidity with a focus on the geometry and physics associated with HVAC air filter media. The aim of this work is the improvement of knowledge surrounding the importance of particle loading on the dynamic properties of air filters.

Chapter 7 describes an experimental study of the physical changes to aerosol aggregates exposed to changes in relative humidity. The purpose of this study was to provide a physical explanation for the impact of relative humidity exposure shown in Chapter 6. The independent measurement of aggregate restructuring while suspended in an airstream and collected on a wire substrate represented the first physical evidence that substantial particle restructuring can occur within filter media. The results highlight the relevance of air conditioning control during standardized tests and further elucidate potential explanations for discrepancies between modeled and experimental results.

Chapter 8 discusses the conclusions to be drawn from the research described in this dissertation and the advancements towards the dissertation goals.

Chapter 9 provides recommendations for improvements to filter performance and system operation as well as future research directions.

2 Literature Review

2.1 Air Filter Performance Modeling

2.1.1 Energy Modeling

The air filter testing methods in ASHRAE 52.2 [67] provide a means of characterizing filter performance but do not stipulate how to determine the energy efficiency of a filter. Two prominent methods have been developed to characterize the energy efficiency of an air filter; quality factor (also referred to as key energy performance or figure of merit) and power calculations.

Quality factor is calculated as [27]:

$$QF = \frac{-ln(1-\varepsilon)}{P} \qquad \text{Equation 2.1}$$

where QF is the quality factor (Pa^{-1}); ε is the particle removal efficiency (-); and P is the pressure drop across the filter (Pa).

The quality factor provides an indication of the performance of a filter (through measurements of efficiency) versus the energy expenditure (through pressure drop). The QF depends on the particle diameter through the filtration efficiency term. Filters with higher filtration efficiency and lower pressure drop will have a higher QF. Quality factor is often used to compare relative performance of flat sheets of filter media [68-72] because it captures both changes in energy use and removal efficiency but is independent of filter thickness [27]. This is an adequate method of comparing relative energy efficiency of filter media but does not provide a means of determining energy consumption for costing equations.

The power required to pass air through a filter is defined as [27]:

$$W = \frac{Q \cdot P}{\eta_s} \qquad \text{Equation 2.2}$$

where W is the instantaneous power (Watts); Q is the flow rate (m^3/s); P is the pressure drop (Pa); and η_s is the fan system efficiency (-) including fan and motor efficiency which is used to determine electrical power requirements.

The average power can then be determined from instantaneous power. The standard method of determining average power for energy and cost calculations (called the Wattage method in this dissertation) is by arithmetically averaging the initial and manufacturers recommended final pressure drop. The energy use of the filter over the operation lifetime is then typically calculated by multiplying the power by the intended operation life [73]. This introduces error in the results by not accounting for the actual pressure drop achieved in the filter or the effect of accumulated dust, which varies depending on installation location.

The metrics Quality Factor and Wattage are incomplete descriptions of filter performance. The QF provides only a means of comparison between filters and does not determine the actual power consumption or energy use during filter operation and therefore cannot be used to compare operation costs of filters. The Wattage model assumes that the power consumption of the filter is constant regardless of the time since the filter was last changed or how much dust has accumulated in the media. This provides an adequate representation of the average power during the filter life but does not provide any indication as to how long the filter should be allowed to operate between changes to achieve that average power rating. The Wattage method also neglects to account for the rate of particle accumulation in the filter, which determines the temporal variation of flow resistance. Since the end result of an energy efficiency comparison is the energy use of the filter, this time parameter is of critical importance and will vary between filters based on the specific filter dust holding capacity and filtration efficiency data, and between installation locations based on particle concentrations.

Given the limitations of these two methods an improved filter model to accurately predict the flow power as a function of dust accumulation and flow rate is required.

2.1.2 Cost Modeling

The air filter power consumption can be used to determine energy use and, from that, operation cost over a certain time frame [74]. A number of air filter manufacturers provide life-cycle cost (LCC) tools or methods to compare the cost of their products [75-79]. These evaluation methods are based on the costing outline provided by Eurovent for filter applications [80]. The limitation to the use of the existing method is that it does not provide a means for determining the dynamic effects of filter operation such as changes in flow rate or dust accumulation. This does not account for differences in loading characteristics of the individual filters or the aerosol concentration in the system and therefore cannot be used to optimize operations. LCC costing methods are limited by the impact of the chosen discount rate to account for value of costs in the future. Considerations of air filters generally exclude the use of discount rates to simplify calculations. This introduces error when calculating costs for long- term projects but is generally minimal for typical lifecycles of air filter comparisons, which are on the order of 1-3 years.

The cost of filter operation has been determined in a number of studies using the method described above. Despite the limitations to the method discussed, the results provide useful insight into filter performance. Arnold et al. [74] provided a comparison of the possibility for reduced total lifecycle cost of an air filtration system by installing more energy efficient filters. The energy consumption was based on an arbitrarily assumed operation time that did not account for differences in loading characteristics between filters but nonetheless showed that gains in efficiency were possible. Sun [73] accounted for different exponential filter loading profiles in an LCC comparison of surface and depth loading filters. Again, the results showed that cost savings were possible but the changeout time was arbitrarily chosen and complete filter loading was assumed to occur in this time without providing a method to account for actual aerosol concentrations. Fisk et al. [81] provided a detailed analysis of the cost and performance of filters based on ASHRAE Dust Spot Efficiency (the classification at the time which was subsequently replaced by MERV). The filter lifetime was determined based on loading characteristics and manufacturers recommended pressure drop rather than a system optimization. The analysis was limited to constant volume systems due to limited model developed at the time.

These methods all assume a constant volume air handling system and simplified filter loading process, which is not suitable for commercial building operation when variable speed drives are installed. A filter power and cost model that accounts for the dynamics of system operation is required to allow for comparison of filter and system changes on cost and indoor air quality.

2.2 Benefits of Air Filter Installations

A number of studies have been performed to investigate the benefits of air filter installations. Experimental methods include measurement of indoor particle concentrations for varying size ranges and impacts on system operation. Modeling of indoor particle dynamics, including the operation of the filtration system, allows for calculation of indoor particle concentration and exposure levels for occupants. Some studies report the impact of filtration systems based on indoor particle concentration changes while others take additional steps to determine how these exposure concentrations will impact the health of occupants.

The primary goal of an air filter is to remove particles from the air stream and thus lower the indoor particle concentration. Many studies have investigated the impact of filtration systems on particle concentrations and system performance:

- Fisk et al. [81] modeled the reduction in indoor particle concentration for installation of 8 different air filters of varying levels of ASHRAE Dust Spot Efficiency. They found that the filters with higher efficiency cost more to operate but provided a cleaner environment. The investigation was limited to analysis using average filter performance based on the standard Wattage model and therefore did not contain information on changes to filter characteristics as dust was deposited.
- Jamriska et al. [82] modified the well known indoor particle dynamics model [83,84] to be used for analysis of filter installations. Their work has shown that the time evolution of indoor concentration is heavily influenced by system design

and outdoor pollution. The model was experimentally validated [85] and is suitable for extension to future analyses of filter performance.

- Noh and Hwang [86] compared the effect of ventilation rate and filter selection on indoor air quality and power consumption. The study found that a minimum of MERV 7 filter was required to reduce indoor particle concentrations below levels found with no ventilation. The filter model accounted for changes in flow rate but neglected particle loading and particle size distributions in the calculations.
- Carlsson and Johnsson [87] have shown that the particle concentration downstream of filters varies by location due to upstream concentration differences and that energy consumption is correlated with filter classification in the European context. They propose that energy consumption could be reduced by selecting filters to meet specific air quality targets. However, they did not provide an analysis of building systems to determine the required filter for specific scenarios.
- Quang et al. [88] performed measurement and modeling analysis of the impact of air filters on particle number concentrations for fine and ultrafine particles. The results showed that installing mixing or outdoor air filters can have significant benefits for reducing indoor concentrations. The model has potential for extension to comparing filter selection and operation choices but was limited to validation with experimental results in this work.
- Zaatari et al. [89] compared experimental measurements of indoor air quality and fan power consumption for a number of rooftop HVAC units. The study found that filter loading and increased filter efficiency caused flow reductions in constant volume systems and power increases in variable air volume systems. The experimental results were not extended to theoretical development of a filter model but highlighted the complex change in system operation with dynamics of filtration processes.

The impact of air filter installations on occupant health can be determined by using epidemiological relations between particle exposure and health endpoints. This methodology follows the approach of studies quantifying benefits from outdoor air pollution reduction interventions [90]. A number of investigations have focused on benefits from improved filtration and those relevant to commercial and institutional system design include:

- Sultan [91] compared the financial benefits associated with reduced exposure to time-weighted indoor particle concentrations when mechanical ventilation with filtration replaced existing natural ventilation systems in Singapore using theoretical models. The results found that the added cost of operation was significantly outweighed by the reductions in morbidity and mortality endpoints from lower exposure concentrations. The study found benefits were greater when the filter was assumed to remove 85% of particles rather than 40% but did not associate these removal fractions with real filtration systems nor were intermediate gradients of filter efficiency investigated.
- Bekö et al. [92] compared the monetized health benefits versus operation costs of HVAC systems operating either with or without an air filter in a constant volume system. The study found that the health benefits of filtration outweigh the costs but did not focus on the impact of filter choice to determine incremental benefits of improved filtration.
- Azimi and Stephens [93] compared the monetized health benefits from reduced exposure to infectious diseases versus filter choice. The study found that filtration provides benefits to occupant health but did not study the impact of exposure to PM.
- Fisk [94] has summarized numerous experimental interventions and modeling studies that compare the impact of filtration on occupant health. The findings show that filtration reduces allergy and asthma symptoms and can have significant impacts on morbidity and mortality through reduced exposure to PM.

Installing an air filtration system has been shown experimentally and theoretically to reduce indoor particle concentrations. Installing filters with a higher efficiency or MERV based on ASHRAE 52.2 will have a greater impact due to lower concentrations of particles in the downstream air. It is clear that providing filtration to a space will improve the health of occupants through exposure reductions. However, the previous studies did not provide the required information to determine what type of filter provides the most benefit or how the filtration system should be designed to optimize results. Improvements to the existing filter energy and cost models are required before such an analysis can be made possible. Using improved dynamic filter models an understanding of the impact of filter selection and operation design can be performed to compare the relative costs and benefits from increased energy consumption and improved occupant health.

2.3 Impact of Particle Deposits on Filter Behaviour

2.3.1 Flat Sheet Tests

Air filter performance is studied predominantly through models and experiments of samples of filter media rather than whole filter investigations. The general trends of performance are applicable for real world application but the specific results have been shown to vary [95]. The majority of studies have focused on performance of a clean filter before any dust loading occurs. While these tests provide insight into the role that certain design characteristics may have on filter performance they do not adequately represent filters throughout the majority of operation due to the significant impact of dust loading.

As particles deposit within the filter media the flow resistance tends to increase [96] due to the drag on deposited particles and growth of aggregate structures [97]. The deposited particles also influence the filtration efficiency of the media by altering the fundamental capture mechanisms. For fibrous media relying only on mechanical capture mechanisms the filtration efficiency increases with dust loading [96,98]. The relationship for filters with electrostatic capture mechanisms is significantly more complex. The filtration efficiency is shown to decline with initial loading of dust within the media [99] but will typically exhibit a subsequent increase [100,101] such that the minimum efficiency does not occur for the clean media.

The majority of studies investigating the impact of different particle geometry and system conditions focus on the impact of surface loaded HEPA filters that form dust cakes and have limited applicability to HVAC filters. Changes in filter operations have been shown to depend on the filter characteristics (fiber diameter, solid volume fraction, fiber charge, etc.) [27,95,102], particle characteristics (size distribution, charge, shape, etc.) [103-

106], and loading conditions (face velocity, relative humidity, etc.) [101,107,108]. The greatest influencing factor on the evolution of filter performance has been particle size. Smaller particles cause a greater increase in flow resistance and filtration efficiency due to greater specific surface area [104,109-111]. System parameters also impact results as they will change the growth of dendrite structures depending on dominant fiber capture mechanisms [112-114].

While the impact of filter and particle characteristics on properties of a loaded filter have been extensively studied, the impact of system conditions, and especially relative humidity, is less well understood. In general, high relative humidity reduces the flow resistance of HEPA filters when loading occurs with hygroscopic particles and has no impact for non-hygroscopic particles [107,115,116]. Joubert et al. [117] performed surface loading of HEPA filters at 0% relative humidity and showed that exposing the loaded filter to a higher relative humidity between 20-60% resulted in a reduction in specific cake resistance that did not depend on the mass loading. It was postulated that the drop in specific cake resistance was a result of a change in size of the particles in the filter cake though no further experiments were undertaken to provide evidence for this hypothesis and the magnitude of the potential impact of relative humidity on filter operation in real systems is unknown.

2.3.2 Full-Scale Filter Test

The significant impact of particle and system properties on filter performance in laboratory testing implies that these impacts will be present for filters loading in real systems. It also implies that filter performance under controlled, standardized conditions such as ASHRAE 52.2 will not accurately predict the performance in real systems where flow rate, particle properties, and system conditions vary significantly. Few studies have explored either performance changes in real systems or a comparison of performance based on laboratory versus real operation.

The flow resistance and filtration efficiency of mechanical filters increases with increased dust loading [28,118-120]. Studies of performance of electret filters has shown significantly more variability in results. The studies all show that flow resistance increases with increased dust loading. The majority of studies have shown significant reduction in filtration efficiency after dust loading [95,118,119,121,122]. A detailed comparison of multiple filters however, has shown that not all electret filters experience the significant change in filtration efficiency [123] throughout operation life.

Whole filter comparisons of filter performance for natural and artificial loading are even scarcer. Stephens and Siegel [124] compared filter efficiency determined from standard ASHRAE 52.2 testing with a whole building efficiency test and found that size resolved efficiency results aligned between both methodologies. Meyers and Arnold [123] showed that the size-resolved efficiency of clean filters was comparable when tested in the field and in the laboratory. The efficiency from the conditioning step in ASHRAE 52.2 did not provide the same degradation of filtration efficiency as did exposure to real operating conditions. Hanley et al. [118] found good agreement for filtration efficiency at a specified flow resistance between filters loaded with natural and artificial dust types.

Though filter performance has been studied extensively there exists a gap in the understanding of how filters behave differently when loaded in real operations versus in the laboratory. Increased understanding of the role that system operation characteristics play on performance changes with loading will allow for improved testing methods and models to be developed.

3 Development and Validation of Filter Energy Model[1]

3.1 Introduction

Two main methods of classifying or comparing air filter energy efficiency exist. The Quality Factor is typically used to describe performance of flat sheets of filter media [27]. The Wattage method uses simplified assumptions to classify flow resistance throughout the life of the filter operation [120]. This does not account for variability in system flow or allow for determination of filter energy use through varying operation lifetimes and schedules. The development of an improved model is critical for comparisons of filter performance that accounts for different operation conditions and locations.

This chapter focuses on the development of a new model based on the data available from ASHRAE 52.2 filter testing to allow for a simple method of determining the response of filters to changes in system operation. A relation for filter pressure drop as a function of airflow rate has been derived and the methods of approximating filtration efficiency have been discussed. The relevant cost calculations to compare filter installations have also been discussed. The model was validated first using the data from lab experiments of Rivers and Murphy [28] and then by a building scale experiment at the Vancouver International Airport (YVR).

The model developed in this chapter will allow for subsequent comparison of the impact of filter selection and system design on energy consumption and indoor air quality. It will allow for an improved understanding of the critical parameters associated with operation costs and can be used by building owners and operators to reduce energy consumption and operation cost of existing system operation through modified performance parameters or filter selection.

---

[1] Content from this chapter has been published. Montgomery, J. F., Green, S. I., Rogak, S. N., & Bartlett, K. (2012). Predicting the energy use and operation cost of HVAC air filters. Energy & Buildings, 47, 643–650.

3.2 Model Development

3.2.1 Deriving Pressure Drop Relations

The instantaneous power required to pass air through a filter is defined by:

$$W = \frac{QP}{\eta_s} \qquad \text{Equation 3.1}$$

From this the average power and energy consumption over the filter operation lifetime can be determined by:

$$W_{ave} = \frac{1}{\eta_s t}\int_0^t P(t)Q(t)dt \qquad \text{Equation 3.2}$$

$$E = \int_0^t W dt = \int_0^t \frac{1}{\eta_s} P(t)Q(t)dt \qquad \text{Equation 3.3}$$

where W is the instantaneous power (watts); P is the pressure drop across the filter (Pa); Q is the air flow rate (m^3/s); η_s is the fan system efficiency (-); W_{ave} is average power (watts); t is the operation time (s) since the last filter change; and E is the filter energy consumption (J).

The equations above assume constant fan system efficiency in their derivation. This fan system efficiency is known to vary during operation with flow rate and flow resistance. The anticipated impact of this assumption is small due to limited potential for fan system efficiency variations compared to other model parameters. The impact of efficiency variations is investigated later in Section 4.3.3.1.

A relation for pressure drop and flow rate as a function of time is required to solve the average power and energy consumption equations. The previous filter power calculations assumed that the system operated at a constant flow rate and did not account for changes in the pressure-flowrate relationships. The flow rate is determined by the system operation and assumed to be known for the purposes of model derivation. The pressure drop through the filter can then be determined as a function of the flow conditions.

The standard filter tests outlined in ASHRAE 52.2 [67] provide an indication of how an air filter will perform during real operation. Examples of results from filter testing are shown in Figure 3.1. The dust holding capacity test provides a relation between the dust mass collected and the pressure drop at a constant flow rate. The dust loading test occurs by flowing dust laden air through the filter and measuring total mass flow. The mass of dust in the filter is related to the time of the test or time of operation by the known volumetric flow rate, particle concentration in the air stream, and filtration efficiency. The clean filter flow test provides a relationship between the pressure drop and flow rate through a clean filter. Both standard tests are based on a 600mm x 600mm filter.

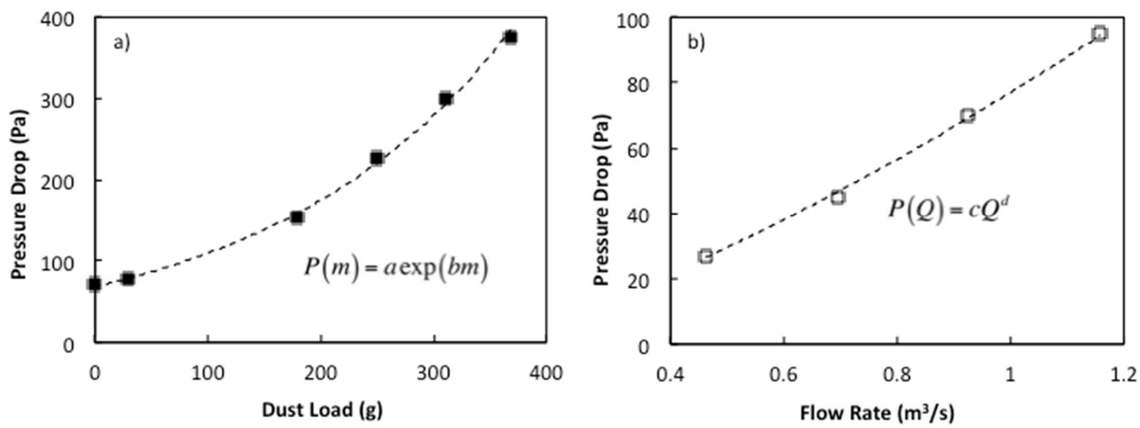

Figure 3.1: Air filter pressure drop relations for (a) filter loading at Q=0.94m^3/s and (b) clean filter flow testing

An exponential curve of the form $P=a\cdot\exp(bm)$ has been shown to provide the best fit to the results of the Dust Holding Capacity Test [73]. The best form for a curve fit to the Traverse Test results has not shown the same level of consistency in the literature. Curves of the following form have been proposed and provide a good fit to the data; $P=cQ$ [27], $P=cQ^2+dQ$ [86], $P=cQ^d$ [29]. A comparison of the fit curves has shown that the form $P=cQ^d$ provides the best fit in most cases and has been used for the following model derivation. The functional pressure drop relations providing the best fit to filter properties are:

$$P(m) = aexp(bm) \quad \text{Equation 3.4}$$

$$P(Q) = cQ^d \quad \text{Equation 3.5}$$

In view of the exponential form of the Dust Holding Capacity Test, and the polynomial form of the clean filter flow test, it is plausible that the two forms can be combined to give:

$$P(Q, m) = a exp(bm) Q^d \quad \text{Equation 3.6}$$

$$a = \frac{P_i}{Q_{design}^d} \quad \text{Equation 3.7}$$

$$b = \frac{1}{DHC} ln\left(\frac{P_f}{aQ_{design}^d}\right) \quad \text{Equation 3.8}$$

where a, b, and d are filter constants which can be determined by ASHRAE 52.2 test data for a specific filter, a is related to the initial filter pressure, b is related to the dust holding capacity, and d relates the flow through the filter to the pressure drop; m is the accumulated dust mass (g); Q is the instantaneous flow rate (m^3/s); P_i is the initial pressure drop (Pa) at design flow rate; Q_{design} is the design flow rate (typically $0.94 m^3/s$) at which the dust holding capacity test was performed; DHC is the dust holding capacity (g) at the manufacturer's recommended final pressure; and P_f is the manufacturer's recommended final pressure drop (Pa) at the design flow rate (typically 375 Pa at 0.94 m^3/s). The constant d is the exponent in the curve fit to the pressure drop versus flow rate of a clean air filter with the form $P=aQ^d$ and is assumed constant through dust loading [29].

3.2.2 Approximations for Filtration Efficiency

The relations for pressure drop derived above are still not suitable for use in determining filter power and energy consumption. A relation between dust accumulation and operation time is required. The dust accumulation is a function of the operation time, filter efficiency, and aerosol concentration upstream of the filter. Assuming system characteristics are known the dust accumulation can be related to operation time through the filter efficiency. Particle removal efficiency is a function of particle size, airflow rate and dust accumulation as will be described below.

3.2.2.1 Constant Filtration Efficiency

Assuming filtration efficiency to be constant throughout the operation time allows for a simple relation between accumulated mass and time. Accumulated mass is then:

$$m = \int_0^t Q \sum \varepsilon_i C_i dt \qquad \text{Equation 3.9}$$

where m is the accumulated dust (g); Q is the flow rate (m^3/s); ε_i is the size resolved filter efficiency (-); C_i is the size resolved aerosol concentration (g/m^3); and t is the operation time (s).

The results from ASHRAE 52.2 testing do not provide measurements of the filtration efficiency for particles below 0.3µm, which is required for a complete understanding of the filter loading and impact on indoor air quality. Kowalski et al. [125] developed a method of approximating the size resolved filtration efficiency based on the measurements from ASHRAE 52.2. The method assumes that the filter efficiency is dominated by diffusion and interception and uses approximations for the single fiber collection efficiency to recreate the size resolved efficiency from experimental measurements of efficiency for particles between 0.3-10 µm. The efficiency is of the form [125]:

$$\varepsilon_i = L_u[1 - exp(-(\varepsilon_D + f\varepsilon_R)S)] \qquad \text{Equation 3.10}$$

$$\varepsilon_D \cong A d_p^{-2/3} \qquad \text{Equation 3.11}$$

$$\varepsilon_R \cong B \frac{d_p^2}{1+d_p} \qquad \text{Equation 3.12}$$

where ε_i is the filter efficiency as a function of particle size (-); L_u is the upper limit of filter efficiency (-); ε_D is the single fiber efficiency for capture by diffusion (-); ε_R is the single fiber efficiency for capture by interception (-), f is the fiber correction factor (typically 0.615); S is the dimensionless fiber projected area (-); A and B are constants based on filter physical properties; and d_p is the incident particle diameter (m). The particle size resolved filter efficiency can then be determined based on efficiency results from ASHRAE 52.2 tests.

This method was validated previously against experimental filter measurements [125] for the range of particle diameter from 0.01 to 10 µm using a limited number of experimental results. The model was confirmed in this work for commercial filters using data in the range from 0.3 to 10 µm and extrapolating to smaller particle sizes (sample results shown in Figure 3.2). The size resolved efficiency can therefore be determined experimentally when possible or approximated using this method from filter performance in ASHRAE 52.2 testing. Extrapolation from ASHRAE 52.2 measurements should be used with caution until further experimental validation of the extrapolation method is performed.

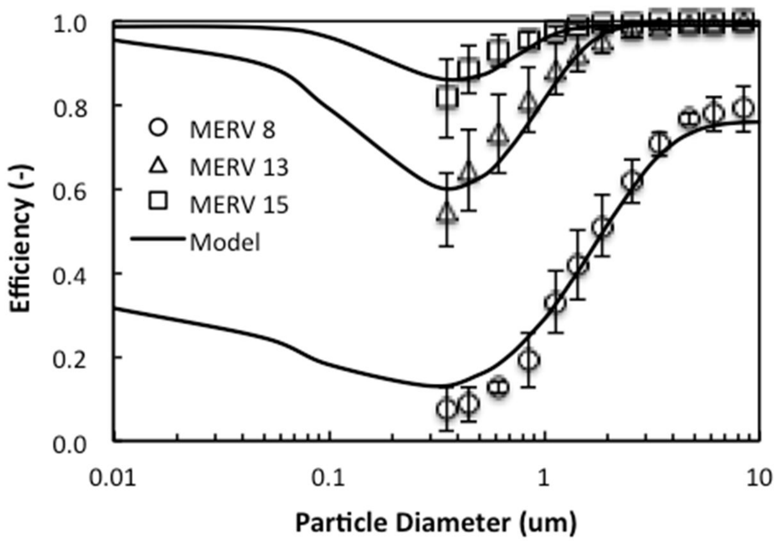

Figure 3.2: Sample comparison of size resolved filter efficiency from ASHRAE 52.2 test results of commercial filters with modeled results.

3.2.2.2 Filtration Efficiency as a Function of Dust Accumulation

The limited availability of experimental data or validated theoretical models providing a relation between size-resolved filter efficiency is a limitation to the current model. The general trend shown during experimental analysis is for the efficiency to increase with dust loading for filters that utilize mechanical capture mechanisms. Filters utilizing both mechanical and electrostatic capture show a more complex relation as described in Chapter 2.

The typical method of accounting for the effect of dust loading in filter cost modeling is to assume a constant value of filtration efficiency equal to the MERV rating of the filter [81]. Two other methods are possible; fitting an empirical curve for efficiency versus dust load to the ASHRAE 52.2 test results or assuming constant filtration efficiency equal to the average efficiency from the ASHRAE 52.2 test results.

An example of a functional form of empirical curve fit to ASHRAE 52.2 test results for efficiency in the three ASHRAE size bins is shown in Figure 3.3. The efficiency versus fraction of DHC results can be fit with a curve of the form:

$$\varepsilon_i = \begin{cases} f_i \left(\frac{m}{DHC}\right)^{g_i} & for\ \varepsilon_i > \varepsilon_{i,MERV} \\ \varepsilon_{i,MERV} & otherwise \end{cases} \qquad \text{Equation 3.13}$$

where ε_i is the particle filtration efficiency (-); $\varepsilon_{i,MERV}$ is the Minimum Efficiency Reporting Value (-); f_i is a constant (-); m is the dust load (g); DHC is the dust holding capacity (g); g_i is a constant (-); and the subscript i denotes the ASHRAE size bin.

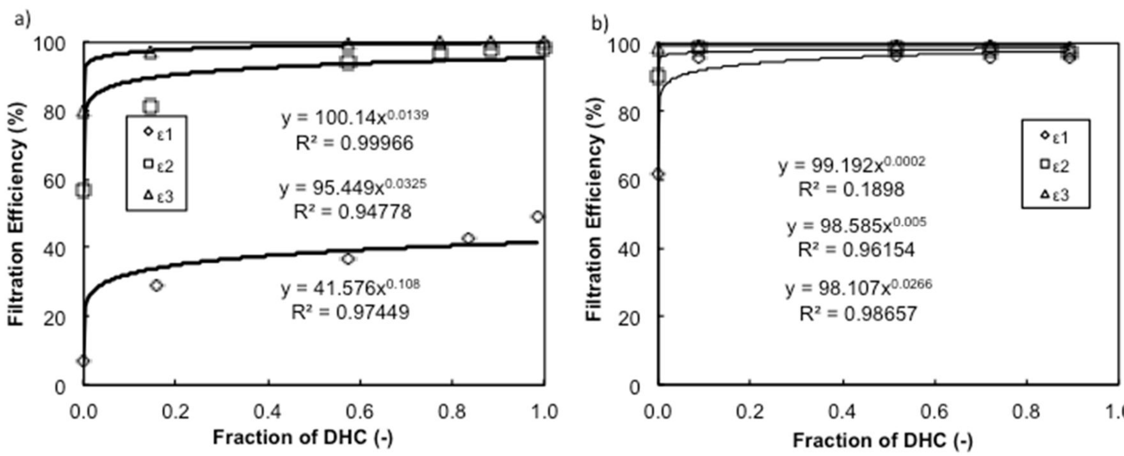

Figure 3.3: Sample filtration efficiency versus dust loading graph with curve fits for (a) MERV 7 and (b) MERV 13 filters.

The use of a single constant value of filter efficiency is the best available option given that the profile of efficiency versus dust loading varies significantly between filters and no single generic functional form has been found that provides an adequate fit for all particle sizes and filter types. Assuming the filtration efficiency is a constant at the MERV will tend to underestimate the filter efficiency during loading with the greatest difference for low MERV rating filters and in the ASHRAE size bin 1 (0.3-1μm). This size bin contains less mass than the larger sizes and so will have relatively lower impact on the overall filter loading. The assumption of constant filtration efficiency (with respect to dust load) equal to the MERV rating will also provide a conservative estimate of the indoor air quality and is therefore the option used in subsequent modeling in this work.

3.2.2.3 Filtration Efficiency as a Function of Flow Rate

Basic filter theory shows that filtration efficiency is a function of face velocity on the filter media and thus air flow rate through the filter [27]. This has also been confirmed experimentally in a number of studies [52,126,127]. When a fibre filter is approximated by an array of parallel cylinders the filtration efficiency as a function of air flow rate can be determined [27,128]. Assuming that diffusion, impaction, and interception are the dominant capture mechanisms present the relation for filtration efficiency is:

$$\varepsilon_i = 1 - exp\left[-k_{i,D}Q^{-2/3} - k_{i,I}Q - k_{i,R}\right] \qquad \text{Equation 3.14}$$

where ε_i is the filtration efficiency (-); $k_{i,j}$ is the characteristic coefficient of collection (a function of particle size and filter choice) for each capture mechanism; Q is the air flow rate (m^3/s); the subscript i denotes the particle size or approximate ASHRAE size bin; the subscript D denotes capture by diffusion; the subscript I denotes capture by impaction; and the subscript R denotes capture by interception.

The equation for filtration efficiency as a function of airflow rate can be simplified further depending on the dominant capture mechanisms (diffusion, interception, impaction). The variation of filtration efficiency with airflow rate has been addressed previously by Noh and Hwang [86] and Rudnick [128]. In their work the aerosol was represented by three particle sizes, 0.1 μm, 1 μm, and 10 μm. In the absence of electrostatic forces diffusion is the dominant capture mechanism for 0.1 μm particles and impaction is assumed as the dominant capture mechanism for 1 μm and 10 μm particles. The relations for efficiency versus flow rate for 0.1 μm, 1 μm, and 10 μm have been used as approximations for the E_1, E_2, E_3 size bins, respectively [86]. The relations are:

$$\varepsilon_1 = 1 - exp\left[-k_{1,D}Q^{-2/3}\right] \qquad \text{Equation 3.15}$$

$$\varepsilon_2 = 1 - exp\left[-k_{2,I}Q\right] \qquad \text{Equation 3.16}$$

$$\varepsilon_3 = 1 - exp\left[-k_{3,I}Q\right] \qquad \text{Equation 3.17}$$

This assumption is valid for the E_2 and E_3 size bins due to the large diameter of particles (>1μm). The filtration efficiency of particles in the ε_1 size range (0.3-1 μm) is likely to depend on diffusion and one or both of interception and impaction; such effects are not fully captured by the simplification used above. A more accurate representation of the dependence of E_1 on flow rate could be achieved by also accounting for the effects of capture by impaction and interception. This would require knowledge of the filtration efficiency at flow rates other than the standard test at 0.94 m^3/s. For the purposes of this model the simplification has been used to prevent the need for additional filter testing beyond the ASHRAE standard tests. Capture of particles smaller than those tested in ASHRAE 52.2 are dominated by diffusion mechanisms due to the small particle diameter (<0.3 μm).

A relation for filter efficiency as a function of airflow rate through a 600 mm by 600 mm filter can be derived from ASHRAE 52.2 test results providing the filtration efficiency of clean filters at 0.94 m^3/s, $\varepsilon_{i@0.94}$. This can be used to determine $k_{i,j}$ to provide a modified version relating to ASHRAE 52.2 test results:

$$\varepsilon_i = 1 - (1 - \varepsilon_{i@0.94})^{D_i} \qquad \text{Equation 3.18}$$

$$D_1 = \left(\frac{0.94}{Q}\right)^{2/3} \qquad \text{Equation 3.19}$$

$$D_2 = D_3 = \left(\frac{Q}{0.94}\right) \qquad \text{Equation 3.20}$$

where D_i are functions determined based on the dominant capture mechanism which is a function of particle size. The effect of airflow rate on filtration efficiency can be significant, as shown for a sample commercial filter in Figure 3.4.

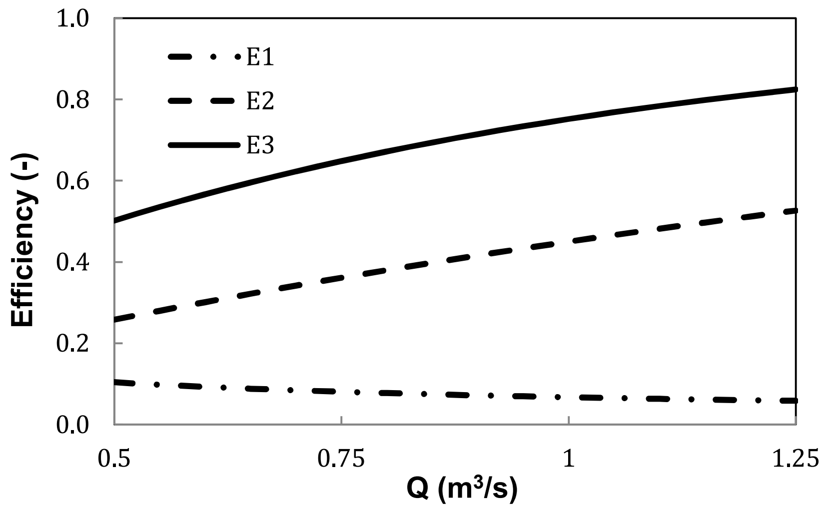

Figure 3.4: Sample filter efficiency as a function of airflow rate for particles in the ASHRAE size bins through a 600mm x 600mm MERV 8 filter.

3.2.3 Calculating Filter Cost

The equations derived for filter pressure drop and efficiency in Sections 3.2.1 and 3.2.2 allow for complete characterization of the air filter throughout its operation lifetime. This can then be used to determine the operation cost of the filtration system.

The annual cost of operating a filter depends on the energy use, installation and disposal costs, and time between filter changes. The equation for annual operation cost is:

$$C_A = 8.76 W_{ave} \$_E + C_L + C_F \quad \text{Equation 3.21}$$

$$C_F = \$_F \frac{31536000}{t} \quad \text{Equation 3.22}$$

$$C_L = \$_L \frac{31536000}{t} \quad \text{Equation 3.23}$$

where C_A is the total annual cost (USD/yr); C_L is the annual installation and disposal cost (USD/yr); C_F is the annual filters cost (USD/yr); $\$_F$ is the price per filter (USD/filter); $\$_L$ is the price of installation and disposal per filter change (USD/filter); $\$_E$ is the price of electricity (USD/kWh); t is the operation time between filter changes (seconds); 8.76 is a conversion factor derived from 8,760 hours in a year; and 31,536,000 is the number of seconds in a year.

The average power can be determined based on the system operation conditions using Equation 3.2. As a simplifying approach the system flow can be approximated as the average flow rate throughout the lifetime of the filter operation. The average power consumption then becomes:

$$W_{ave} = \frac{Q^d}{\eta_s \eta_o t \sum \varepsilon_i C_i} \frac{a}{b} [exp(bQ\eta_o t \sum \varepsilon_i C_i) - 1] \qquad \text{Equation 3.24}$$

where W_{ave} is average power (Watts); η_s is the fan system efficiency; η_o is the fraction of the year that the system is operating; C_i is the particle mass concentration in the air stream incident on the filter in the size bins i (g/m^3); and all other variables are as described above.

3.3 Model Validation

3.3.1 Methodology

The air filter pressure drop and energy use model was validated in two steps. First, the theoretical pressure drop was compared to laboratory measurements from Rivers and Murphy [28] and a subset of commercial filter data provided for consideration by the Vancouver Airport Authority to determine typical model error. The model was then compared to full-scale field experiments for a selection of air filter combinations to compare predicted and actual energy required to operate air filters in a real system.

3.3.1.1 Laboratory Experiments

The data used for the laboratory experimental validation was collected by Rivers and Murphy [28] to determine air filter operation characteristics in a variable air volume system. The experimental data was collected by a means similar to ASHRAE 52.2 testing. Full size air filters (600 mm x 600 mm) were tested to determine the pressure drop versus flow rate for a clean filter for flow from 0.47m^3/s to 1.18m^3/s. The filters were then loaded at a constant flow rate of 0.94 m^3/s to determine the relation for pressure drop versus dust load to a final pressure of approximately 375 Pa (dust holding capacity test) for MERV 13 and 14 filters and 250 Pa for filters of MERV 12 and under. The filter was then tested to determine the pressure drop versus flow rate for a loaded filter for flow from 0.47 m^3/s to 1.18 m^3/s.

The filter model parameters *a*, *b*, and *d* were determined using the results available from typical ASHRAE 52.2 testing. This includes fitting curves to the pressure drop versus flow through a clean filter and pressure drop versus dust loading at 0.94 m^3/s. The model was then used to predict the pressure drop versus flow for clean and loaded filters as well as the pressure drop during dust loading. The pressure drop versus flow for the loaded filter is not used in the model derivation and typically not available from manufacturers' data and therefore represents an independent dataset for comparison of the theoretical and experimental work. The error associated with using the model to predict air filter pressure drop compared to the experimental results was determined and discussed below.

3.3.1.2 Field Experiments

3.3.1.2.1 Experimental Set-up

The air filter field experiments compared predicted versus actual energy consumption of 6 filter installations in 6 different air-handling units all serving an airport terminal. The air-handling units were chosen to have similar capacities, serve the same space, and operate with similar controls protocols on a 24hr schedule. The filters to be tested were chosen to represent existing air filter conditions at the airport (a 50 mm thick MERV 8 pleated prefilter, and a 300 mm thick MERV 13 box filter) and filters previously estimated to be more energy efficient using the air filter energy model [129]. The study included Box and V-type filters from 4 different manufacturers and tests operation with and without a prefilter. Table 3.1 shows the filter and air handling unit information for the experimental validation.

Table 3.1: Filter information for field experiments

Filter Manufacturer	AHU	$N_{Filters}$ [a]	Average Flow (m^3/s)	Prefilter MERV	Prefilter a	Prefilter b	Prefilter d	Final Filter Label	Final Filter Type	Final Filter MERV	Final Filter a	Final Filter b	Final Filter d
A	21	10.5	0.71	8	90.1	0.006	1.575	I	V	13	77.1	0.005	1.383
A	22	7.5	0.64		N/A			I	V	13	77.1	0.005	1.383
A	23	10.5	0.64	8	90.1	0.006	1.575	II	Box	13	131	0.006	1.49
B	25	6	0.8		N/A			III	V	13	101.8	0.004	1.395
C	26	6	0.85		N/A			IV	V	13	63.9	0.005	1.587
D	27	7.5	0.56		N/A			V	V	14	75	0.003	1.92

a - $N_{filters}$ indicates the number of 600mm x 600mm filters in the AHU filter bank. 300mm x 600mm filters are counted as 0.5 filters.

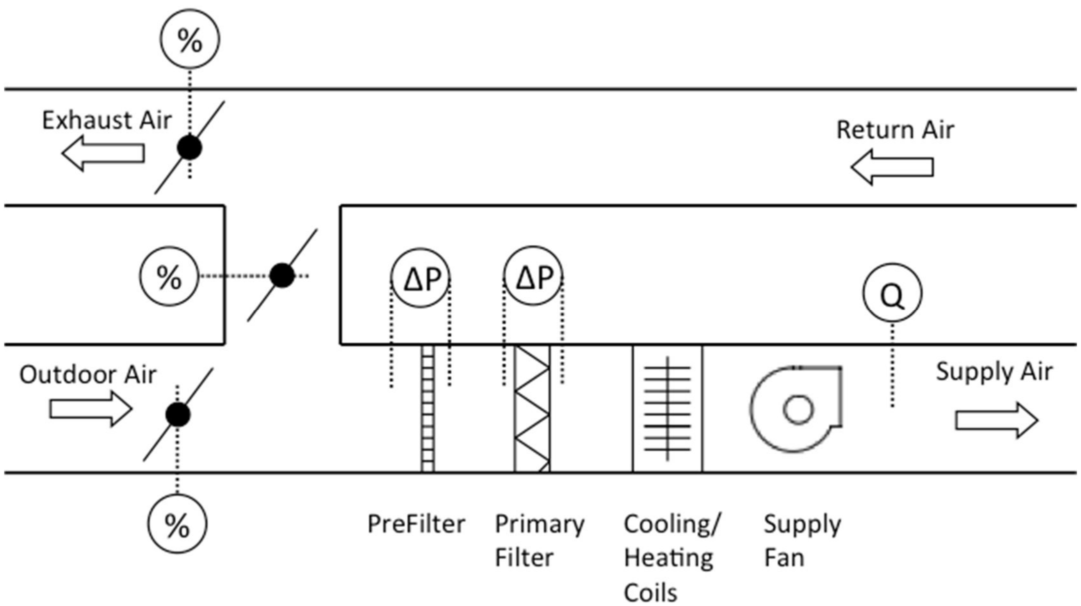

Figure 3.5: Schematic of field experimental set-up for model validation

The air-handling system operates with variable-air-volume controls to meet the ventilation and temperature demands of the airport terminal. Each air-handling unit has similar controls features but operates independently to supply air to different zones. The system controls and operation were not modified for this experiment to ensure the validation was performed for real system operation. The building automation system is used to record filter pressure drop and damper conditions for use in experimental calculations. The building automation system had been recently upgraded and calibrated. The pressure measurements were verified using handheld pressure transducers. The damper positions were not calibrated again as part of this experiment and introduce uncertainty in to the results. Hot wire anemometers were used to determine instantaneous airflow rate in each air handling unit supply air ductwork following the procedure of a duct traverse test outlined by ASHRAE [130] and then converted to flow through the filter bank based on relative cross sectional areas. The data was recorded at 5-minute intervals for the duration of the experiment. A schematic of the experimental set-up for field measurements is shown in Figure 3.5.

3.3.1.2.2 Comparison with Theory

The theoretical predictions for filter energy use can be compared with the experimentally measured energy required to pass flow through the filters. The comparison requires a single common measurement of flow velocity in each AHU supply duct using the hotwire anemometers as a means of determining system conditions. The flow measurement is then used in the model to predict pressure drop, filter loading, and energy use. The experimental calculation uses the same measured airflow along with measured filter pressure drop to calculate energy consumption.

The volume flow rate through each filter can be determined for each air-handling unit by:

$$Q_{filter} = \frac{V_{duct} A_{duct}}{N_{filters}} \qquad \text{Equation 3.25}$$

where Q_{filter} is the volume flow rate through each filter in the filter bank of the AHU (m^3/s); V_{duct} is the average velocity determined from hotwire anemometer in the supply air duct of the AHU (m/s); A_{duct} is the duct cross sectional areas in the supply duct of the AHU (m^2); and $N_{filters}$ is the number of filters in the filter bank of the AHU.

The experimental filter flow power use during each 5-minute time interval and the cumulative flow filter energy consumption can then be determined by:

$$W_{exp,j} = P_{exp,j} Q_{filter,j} \qquad \text{Equation 3.26}$$

$$E_{exp} = \sum W_{exp,j} \Delta t_j \qquad \text{Equation 3.27}$$

where $W_{exp,j}$ is the experimentally determined instantaneous power required (watts); $P_{exp,j}$ is the instantaneous pressure drop across the filter bank (Pa); $Q_{filter,j}$ is the volume flow rate through each filter (m^3/s); E_{exp} is the experimentally determined cumulative energy use required by each filter (J); Δt_j is the time interval (s) for time step j.

The calculations above allow for comparison of flow power only and are not measurements of the electrical power consumption within the units.

The mass accumulation in the air filters must be estimated in order to determine the theoretical filter power and energy. The hourly average outdoor particle concentrations in the PM_{10} and $PM_{2.5}$ size ranges were obtained from a regional PM monitoring site located at the airport [131]. Indoor particle concentrations were determined by typical indoor-to-outdoor particle concentration ratios [19] for the E_1, E_2, and E_3 size ranges [67] and are 1.2, 0.9, and 0.6, respectively. These values have been measured in residences and are not necessarily applicable to an airport application. Measurements of $PM_{2.5}$ I/O ratios within retail spaces have shown similar values and attest to the significant variability[132]. Future studies can be improved with specific measurement of indoor and outdoor concentrations in the space. The concentrations in the three ASHRAE size bins for each air-handling unit were then estimated by:

$$C_1 = \frac{3}{5}(1.2)(1 - f_{OA})PM_{2.5} + \frac{3}{5} f_{OA} PM_{2.5} \qquad \text{Equation 3.28}$$

$$C_2 = \frac{2}{5}(0.9)(1 - f_{OA})PM_{2.5} + \frac{2}{5} f_{OA} PM_{2.5} \qquad \text{Equation 3.29}$$

$$C_3 = (1.2)(1 - f_{OA})(PM_{10} - PM_{2.5}) + f_{OA}(PM_{10} - PM_{2.5}) \qquad \text{Equation 3.30}$$

where C_i is the concentration of particles in the air stream incident on the filters in size bin i ($\mu g/m^3$); 3/5 is the fraction of $PM_{2.5}$ which is assumed to consist of PM_1; f_{OA} (-) is the fraction of outdoor air (-) determined using the Building Automation System (BAS). The subscripts 1, 2, and 3 represent the three particle size bins for ASHRAE filter testing

[67]; size bin 1 between 0.3-1μm, size bin 2 between 1-3μm, and size bin 3 between 3-10μm. For primary filters installed downstream of a prefilter the concentration reaching the primary filter was determined by accounting for the filtration efficiency of the prefilter.

The theoretical filter accumulated mass, pressure drop, power, and cumulative energy consumption are then determined by:

$$m_j = \sum_0^n C_{i,j}\varepsilon_{i,j}Q_{filter,j}\Delta t_j(10^{-6}) \quad \text{Equation 3.31}$$

$$P_{the,j} = aexp(bm_j)Q_{filter,j}^d \quad \text{Equation 3.32}$$

$$W_{the,j} = P_{the,j}Q_{filter,j} \quad \text{Equation 3.33}$$

$$E_{the} = \sum W_{the,j}\Delta t_j \quad \text{Equation 3.34}$$

where m_j is the mass accumulated (g) in the filter during timestep *j*; $C_{i,j}$ is the mass concentration (μg/m^3) of the particles in in the airstream incident on the filter in size bin *i* during timestep *j*; $\varepsilon_{i,j}$ is the filter efficiency (-) for particles in size bin *i* during timestep *j*; $Q_{filter,j}$ is the flow rate (m^3/s) through each filter during timestep *j*; Δt_j is the time interval (s) for time step *j*; $P_{the,j}$ is the theoretically calculated filter pressure drop (Pa) during timestep *j*; $W_{the,j}$ is the instantaneous filter power required to pass air through the filter in timestep *j*; E_{the} is the theoretically calculated cumulative energy (J) use of each air filter; and *a*, *b*, and *d* are filter constants determined from ASHRAE 52.2 testing.

3.4 Results

3.4.1 Lab Validation

Figure 3.6 shows a typical comparison of model and laboratory experimental results for filter pressure drop versus flow for a clean filter or loaded filter (a) and pressure drop versus dust load during a dust holding capacity test (b). This experimental data can be used to validate the air filter model and determine the model error in predicting pressure drop through a filter for the range of conditions tested by Rivers and Murphy [28].

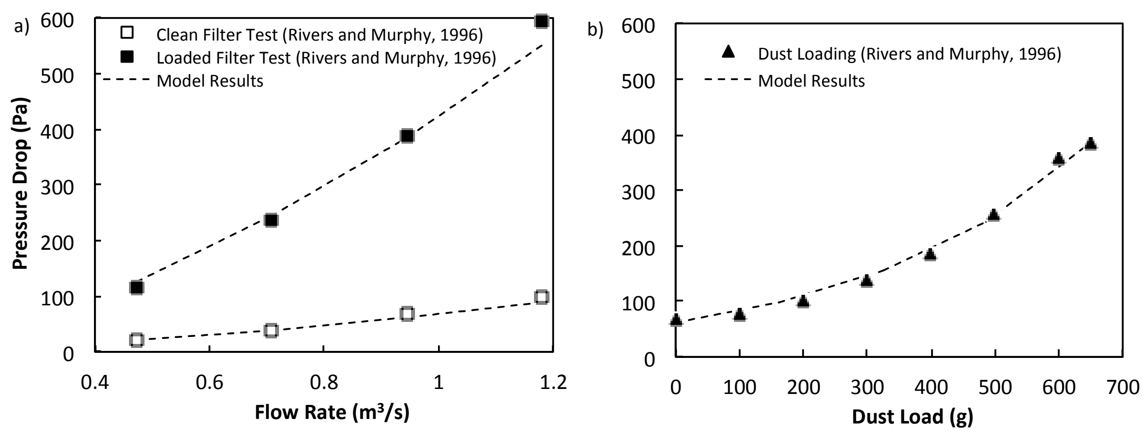

Figure 3.6: Comparison of typical model results with lab experiments of Rivers and Murphy [28] for (a) resistance versus flow rate and (b) resistance versus dust load at 0.94m^3/s.

The comparison of typical model predictions shows good agreement with experimental results for pressure drop versus flow of a clean filter and for the dust loading test as expected as these are used to determine the model constants. The model also shows good agreement with the experimental results for pressure drop versus flow of a loaded filter. No experimental data is available for pressure drop versus flow rate for intermediate levels of filter loading.

Figure 3.7 shows the average error of the model prediction versus the experimental results for resistance versus flow rate of clean (a) and loaded (b) filters. The maximum, minimum and standard deviation of error is also shown for comparison. The model typically predicts the pressure drop to within ±10% for clean and loaded filters. The best results are shown for flow rates between 0.75 m^3/s and 1m^3/s due to the influence of the dust loading test at a flow rate of 0.94 m^3/s on determining model parameters. The model predictions are closer to experimental results for clean filters than for loaded filters. The maximum error for clean filters is +4%/-12% compared to the maximum error for loaded filters of +10%/-19%.

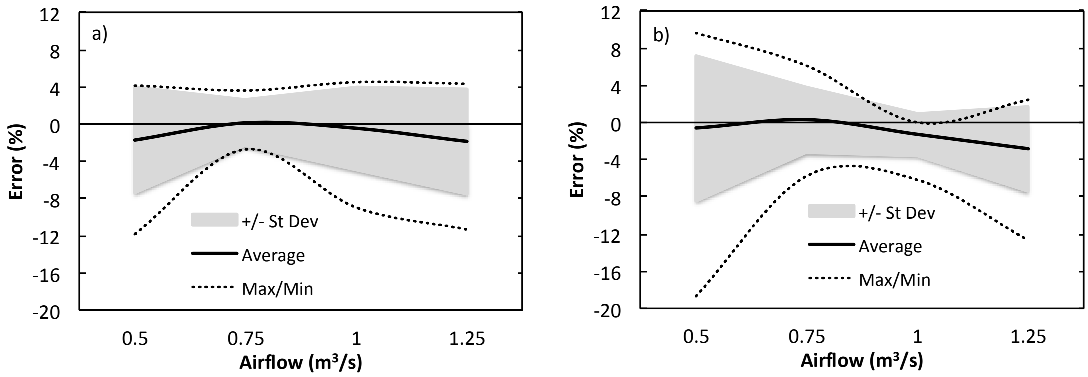

Figure 3.7: Model error versus laboratory testing [28] for predicting filter flow resistance versus flow rate in a) clean and b) loaded filters.

Figure 3.8 shows error in using the model to predict the pressure drop versus dust loading during the dust holding capacity tests at 0.94 m^3/s. The average error varies between 1% and 9% during the loading tests. The maximum error in model prediction of pressure drop during dust loading is +34% and -9%. The model best predicts experimental results for clean or fully loaded filters while overpredicting pressure drop at intermediate values of dust loading. This indicates that the use of an exponential format to relate dust load to pressure drop at a constant flow rate is not a perfect fit. Improvements in model accuracy would be possible with modifications to the equation format but would result in loss of simplicity.

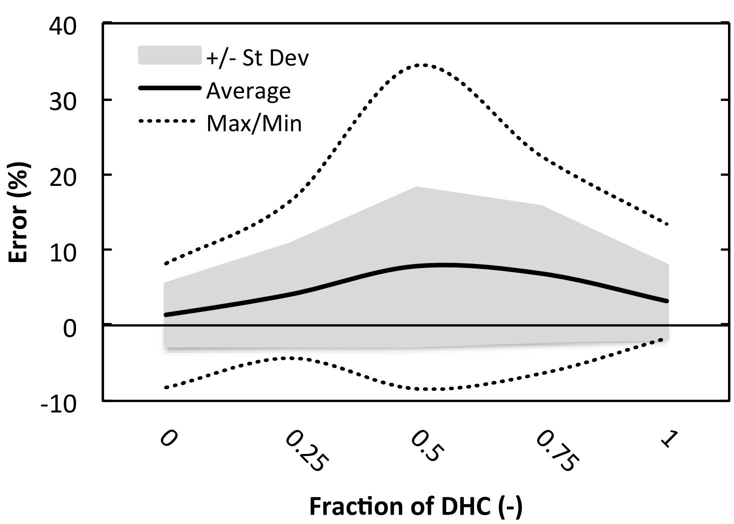

Figure 3.8: Model error versus laboratory testing [28] for predicting filter flow resistance versus dust loading at an airflow rate of 0.94 m^3/s.

The model developed to predict air filter pressure drop under variable flow and loading conditions using data available from typical ASHRAE 52.2 test results shows good agreement with the experimental results from laboratory testing. The model provides the best predictions when filters operate with a face velocity of 0.94 m^3/s (typical design flow) and has greater error as the flow deviates from design conditions. The error in predicting pressure drop for laboratory experiments is ±10% for clean and loaded filters versus flow rate. Model predictions of pressure drop versus dust loading is typically within 16%/-3% of experimental results.

3.4.2 Full-Scale Validation

Laboratory scale validation provides an indication of the ability of the model to capture the air filter operation characteristics over the range of flow and loading conditions tested by standard ASHRAE 52.2 testing. These are highly controlled tests and do not necessarily represent real conditions as the tests are performed on a single filter not a filter bank, are accelerated to be completed in hours instead of months, and use a single dust type instead of the variable conditions seen during real operation. Further model validation has been performed using real HVAC installations with the methods and filters described in Section 3.3.1.2.

Initial model comparisons with experimental results were performed for the six air-handling installations described in Table 3.1 assuming the filter bank was completely sealed and did not allow for any air to bypass the filters. Figure 3.9 shows the error of the model in predicting the cumulative energy use of the filter bank over 14 months of operation.

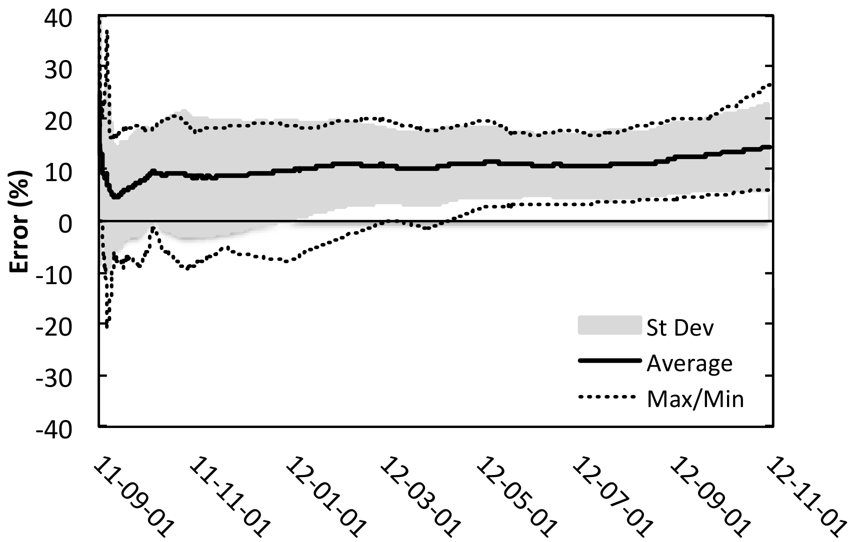

Figure 3.9: Model error in predicting air filter flow energy before bypass correction

The air filters typically show reasonable agreement between the model and the experimental results. The error varies over the duration of the validation period as the model accuracy varies with dust accumulation and operation parameters such as airflow. The average error at the end of 14 months of operation is 14.4% with a typical range of 6% to 23%. The typical error throughout the year of testing was in the range of +25% to -10%. The over-prediction of model energy consumption relative to the experimental measurements indicates that for actual operation the filter pressure drop is lower at a given flow rate than during the ASHRAE tests. One explanation for this behavior is that a portion of the airflow is bypassing the filter and not contributing to the experimental pressure drop. The model can be adjusted to account for this air bypass to reduce model error.

Filter bypass is an important parameter that has been shown to be present in all commercial HVAC filter systems. Bypass is the fraction of air that passes the filter bank through cracks around the filter edges present due to the mounting methods. This air does not pass through the filter media and is therefore not subject to filtration. Typical filter bypass in commercial systems varies widely [133]. A bypass of 10% has been chosen as a representative value and applied to the model for use in predicting the filter energy use.

Figure 3.10 shows the error of the model in predicting the cumulative energy use of primary air filters installed in the study with an assumed 10% filter bypass.

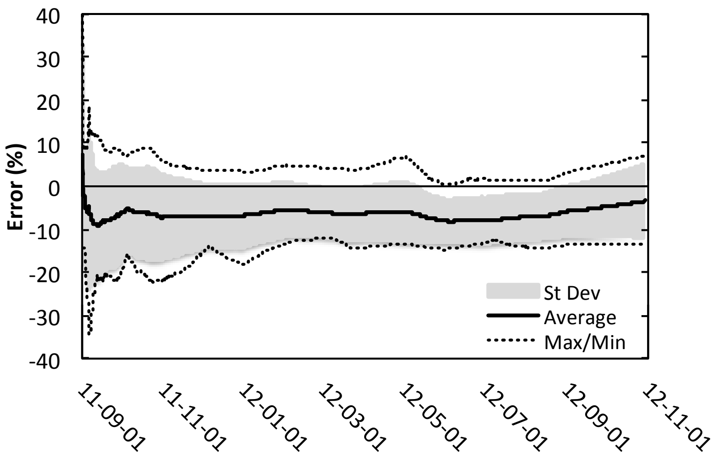

Figure 3.10: Model error in predicting air filter flow energy after 10% bypass correction

The model shows better prediction of experimental results when a standard 10% filter bypass is included in the calculations. The average error in cumulative energy after 14 months of operation is -3.4% with typical error in the range of +5% to -11% The typical error in predicting the cumulative energy use throughout a year of operation is within the range of +5% to -15%. The improvement in overall model accuracy when filter bypass is included indicates that it is an important parameter to consider. The assumption of 10% filter bypass may be an overestimate resulting in a slight under-prediction of the average cumulative energy. Applying a standard 10% filter bypass is an adequate option for model predictions as specific measurement of filter bypass in a given installation is not feasible.

3.5 Discussion

The model predictions of filter pressure drop show good agreement with laboratory experiments for clean and loaded filters. The model is typically within ±10% for all conditions of airflow and loading presented in this work. This good agreement indicates that the model is valid for use in predicting air filter operation. The error resulting from model prediction of cumulative air filter energy use throughout 14 months of operation in real installations is larger than those of the laboratory experiments. The additional error seen in validation with field experiments is a result of the greater variability in conditions for real air handling installations such as filter bypass, variations in flow during loading, different particle characteristics, and uncertainties in filter efficiency.

Filter bypass is minimized in laboratory testing and can vary between real filter installations and type of filter installed resulting in increased model error. The updated model assumes a 10% filter bypass in keeping with representative values from previous works [133]. Filter bypass varies with airflow and dust loading of a filter and is a difficult parameter to predict before filter installation. Model results could be improved with more accurate determination of bypass but would require measurement of each filter installation, which is prohibitive for a model with the purpose of predicting operation before installation and as such a fixed bypass is best used.

The comparison of laboratory testing showed that the model error is greater for operation below the design flow rate of 0.94 m^3/s per filter. The air-handling units used for the field validation operated with airflow below design condition, which would add to error in energy predictions. Field installations can be expected to have closer agreement between model and experimental results when the system operates nearer design flow.

An additional challenge with the model and validation using a field experiment is the uncertainty in accumulated dust. The air filters were not weighed during the experiments as this would result in disturbance in the operation. Dust load was predicted based on outdoor particle concentrations from a local measurement station, typical indoor to outdoor particle concentration ratios, and predicted filter efficiency. This will not reflect the exact concentration of particles in the airstream incident on the air filter, which will lead to error in the model results. Air filter efficiency is a difficult parameter to estimate throughout the lifetime of system operation. The efficiency as a function of particle size bin has been included in the model but adequate representations of the changes in filter efficiency with dust loading have not yet been determined [134]. The model used assumes a constant filter efficiency of the MERV as determined from ASHRAE 52.2 testing for each filter. Fibrous filters that collect particles by mechanical capture mechanisms (no electric charge) have been shown to have increasing collection efficiency with increased dust loading due to the collection efficiency of the particle aggregates within the media. The model will tend to under-predict the filtration efficiency and thus the accumulated mass as the filter operation progresses adding to the model error.

Tighter control of the experimental environment during field-testing would provide for better agreement between the model and experimental results. However, this would not be representative of real air-handling system operations and would more closely resemble a laboratory validation. The agreement between model and experiment of +5% to -20% for predicting the operation of real air handling systems provides confidence in the use of the model to determine impacts of changes to filter system operation.

3.6 Conclusions

An air filter operation model to predict pressure drop and energy consumption was developed and validated using laboratory and field experiments. The model error in predicting filter pressure in a laboratory setting is generally within ±10%. The best agreement is found for clean filters operating at the design flow rate of 0.94 m^3/s per filter. The model error is typically between +25% to -10% when compared to field experiments without a filter bypass correction. The error is reduced to the range of +5% to -20% throughout 14 months of operation when a standard 10% filter bypass is assumed in the model calculations.

The comparison of model prediction with experimental measurement shows that the model is adequate for predicting filter performance over the range of conditions typical of real variable air volume HVAC systems. The model can be used for a number of purposes that previous air filter energy calculation methods could not due to the inability to predict operation through varying flow and loading conditions. The model can be used to compare between air filter selections to determine relative energy efficiency in real operation scenarios to reduce building energy consumption. Optimum system operation and filter operation lifetime can also be determined for individual locations accounting for local particle concentrations, electricity prices, and flow conditions. If combined with existing epidemiological models the new filter model will also allow for a comparison of the impact of system changes on relative cost of operation and occupant benefits from improved indoor air quality.

The filter model validated in this work has a number of limitations that can be improved with further development. Air bypass around the filter installations has been accounted for in the model by assuming a constant ratio of 10% of total flow. Filter bypass varies between installations as well as with increased dust loading due to changes in flow resistance of the filter media. Including bypass characteristics specific to a filter installation or eliminating filter bypass in the field are methods that would allow for more accurate prediction of filter operation and better system performance.

The characteristics of the dust and air conditions throughout the experiment can also add to uncertainty of the model predictions. The ASHRAE 52.2 testing used to characterize the filters and the system conditions (relative humidity, etc.) are fixed. The flow resistance and filtration efficiency of flat samples of filter media are dependent on the properties of the dust captured [104,135] and the relative humidity [115,117]. These conditions are not constant and not controlled throughout the real operation and will likely introduce an unknown level of error in the modeling.

The current model accounts for variation in filter efficiency with changes in flow rate but does not account for changes as the filter loads due to insufficient knowledge on the characteristics of particle loading. Additionally, the model has been limited to filters that remove particles by mechanical capture mechanisms. Electret filter media can be included in future models by accounting for the differences in behavior of pressure drop and filtration efficiency with dust loading through modifications to the base model relationships as required. Additional research is required into the impacts or particle loading on electret filters before sufficient data is available to allow for model predictions.

4 Understanding Air Filter Operation Costs[2]

4.1 Introduction

The studies to date comparing the costs of air filter system operation have utilized simplified models that do not account for variation in flow conditions, particle concentration, or system operation time [74,81,92]. The results have been limited with respect to the ability to compare between the operating cost and energy consumption of different filter selection within the same system or the appropriate operating conditions to optimize the annual operation cost. As building owners and operators focus more on reducing system costs a need for a comparison method has emerged.

The model developed in the previous chapter can be used to perform cost comparisons between different types of filters or different system configurations. This is the first model developed that incorporates the variables associated with both filter and system temporal variations allowing for a comparison of filter performance under different operation contexts. The model was used in this chapter to develop an understanding of filter operation cost and energy consumption in HVAC systems. The analysis was conducted using a filter retrofit at the Vancouver International Airport as a case study to highlight the model use to facility operators in making decisions regarding filter and system choices. The annual operation cost and energy consumption was determined for a number of air filter combinations that meet filtration efficiency requirements at the airport to inform future filter selection. A study of the role of filter and system parameters on annual operation cost was also performed to extend the relevance of the investigation to installations in other locations with varied conditions.

The model use is applicable for comparison of any filter types or system changes. The results from this study can be used by other building operators to inform system changes

---

[2] Content from this chapter has been published. Montgomery, J. F., Green, S. I., Rogak, S. N., & Bartlett, K. (2012). Predicting the energy use and operation cost of HVAC air filters. Energy & Buildings, 47, 643–650.

to reduce cost. Indoor air quality and occupant health impacts can be included in future expansions of the model to compare operation costs with benefits to occupants.

4.2 Model

The Vancouver Airport Authority has used the filter model developed in the previous chapter to inform the purchase, installation, and operation of the air filtration system at the Vancouver International Airport. The specific operation parameters of the air handling system for which the model was to be applied were stipulated in discussion with the operations personnel at the airport. The results of this study are specific to the airport operations but the general trends and the procedure are applicable for all installations. The parameters were varied in Section 4.3.3 to develop a deeper understanding of the potential outcomes for systems that operate in a similar manner but are subject to different cost and operation characteristics.

A summary of the properties of air filters considered for the YVR air filter study are shown in Table 4.1. The filter MERV and manufacturers were limited based on specifications of system operation at the airport. The filtration efficiency, MERV, DHC, and initial flow resistance of each filter were determined in accordance with ASHRAE 52.2-2012 testing methods [67]. The model variables, a, b, and d, were determined using the equations developed in Chapter 3. The filter price was determined from the bid submissions from filter suppliers. These prices do not necessarily reflect the standard commercial sale price due to the potential for economy of scale in selling to and dealing with an entity such as the airport but are none-the-less useful for investigation of the potential of the model. An investigation of the effect of filter price variation is performed in Section 4.3.3.3.

Table 4.1: Properties of filters considered for the YVR air filter study

Filter No.	Manufacturer	Filter Type	E1 (-)	E2 (-)	E3 (-)	MERV	DHC (g)	Initial Resistance (Pa)	Model variables			Price (CAD)
									a	b	d	
1	A	2" Pre	0.13	0.57	0.80	8	106	65	73.0	0.016	1.62	5.0
2	A	4" Pre	0.13	0.65	0.85	8	238	65	55.2	0.007	1.84	9.0
3	A	Box	0.87	0.98	0.99	15	192	155	170.1	0.005	1.50	81.6
4	A	Box	0.61	0.95	1.00	13	269	157.5	172.8	0.003	1.50	64.8
5	A	Bag	0.89	0.98	1.00	15	605	92.5	102.7	0.002	1.55	23.7
6	A	V	0.65	0.87	0.99	13	352	90	101.8	0.004	1.39	110.1
7	B	2" Pre	0.15	0.50	0.75	8	104	82.5	87.7	0.011	1.36	6.6
8	B	Box	0.82	0.95	0.98	14	220	162.5	160.4	0.004	1.48	38.3
9	B	Bag	0.90	0.97	0.99	15	308	102.5	128.0	0.004	1.11	26.8
10	B	V	0.72	0.92	0.99	13	340	55	63.9	0.005	1.59	122.1
11	C	2" Pre	0.07	0.43	0.73	8	179	80	90.1	0.006	1.58	4.0
12	C	4" Pre	0.08	0.47	0.75	8	156	75	84.3	0.008	1.74	6.6
13	C	Box	0.61	0.93	1.00	13	195	115	131.0	0.006	1.49	85.0
14	C	Bag	0.79	0.99	1.00	13	288	127.5	138.1	0.004	1.10	22.2
15	C	V	0.61	0.90	0.99	13	350	70	77.1	0.005	1.38	49.4
16	D	4" Pre	0.25	0.60	0.80	8	286	55	54.2	0.006	1.23	7.2
17	D	Box	0.61	0.95	1.00	13	402	135	122.7	0.003	1.59	48.5
18	D	Bag	0.61	0.95	1.00	13	295	75	82.8	0.006	1.59	19.3
19	D	V	0.80	0.95	1.00	14	670	67.5	75.0	0.003	1.92	79.0
20	E	2" Pre	0.10	0.49	0.80	8	97	47.5	53.7	0.017	1.64	7.0
21	E	2" Pre	0.11	0.57	0.76	8	165	47.5	53.4	0.010	1.48	7.0
22	E	4" Pre	0.04	0.41	0.79	8	184	30	34.1	0.011	1.57	7.0
23	E	Bag	0.86	0.98	1.00	15	356	120	135.5	0.003	1.41	45.0
24	E	V	0.76	0.96	0.98	14	300	90	108.6	0.005	1.59	150.0

Filter installation and disposal price is related to filter size and time spent carrying them to and from the air-handling units as well as disposal costs. Arnold et al. [74] provide estimates for installation and disposal prices of filter change-out based on standard 600 mm x 600 mm filters of various types. The installation and disposal prices used are 0.36 CAD for prefilters, 2.43 CAD for bag filters, and 4.73 CAD for Box and V-type filters. Filter installation and disposal costs are functions of the labour wages and size of air handling units. Since filter installation and disposal cost is typically a very small fraction of the annual filter cost, the associated errors will have minimal effect on the overall outcome of this study.

The constant air flow rate through each 600 mm x 600 mm filter was assumed to be 0.94 m^3/s (2000 CFM), corresponding to a face velocity of 2.54 m/s (500 fpm), which is the typical filter design speed and the system design rating at the airport. The air stream passing through the filters was assumed to be comprised of 30% outdoor air and 70% indoor air for the purpose of determining particle concentration. This is the minimum outdoor air set-point for the airport air handling system. The fan system efficiency (η) was assumed to be 0.55 based on efficiency rating of the equipment specifications at airport. The efficiency was determined based on as-built equipment installations and measurement and balancing reports. Variability of fan system efficiency is expected throughout operation but is not expected to have a significant impact on the results (see Section 4.3.3.1). The price of electricity ($\$_E$) was assumed to be 0.04 CAD/kWh, a value typical for the airport operations but not representative of a standard commercial consumer in Vancouver.

In order to estimate the rate of dust accumulation in the air filters a typical aerosol concentration in the airstream of the important size ranges was required. Average daily values of PM_{10} and $PM_{2.5}$ in outdoor air at the Vancouver International Airport are documented by the B.C. Ministry of Environment [131]. These values were used to determine the outdoor air concentration of particles in the E_3 (3-10 μm) and E_2 (1-3 μm) size range as 7 μg/m^3 and 2 μg/m^3, respectively. Using information from ongoing measurements of $PM_{2.5}$ and $PM_{1.0}$, the outdoor air concentration of particles in the E_1 size range (0.3-1 μm) was predicted to be 3 μg/m^3. Indoor particle concentrations were determined by typical indoor-to-outdoor particle concentrations ratios [19] for the E_1, E_2, and E_3 size ranges and are 1.2, 0.9, and 0.6, respectively. Using this information regarding particle concentrations and the assumption of 30% outdoor air, the final particle concentration in the air stream incident on the filters for E_1, E_2, and E_3 size ranges was calculated to be 3.4, 1.9, and 5.0μg/m^3, respectively. The filtration efficiency used for each size bin is the efficiency used in determining the MERV as calculated from ASHRAE 52.2-2012 test methods. The filter's rated final resistance is 250 Pa (1" w.g.) for all prefilters and 375 Pa (1.5" w.g.) for all primary filters. The Dust Holding Capacity is the amount of accumulated dust in the filter at the designated final resistance.

4.3 Results and Discussion

4.3.1 Model Results

For each filter, the power required and annual filter costs were calculated for a range of operation times. The operation time is defined as the time since the last filter change. The air-handling system is assumed to operate 24hrs per day (as per airport scheduling). The Time to DHC, which is defined as the operation time to filter rated final resistance, has also been calculated. These results were then used to determine the minimum annual cost of filter operation. An example of the data obtained is shown in Figure 4.1.

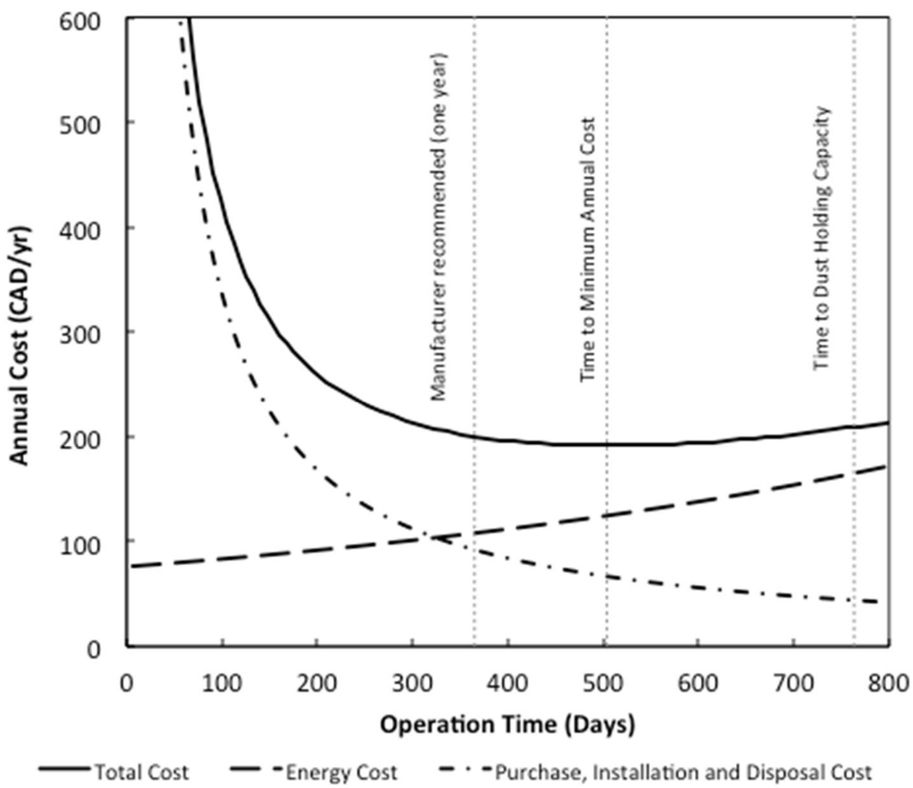

Figure 4.1: Sample filter model result

As shown in Figure 4.1, the total annual filter cost is the capital cost (annualized) of the filter purchase, installation, and disposal, plus the flow power cost. When plotted as a function of filter operation time (the time period between filter changes), the capital cost decreases hyperbolically whereas the energy cost increases exponentially owing to dust accumulation. As a result, the total annual filter cost is “U” shaped, with a minimum at a particular operation time that does not necessarily correspond with the manufacturer’s recommended changeout frequency (typically 6 months for prefilters or one year for primary filters).

A summary of the filter performance, determined using the model and filter data from ASHRAE 52.2-2012 test results is presented in Table 4.2. The data presented in Table 4.2 is for the performance of each filter installed alone in the air handling system. The cost of operation of a prefilter and primary filter in the air handling system was also calculated for comparison in Section 4.3.3.2. The cost of prefilter used is that of the least costly prefilter option from the manufacturer of the given primary filter (determined from the results of Table 4.2). Mixing of prefilters and primary filters between manufacturers was avoided to simplify the results and because it is standard practice to purchase prefilters and primary filters from the same source. The results of the filter model developed in this work are based on optimizing the operation time to achieve minimum annual operating cost.

Table 4.2: Summary of data for all filters installed with no filter upstream

Filter No.	Filter Type	MERV	Time to DHC (days)	Annual Cost at Final Resistance (CAD)	Minimum Annual Cost (CAD)	Operation Time To Minimum Cost (days)	Minimum Annual Cost with Prefilter (CAD)
1	2" Pre	8	235.3	117.9	91.3	116.1	N/A
2	4" Pre	8	492.4	84.7	65.7	239.2	N/A
3	Box	15	241.0	280.8	275.3	293.8	278.0
4	Box	13	371.5	222.2	221.8	349.8	240.6
5	Bag	15	750.3	133.8	108.0	357.9	156.7
6	V	13	489.8	207.8	207.1	457.8	215.2
7	2" Pre	8	243.8	105.1	96.2	151.1	N/A
8	Box	14	284.0	201.7	199.9	245.9	258.0
9	Bag	15	383.2	164.5	152.6	250.9	222.1
10	V	13	455.8	203.9	203.2	428.9	234.2
11	2" Pre	8	466.5	99.0	78.9	190.3	N/A
12	4" Pre	8	389.2	98.6	83.1	193.8	N/A
14	Bag	13	369.1	166.5	153.2	231.2	263.8
14	Box	13	270.5	257.1	256.0	294.4	206.3
15	V	13	491.4	146.0	136.0	353.8	179.2
16	4" Pre	8	584.8	81.2	60.1	253.4	N/A
17	Box	13	555.2	166.1	155.7	383.1	183.0
18	Bag	13	407.4	135.7	111.9	225.1	147.2
19	V	14	862.5	143.4	128.7	578.9	157.1
20	2" Pre	8	225.7	92.8	80.5	138.5	N/A
21	2" Pre	8	342.9	78.8	67.1	193.2	N/A
22	4" Pre	8	463.5	73.4	51.0	219.7	N/A
23	Bag	15	445.9	179.4	171.8	327.6	189.9
24	V	14	395.2	269.5	267.6	436.2	241.0

Figure 4.2 compares the operation life-time of the filter as determined by the Wattage model and the model developed in this work. The long operation lengths seen are in part due to the extremely low particle concentration in the air, typical of the Vancouver area, and would be shorter for locations with higher aerosol concentrations. The operation time for the Wattage method is the operation time to reach the dust holding capacity of the filter based on calculations using the MERV and the aerosol concentration in this work.

The operation time to minimum annual cost is the recommended change-out period as determined using the new model.

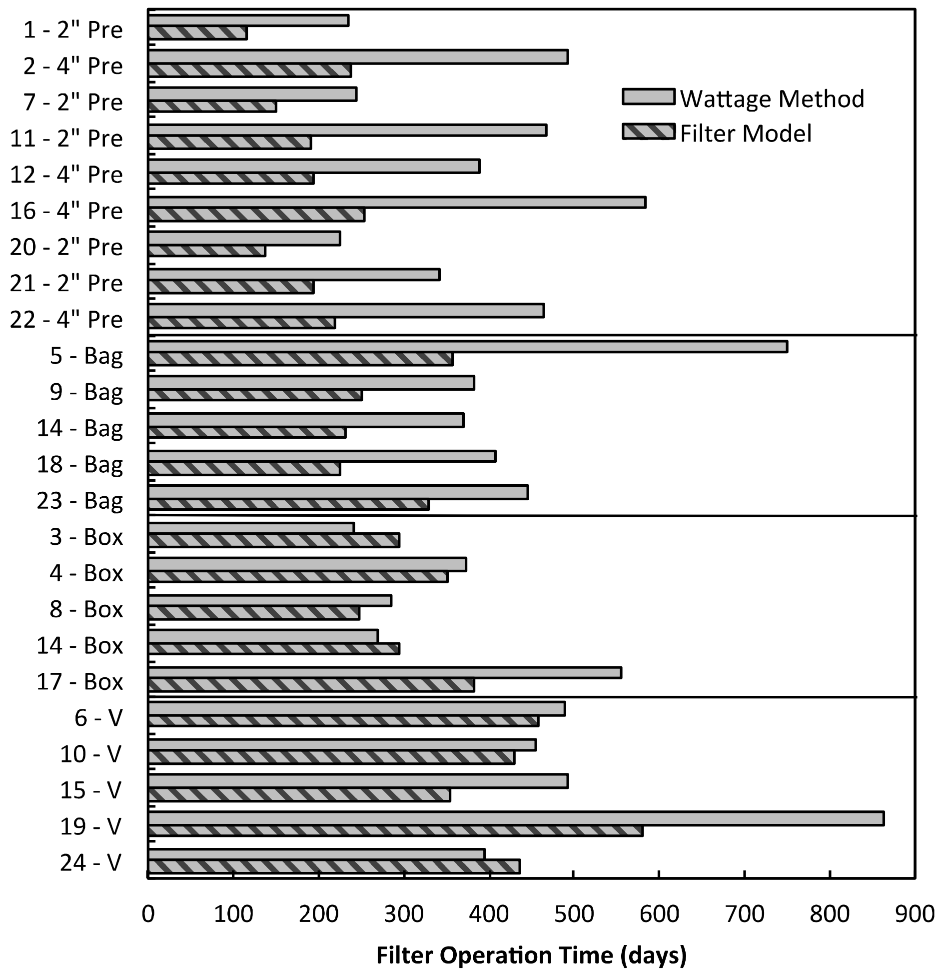

Figure 4.2: Comparison of the filter operation time as determined using the new and previous cost model

The filter life expectancy varies greatly between filters and provides an indication of the desired length of time between filter changes. The operation Time to Dust Holding Capacity is in the range 6-16 months for prefilters, 1-2 years for primary filters without a prefilter, and 2-3 years for a primary filter with a prefilter. The Operation Time to Minimum Annual Cost is typically 6-9 months for prefilters, 0.75-2 years for primary filters without a prefilter, and 1-2 years for a primary filter with a prefilter. A comparison between the operating life of prefilters shows that 100 mm (4”) prefilters do not necessarily last longer than 50 mm (2”) prefilters. The Time to DHC shows that V-type filters last the longest in general, followed by Bag and then Box type filters. The Operation Time to Minimum Cost also shows that V-type filters can operate for the longest followed by Bag and Box type filters showing similar operation times. Therefore the filters that would be expected to last the longest in a system are the V-type.

The best practice would be to set alarms on the filter pressure data from the building automation system for a pressure associated with the Operation Time to Minimum Annual Cost and provide filter changing within a predetermined timeframe from that point. Operating the filter for time periods greatly longer or shorter than this can significantly increase the cost of filter operation. The significant difference between filter life expectancy as determined by minimizing for cost versus operation to dust holding capacity shows the potential for significant savings if system length is based on cost reduction measures.

The average power consumption of the filters over the operation lifetime is shown in Figure 4.3. The power used in the Wattage model is a simple average of the initial resistance and the resistance at Dust Holding Capacity. It does not represent actual predicted power requirement but is rather a means of comparing hypothetical filter power. The power determined using the filter model developed in this work is the average power of the filter for operation to minimum annual cost.

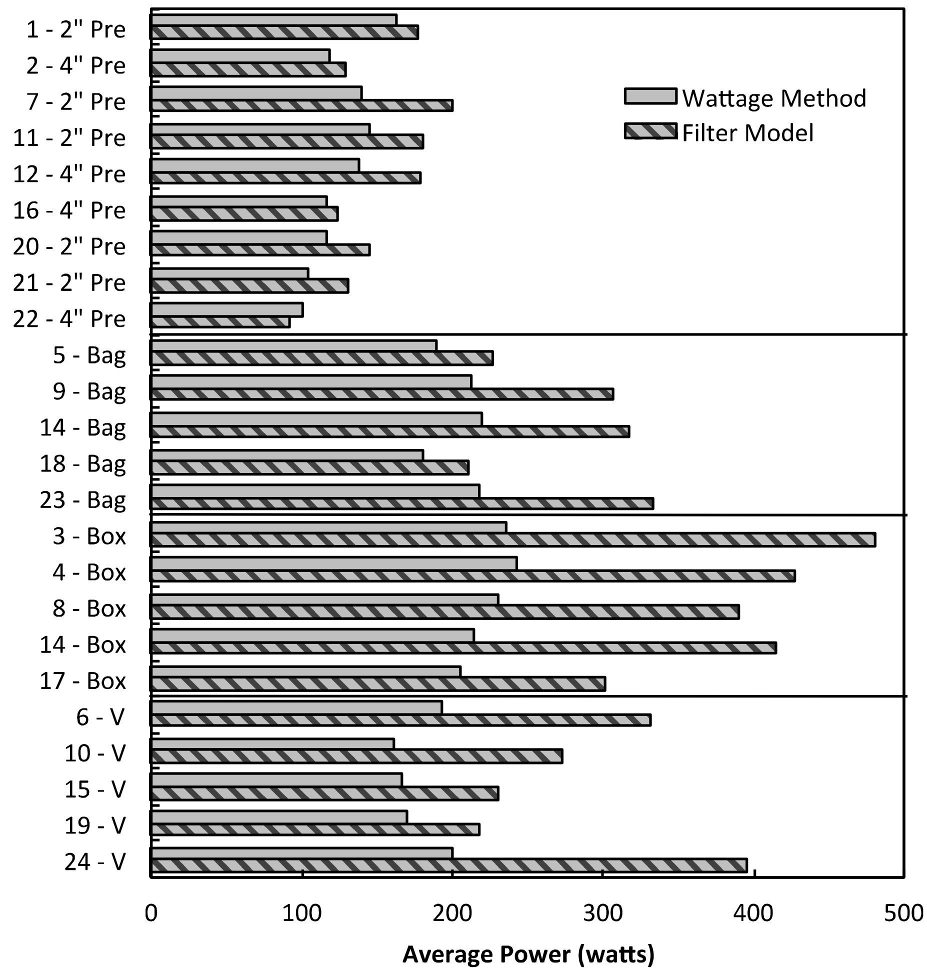

Figure 4.3: Comparison of the average filter power as determined using the new and previous cost model. Note: The Wattage method only provides for calculation of a single power for the filter and does not represent potential actual filter power requirements.

Of the primary filters investigated, the average power required for operation to minimum cost is lowest for V-type filters and bag filters which have a typical range of approximately 200-400 watts while box filters have a higher power requirement of approximately 300-500 watts. V-type filters generally have a slightly lower power requirement than bag filters. The power requirement of prefilters is in the range of 100-200 watts and no general distinction is seen between the average power required for 50 mm (2”) and 100 mm (4”) prefilters. From the standpoint of operation energy use, V-type filters are the most energy efficient filter type to install. It is also more energy efficient to install a primary filter without a prefilter given the conditions assumed in this study. Values of model parameters, such as filter purchase price, electricity price, aerosol concentration, etc., for specific installations must be considered when determining the most cost effective filtration solution.

Figure 4.4 compares the annual cost of operating an air filter when determined using the Wattage and the new filter model. The Wattage method determines filter cost when it is allowed to operate until Dust Holding Capacity is reached (at a resistance of 250 Pa for prefilters and 375 Pa for primary filters). The Minimum Annual Cost is determined using the new filter model by calculating the annual cost of operation for the range of possible filter resistances and then determining the minimum value. The two costs typically differ by a small amount but in some cases the Minimum Annual Cost is significantly lower.

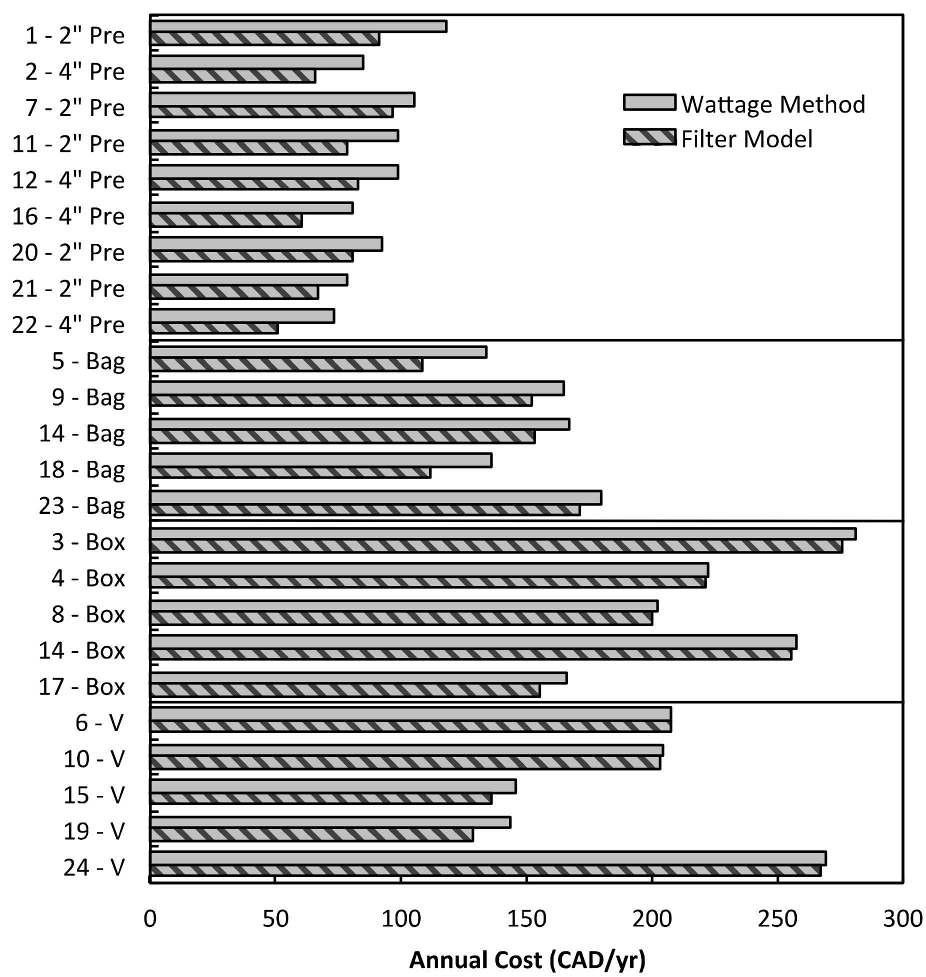

Figure 4.4: Comparison of the annual operation cost as determined using the new and previous cost model

The Minimum Annual Cost of operating a primary filter without an associated prefilter is within the range of 100-300 CAD. The least costly option is a bag filter (100-175 CAD) followed by V-type (125-275 CAD) and Box (150-275 CAD) filters. If a prefilter is installed upstream of the primary filter, the cost of operating the system is increased in the case of most filters, typically by approximately 20% though there is considerable variability. The annual cost of operating a prefilter alone is typically in the range of 50-100 CAD. No general trend regarding cost versus thickness of prefilter has been shown. Installing a prefilter upstream of a primary filter acts to protect the more expensive primary filter. If the installation is deemed to be safe for a primary filter alone then there is potential for cost savings in this application, which is characterized by low aerosol concentration and electricity prices.

4.3.2 Comparison with Previous Filter Models

The results obtained using the Filter Energy and Cost Model proposed in this dissertation differ from those of the Quality Factor or Wattage method. The simplest means of representing these differences is by a ranking scheme, the results of which are shown in Table 4.3 for only the primary filters investigated. The new model uses the calculated Minimum Annual Cost to rank filters from least to most costly. The Wattage method uses the average of initial and final power (Wattage) based on operation to DHC from most to least energy efficient. The Quality Factor uses the QF method calculated for the E_1 size bin to rank filters from lowest to highest.

All three methods rank Box filters poorly while Bag and V-type filters are mixed near the top of all ranking schemes. The Wattage method is biased towards V-type filters because it accounts only for the energy use of the filter and not the purchase price or life expectancy of the filter. The QF method is slightly biased towards bag filters and filters with a higher MERV because of the strong influence of filtration efficiency in the calculations. These differences in the calculation methods can also cause significant differences in individual filter ranking. An example of this is Filter No. 15 which is ranked 4th by the model presented here, 2nd using the wattage method due to energy efficiency, and 11th using the QF method due to low filtration efficiency in the E_1 size range.

Table 4.3: Filter rankings by different evaluation methods

Filter No.	Filter Type	MERV	Rank Based on Minimum Annual Cost ($)	Rank Based on Wattage	Rank Based on QF E1
3	Box	15	15	14	4
4	Box	13	12	15	15
5	Bag	15	1	5	2
6	V	13	11	6	10
8	Box	14	9	13	6
9	Bag	15	5	9	1
10	V	13	10	1	9
13	Box	13	13	10	13
14	Bag	13	6	12	7
15	V	13	4	2	11
17	Box	13	7	8	14
18	Bag	13	2	4	12
19	V	14	3	3	5
23	Bag	15	8	11	3
24	V	14	14	7	8

*Only primary filters are included in the comparison of filter rankings
Similar differences in ranking schemes are seen amongst the prefilters

The main cause for the differences in results between the new model and the Wattage method is in accounting for actual filter life. The Wattage method does not incorporate the particle collection efficiency of the filter or the concentration of particulate matter in the air stream. These two factors provide the necessary data to determine how quickly the filter will clog and thus require replacement, which affects the annual cost of operation. Without this information it is not possible to determine the optimized operation time for minimum annual cost.

The QF method produces a number that is useful for crude ranking of filters based on the average flow resistance over the life of the filter and the particle filtration efficiency. This number does not incorporate the concentration of particles in the air stream in determining the QF. There is also no method of converting QF to a dollar value for comparing energy cost or incorporating installation and disposal cost in the comparison method to determine an operation life to achieve minimum cost.

4.3.3 Effect of System Parameters on Annual Cost

The variables used to obtain model predictions in Section 4.3.1 and 4.3.2 are specific for filters used in Vancouver, Canada. These variables, and thus the model results will change depending on the filter installation location. An investigation of the effect of changing the variables used is shown in the following sections. Data for a limited selection of primary filters is shown for the purpose of clarity in the following figures. The analysis and conclusions were drawn from the complete set of primary filters in this study.

4.3.3.1 Effect of Fan System Efficiency (η_s)

The fan system efficiency will change depending on the air-handling unit in which the filter is installed and the operation conditions. Efficiency will also vary throughout the lifetime of filter operation with the changing resistance due to accumulation of mass changing the location on the fan curve at which the unit is operating. These conditions are extremely difficult to predict without investigating the system in question and therefore it is a necessary simplification to assume a single constant efficiency. The selection of this efficiency will change the results of the energy and cost model as shown in Figure 4.5. The fan system efficiency can have a large effect on the annual cost of operating a filter if a large range of efficiencies is investigated such as the difference from 0.4 to 0.9. Typical changes in Minimum Annual Cost for a change in efficiency of ±0.1 from 0.6 are ±40 CAD. This will change the calculated annual cost by ±15% which can make a significant difference in the cost of the system but if the same efficiency is applied to all filters being compared the chosen efficiency value does not change the relative performance.

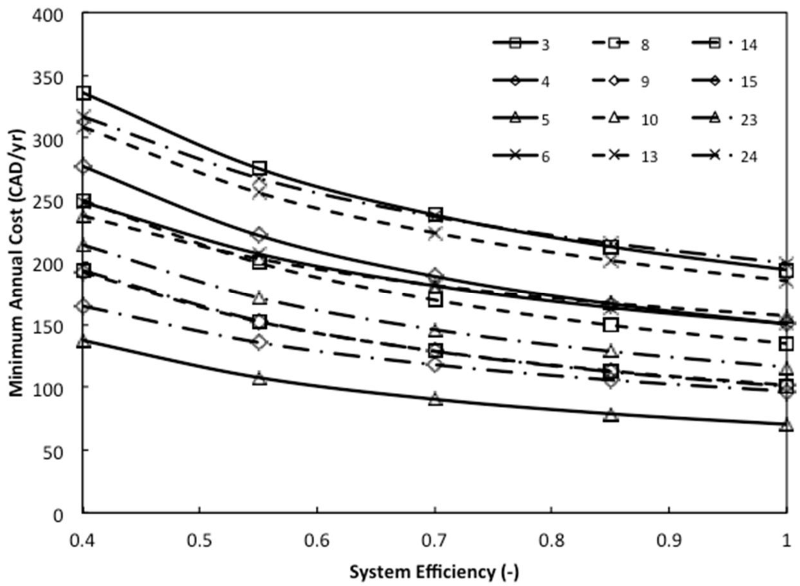

Figure 4.5: Effect of fan system efficiency on Minimum Annual Cost of primary filters installed without prefilters.

4.3.3.2 Effect of Electricity Price ($\$_E$)

Electricity prices vary significantly between countries and regions and will have a large impact on the cost of a filter installation. The base case for this study, 0.04 CAD/kWh representing Vancouver, is amongst the lowest prices worldwide. Figure 4.6 shows changes in the Minimum Annual Cost for a selection of primary filters installed without a prefilter as the assumed price of electricity is increased. Increasing the price of electricity increases the cost of operation for all cases and has the largest impact on filters requiring large flow power to overcome resistance. This increases the economic viability of more expensive, energy efficient filters. This also has the effect of lowering the Operation Time to Minimum Annual Cost. In the case of filters in this study, the higher purchase price of V-type filters is not overcome by assuming an increased price of electricity and bag filters are typically the least costly option even when 0.4 CAD/kWh is assumed, though in a number of cases the Minimum Annual Cost of V-type filters has decreased to the level of associated bag filters.

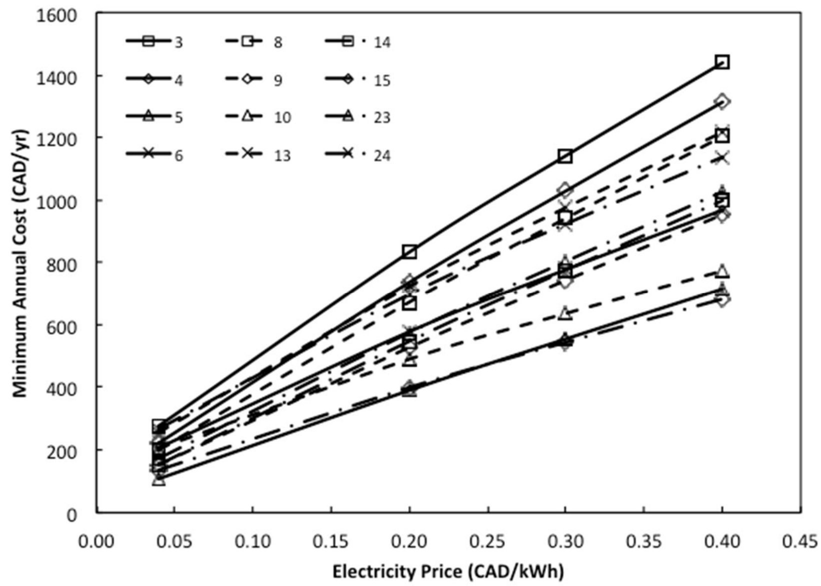

Figure 4.6: Effect of electricity price ($\$_E$) on Minimum Annual Cost of primary filters installed without prefilters

Figure 4.7 shows the difference in Minimum Annual Cost for each primary filter installed with a prefilter versus the primary filter installed alone in the system. The additional cost of a primary filter installed with a prefilter increases as the cost of electricity is increased. This indicates that for installations with high electricity prices the increased cost of added power consumption with a prefilter is not offset by the increase in operation time of the primary filter. For installations where electricity costs are high it becomes increasingly attractive to forego the installation of a prefilter in the filtration system and to rely solely on the primary filter due to the reduced energy consumption.

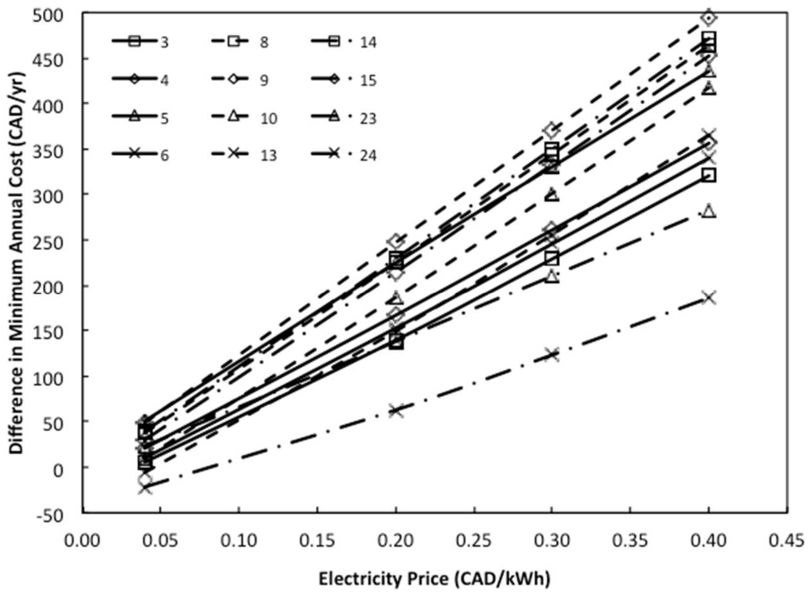

Figure 4.7: Difference in Minimum Annual Cost of a system operating with prefilter and primary filter versus primary filters alone for varying electricity price ($\$_E$)

4.3.3.3 Effect of Filter Price ($\$_F$) and Installation and Disposal Price ($\$_L$)

The cost of installation and disposal is typically shown to be a small percentage of the overall cost of operating an air filter. A four-fold increase in the price of installation and disposal cost increases the annual cost by less than 5% for filters in this study. This increase does not affect relative cost performances of the filters and does not change the relative performance of filters investigated.

The price of purchasing filters can vary widely between regions and installations. The effect of these variations on the Minimum Annual Cost has been investigated (results not shown). A change in filter price of ±25% from the base case results in variations in Minimum Annual Cost of ±10%. Variations in cost of this order do not change the relative cost of operations of filters if applied to all filters in a study. However, if the estimates of price for individual filters vary significantly, for instance a reduction in V-type filter price, then the outcome of a cost comparison can vary. Increasing the assumed price of a filter will increase the Minimum Annual Cost and reduce the Time to Minimum Cost. Decreasing the price of a filter has the reverse effect.

4.3.3.4 Effect of Particle Concentration (C_i)

The concentration of particulate matter in the outdoor air varies significantly depending on the installation location. The effect of increasing the particle concentration from the base case ($C_{i,o}$) on the Minimum Annual Cost of primary filters installed without prefilters is shown in Figure 4.8. Increasing the concentration in the air stream causes the energy cost to increase more sharply with increased operation time. This increases the Minimum Annual Cost for filters and reduces the Time to Minimum Cost. The effect is greater for more expensive filters such as V-type filters.

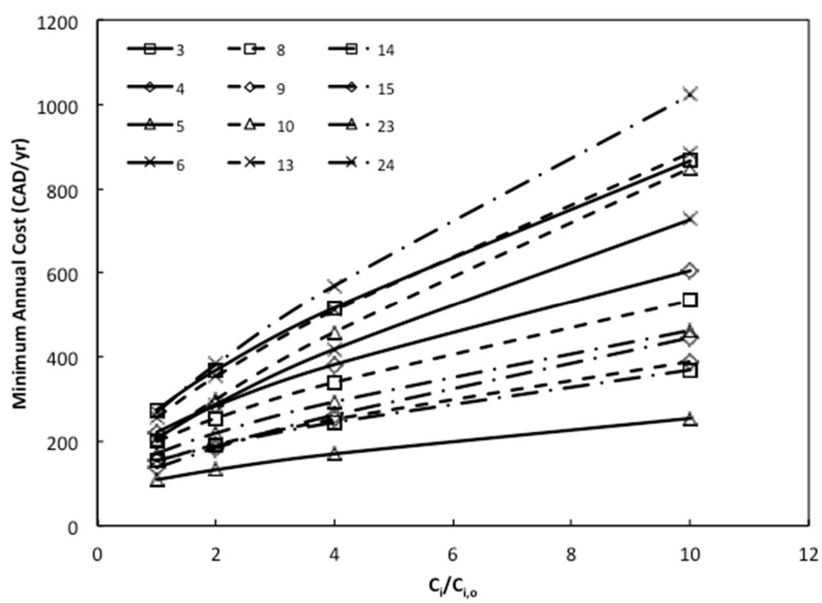

Figure 4.8: Effect of particle concentration (C_i) on Minimum Annual Cost for primary filters without prefilters

Figure 4.9 shows the difference in cost of the filtration system if a prefilter is installed upstream of the primary filter, rather than the primary filter alone, for varying levels of particle concentration in the airstream. In locations such as Vancouver where the annual average PM_{10} concentration is low, approximately 10 μg/m^3, it may be economically attractive to forego the prefilter. As the particle concentration is increased the relative annual cost of a system with a prefilter installed is reduced. The slopes of the curves in Figure 4.9 are more severe for primary filters with higher purchase price. At $C_i/C_{i,o}$ equal to 2 the outdoor air particle concentration is approximately 20 μg/m^3 which corresponds to the WHO air quality guideline for annual mean outdoor concentration [17]. For this level of particulate matter approximately 50% of primary filters would benefit from a prefilter. At $C_i/C_{i,o}$ equal to 3 the outdoor air particulate matter concentration is approximately 30 μg/m^3. For this level of particulate matter the majority of primary filters would benefit from having a prefilter installed upstream. The majority of urban environments have even higher concentrations of particles [17], therefore, in the majority of installations it would be beneficial to install a prefilter upstream of the primary filter.

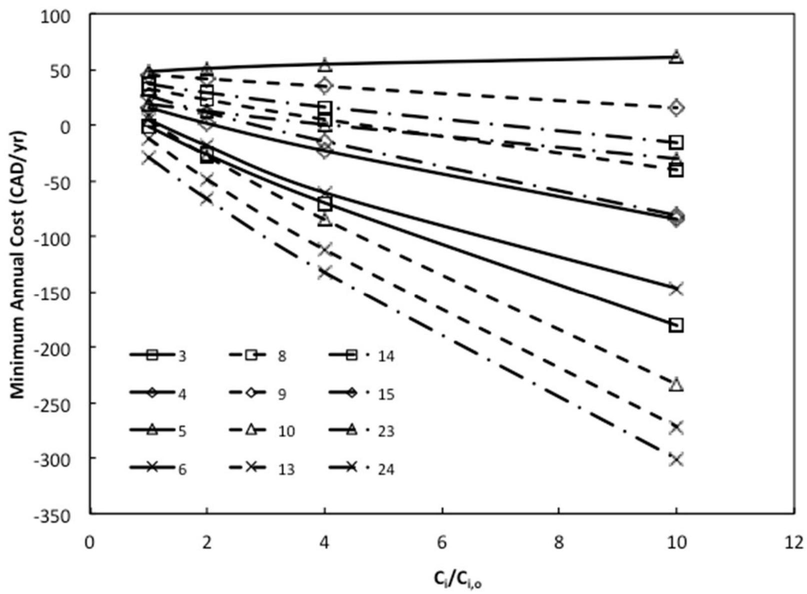

Figure 4.9: Difference in Minimum Annual Cost of a system operating with prefilter and primary filter versus primary filters alone for varying particle concentrations (C_i)

4.3.4 Effect of Filter Design Parameters on Operation Cost

The filter design parameters impact the initial performance of the clean filter and the change in performance throughout the operation lifetime. The two main characteristics of an air filter are the filtration efficiency and the flow resistance. Filtration efficiency is characterized by the size resolved efficiency and impacts the operation cost through the rate of mass accumulation. The flow resistance is characterized by three parameters; the dust holding capacity, the initial pressure drop, and the relation between flow resistance and airflow rate, which are captured in the model variables *a*, *b*, and *d*. A change or uncertainty in any of these parameters can impact the filter operation cost and comparison between filter choices. The impact of changes in filtration efficiency (ε_i), initial pressure drop (through variable *a*), dust holding capacity (through variable *b*) will be investigated in the subsequent sections. Variable *d* is not investigated as the flow rate is assumed constant in this evaluation.

4.3.4.1 Effect of Filter Efficiency (ε_i)

The efficiency of an air filter changes throughout the operation life as dust particles are deposited in the filter media. A single value has been assumed for the purposes of these calculations, which will affect the results. Increasing the filter efficiency tends to have a similar effect as increasing the concentration of particles in the air. The degree of change is significantly lower for efficiency variations as the possible changes in efficiency are limited to approximately ±10 percentage points, which has a limited effect relative to possible changes in other variables.

4.3.4.2 Effect of Initial Pressure

Figure 4.10 shows the change in normalized Minimum Annual Cost for changes in initial pressure drop (assuming constant flowrate) using normalized changes in variable *a* for a selection of Primary filters in this study. An increase in the initial pressure drop of the filter causes an increase in the annual cost of operation due to higher energy costs. Similarly, a filter's operation cost is reduced with decreasing flow resistance. The results in Figure 4.10 show that for a change in initial pressure drop of ±25% there is an associated change in Minimum Annual Cost of approximately ±15%. The relationship shows a slightly non-linear profile throughout the range investigated. Though these variations are small compared to the potential impact of system parameters such as electricity price and particle concentration they are likely to impact each filter independently and therefore can result in substantial impact when comparing between different filters to determine the most efficient option for system operation.

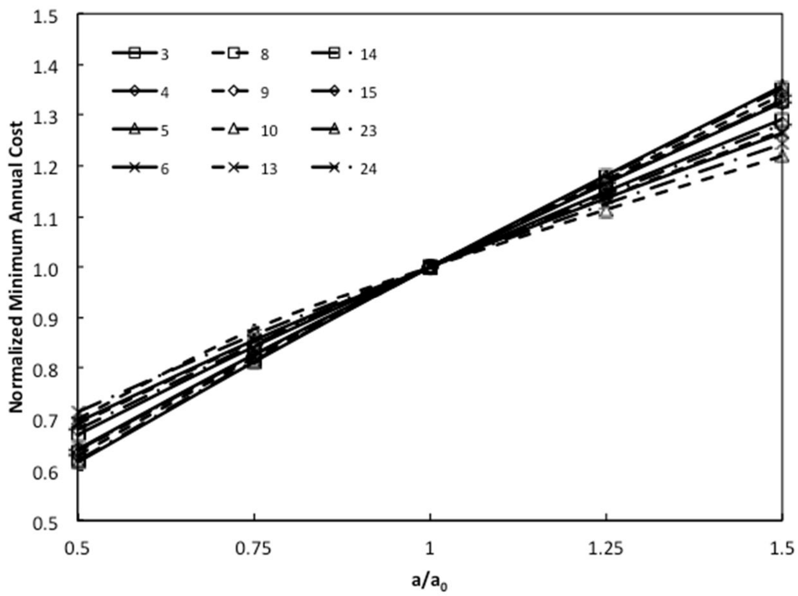

Figure 4.10: Impact of changes in filter parameter 'a' on minimum annual cost of operation

4.3.4.3 Effect of Dust Holding Capacity

Figure 4.11 shows the change in normalized Minimum Annual Cost for changes in dust holding capacity using normalized changes in variable *b* for a selection of Primary filters in this study. An increase in variable *b* (corresponding to a decrease in the dust holding capacity for fixed initial pressure drop) results in an increase in the annual cost of filter operation. The results in Figure 4.11 show that for a change in initial pressure drop of ±25% there is an associated change in Minimum Annual Cost of approximately ±10%. This shows that the filter operation cost is more strongly influenced by the initial pressure drop than it is by dust holding capacity. The dust holding capacity is also a parameter that is specific for a given filter and variability of a single filter's performance may have significant impact on the relative comparison of energy efficiency.

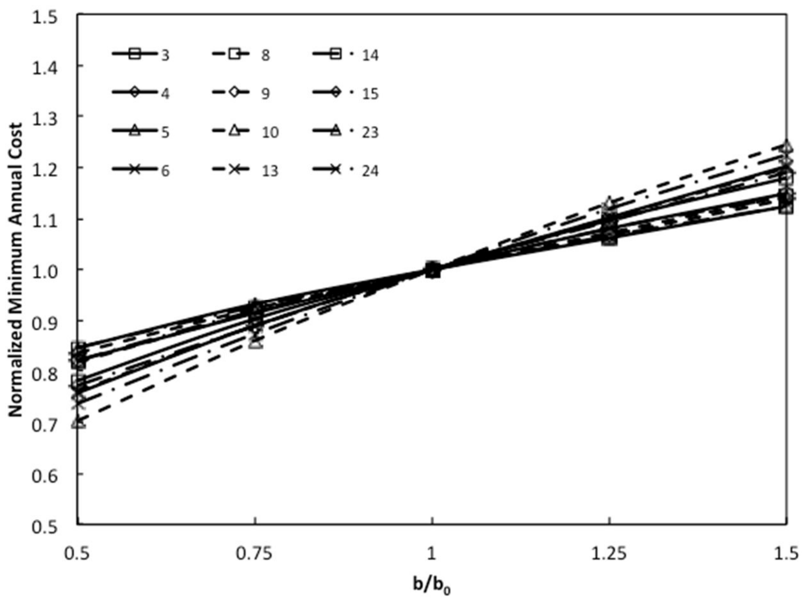

Figure 4.11: Impact of changes in filter parameter '*b*' on minimum annual cost of operation

4.4 Conclusions

The new model developed in this dissertation to predict filter energy efficiency and annual cost of operation has been used to compare twenty-four different filters from five manufacturers. The model has been limited to constant flow rate applications to simplify the calculations. The results show that V-type filters are the most energy efficient type of filter investigated. Bag filters, however, are the lowest cost option due to the significantly lower purchasing price of the filter. It has been shown that the annual cost of operation of a filtration system can be reduced if the filter is changed once it reaches a resistance corresponding with the operation time to minimum annual cost rather than simply using the manufacturer's suggested final resistance. Detailed knowledge of the air handling system and installation are required to determine this resistance value as it will vary with system parameters.

The model parameters that have the largest effect on Minimum Annual Cost are the price of electricity and the concentration of particulate matter in the air stream. Parameters having a smaller effect include the cost to install and dispose of filters, the price of purchasing the filter, and the particle collection efficiency of the filter. Increasing the price of electricity causes an increase in the minimum annual cost of operation for all filters but has a smaller effect on more energy efficient models. Increasing the concentration of particles in the airstream increases the minimum annual cost of operating the filtration system and has a stronger effect on filters of higher purchase price. For model conditions typical of Vancouver, Canada it has been shown that foregoing a prefilter in the air handling system can reduce the annual cost of operation. Increasing the price of electricity makes forgoing the installation of a prefilter more attractive while increasing the concentration of particulate matter in the airstream tends to make including a prefilter more economically viable.

The model introduced here provides a method of comparing relative energy efficiency performance between filters for any installation. A comparison of the output of the proposed model with the Quality Factor and Wattage methods was performed to highlight the possible differences in filter choice that would be made using alternative approaches. The outcomes have been shown to differ due to data not incorporated in the older models such as filtration efficiency and particle concentration.

The impact of filter design parameters (ε_i, a, and b) have shown that the annual operation cost can vary significantly between different filter types or the same filter design if the construction methodology allows for variability. The most critical filter design parameter for a specific MERV is the initial pressure drop due to the substantial impact it has on energy costs. Reduction in flow resistance of the filter media and bulk filter design has the potential to improve energy efficiency at a given design condition.

5 Financial Implications of Modifications to Building Filtration Systems[3]

5.1 Introduction

ASHRAE provides guidelines for air filter use [23] and classification [67] that has allowed for the development of an air filter energy and cost model presented in previous chapters. The guidelines recommend that filters with a MERV 6 or higher be installed if the national outdoor air quality standard or guideline is exceeded for PM_{10} or MERV 11 if $PM_{2.5}$ guidelines are exceeded. Filter efficiency guidelines in Europe are dictated based on desired indoor air quality categories set forth in EN15251 [136] but specific desired indoor particle concentrations are not stipulated. The LEED rating system advocates the installation of MERV 13 filters to achieve indoor air quality credits, without specifying an IAQ target or considering the implications of increased energy consumption associated with high efficiency filters. These prescriptive methods do not account for the potential tradeoff between filter energy consumption and the need to provide a specific indoor air quality while accounting for local conditions. Carlsson and Johnsson [87] have shown that the particle concentration downstream of filters varies by location due to upstream concentration differences and that energy consumption is correlated with filter classification in the European context. Energy consumption could be reduced by selecting filters and systems to meet specific air quality targets rather than selecting the filter based on standardized performance.

Filtering the air introduced to the indoor environment can significantly improve occupant health. Modeling efforts have found that the monetized reductions in morbidity and mortality may outweigh the costs of improved filtration by an order of magnitude [91,92,137]. The efficiency of the filter used has been shown to impact operation cost

[3] A version of this chapter has been published. Montgomery, J. F., Reynolds, C. C. O., Rogak, S. N., & Green, S. I. (2015). Financial Implications of Modifications to Building Filtration Systems. Building and Environment, 85, 17–28.

and IAQ [85,91,92,138] but the impact of specific MERV has not been investigated. The impact on indoor air quality, system costs and associated financial benefits from improved occupant health as a result of modifications to the filters installed and the system operation is unknown. Additionally, the filtration efficiency required to meet expected air quality guidelines and the cost of operating these systems has not previously been investigated.

The purpose of this chapter is to develop theoretical models of the financial costs and benefits of HVAC air filtration systems in a number of cities throughout the world representing a broad range of outdoor air quality, electricity prices, and economic indicators (used to scale labour rates, and morbidity and mortality costs). The models will be used to provide insight into the impact of changes to efficiency (MERV) and air handling system operation. Relative impacts of changes to the air flow characteristics such as fraction of recirculated and return air, and the use of increased ventilation rates will be compared based on impacts to system operation cost, indoor air quality, and monetized occupant health outcomes from PM exposure. The results from this work will help to inform industry practitioners and policy makers to understand the impact of system design considerations on occupant exposure to indoor particles, and the potential implications of indoor air quality policies and guidelines. The model developed in this work was implemented as a spreadsheet that building practitioners can use with input parameters appropriate to specific design or policy questions [139].

5.2 Model and Methodology

Changes in air filtration system parameters will affect the indoor air quality, system operation cost and occupant exposure to airborne particles. To understand the impact on each aspect of the system a number of models have been adapted from previous works and integrated in a novel manner as described below.

A model commercial office building is used to evaluate the impact of modifications to the airflow and filtration system. The office building is assumed to contain an indoor volume of 6,400 m^3 with a floor area of 1,600 m^2 which is typical of the size bin constituting the largest total floor space from the EIA Commercial Buildings Energy Consumption Survey [140]. Occupant density (0.07 people/m^2), and required baseline outdoor air ventilation rate (10 L/s/person plus 1 L/s/m^2) are determined based on the requirements for IAQ Category A for an open office space [141]. The base model assumes a 100% outdoor air system (other air mixes are also investigated) with flow rate equal to the baseline ventilation rate, an infiltration rate of 0.25 ACH [142], and a size resolved (0.001-100 μm) ambient particle concentration to match the annual average PM_{10} and $PM_{2.5}$ concentrations in London, UK [143]. No energy recovery system has been assumed for the model. The building air system is assumed to operate continuously when occupants are present and thermal requirements are met through separate energy control. The air control is assumed to operate with variable fan speed control to maintain constant flow rate throughout operation. The results of this work relate specifically to buildings capable of achieving these controls parameters. The use of alternative base scenarios could provide additional information for specific buildings of interest and can be determined using the model. Outdoor particle concentrations are scaled to match local conditions for comparisons of different cities where indicated. Filter banks are sized in the model to provide a nominal face velocity of 2.5 m/s to match air filter testing specifications [67]. The model assumes a baseline filter bypass of 10% as a representative value. Previous modeling has shown the potential for filter bypass between 1-38% for straight, L-shaped, or U-shaped gaps of 1 mm or 10 mm [144]. A schematic of the airflow branches and potential filter locations is shown in Figure 5.1.

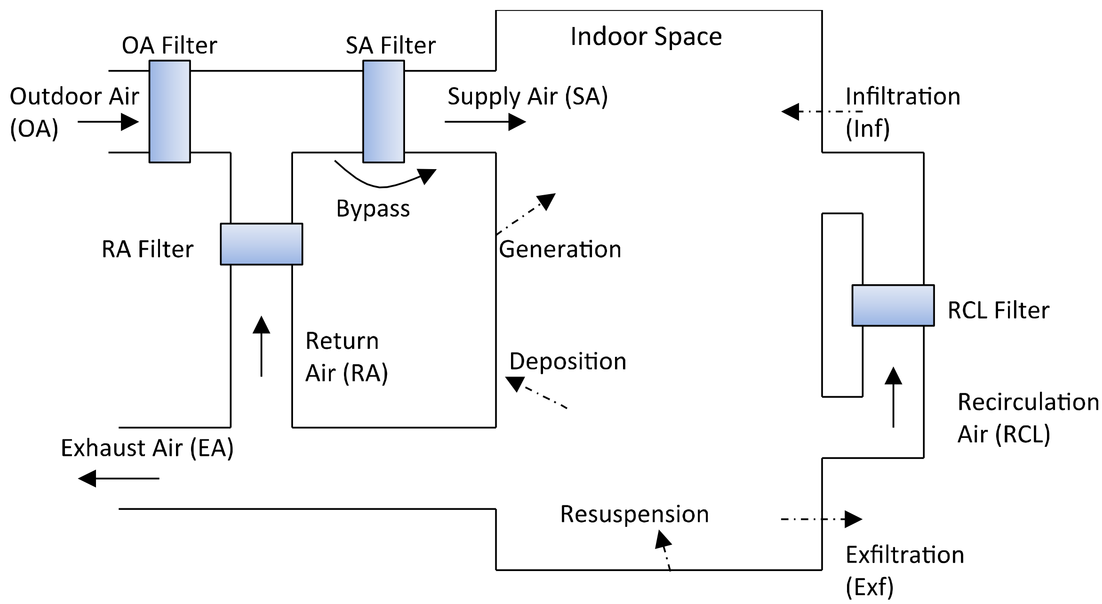

Figure 5.1: Schematic of building airflows, potential filter locations, and particle dynamics. A typical building will be designed with one or more of the branches of airflow. Typical filtration systems utilize only a supply air filter while filters are sometimes present in other locations.

5.2.1 Indoor Aerosol Dynamics Model

The indoor particle concentration within the model building is determined through a mass balance on particles in discrete size bins as previously developed [82,83,145] and experimentally validated [85]. Equations 5.1-5.4 describe the mass balance and steady state solution for the indoor aerosol concentration.

$$\frac{dC_{IA}}{dt} + \alpha C_{IA} = \beta \qquad \text{Equation 5.1}$$

$$\alpha = \frac{k}{V_B}\left[-Q_{RA}(1-\varepsilon_{RA})(1-\varepsilon_{SA}) + Q_{RA} + Q_{Exh} + Q_{Exf} + Q_{RCL}\varepsilon_{RCL} + V_B\lambda_d\right] \qquad \text{Equation 5.2}$$

$$\beta = \frac{C_{OA}}{V_B}\left[Q_{OA}(1-\varepsilon_{OA})(1-\varepsilon_{SA}) + Q_{Inf}P_{Bldg}\right] + \frac{G}{V_B} + \frac{RL_{fl}A_{fl}}{V_B} \qquad \text{Equation 5.3}$$

$$C_{IA,\infty} = \frac{\beta}{\alpha} \qquad \text{Equation 5.4}$$

where C_{IA} is the indoor aerosol concentration (#/m^3); C_{OA} is the outdoor aerosol concentration (#/m^3); $C_{IA,\infty}$ is the steady state indoor aerosol concentration (#/m^3); k is the mixing factor (assumed 1 for well mixed); V_B is the building volume (m^3); Q is the air flow rate (m^3/s); ε is the filtration efficiency (-); λ_d is the particle deposition rate (s^{-1}) including both surface deposition and coagulation; P_{bldg} is the building penetration factor (-); G is the emission rate (s^{-1}); R is the resuspension rate (s^{-1}); L_{fl} is the floor dust loading (#/m^2); A_{fl} is the floor area (m^2); and the subscripts RA, Exh, Exf, Inf, RCL, and OA denote return air, exhaust air, exfiltration, infiltration, recirculated air, and outdoor air, respectively.

Typical values for parameters in Equations 5.1-5.4 were identified in the literature. A description of the values used in this work is provided in : Supplemental Information – Chapter 5. A number of these parameters have been developed theoretically and are expected to vary significantly between buildings. An investigation of the impact of variability in these parameters is presented in Section 5.3.5. The models accuracy can be improved if experimental data is obtained for these values specific to a building of interest.

5.2.2 Air Filtration Model

The cost of operating air filters depends on properties of the air system (flow rate, efficiency, etc.) and the local conditions (particle concentration, electricity prices, etc.). Models have been developed to predict the operation cost and power consumption throughout the filter lifetime [129,134]. The simplest form of filter modeling assumes a constant airflow system with filtration efficiency equal to the reported MERV while accounting for increases in flow resistance with dust accumulation. This limits the filter cleaning capacity to the minimum value reported during standard testing which will limit the potential benefit for mechanical filters investigated herein. The average annual power consumption (Watts) and annual operation cost (USD/yr) of a filter can be determined by:

$$W_{ave} = \frac{Q^d}{\eta_s \eta_o t \Sigma \varepsilon_i C_{IA,i}} \frac{a}{b} [exp(bQ\eta_o t \Sigma \varepsilon_i C_i) - 1] \qquad \text{Equation 5.5}$$

$$C_A = 8.76 W_{ave} \$_E + \frac{31536000(\$_F + \$_L)}{t} \qquad \text{Equation 5.6}$$

where W_{ave} is average power (Watts); Q is the air flow rate (m^3/s) through the filter; η_s is the fan system efficiency (0.55); η_o is the fraction of the year that the system is operating (0.31); t is the operation time (s) to filter change; ε_i is the average filtration efficiency of the particles size bin *i* (accounting for 10% filter bypass); C_i is the particle mass concentration in the air stream incident on the filter in the size bins *i* (g/m^3); C_A is the annual cost of operating the air filter (USD/yr); $\$_E$ is the local electricity price (USD/kWh); $\$_F$ is the filter purchase price (USD/filter); $\$_L$ is the price of filter installation and disposal (USD/filter); 8.76 is a conversion factor derived from 8,760 hours in a year (used to annualize the energy cost); and 31,536,000 is the number of seconds in a year (used to annualize the labour and purchase costs). The variables *a*, *b*, and *d* are determined from ASHRAE 52.2 testing [134]; *a* is related to the initial filter pressure, *b* is related to the dust holding capacity, and *d* relates the flow through the filter to the pressure drop (34). The subscript *i* denotes the particle size bin.

A summary of parameter values used is provided in : Supplemental Information – Chapter 5. The filter parameters used assume that flow resistance increases with increased MERV. In reality there is a large degree of variability in flow resistance of filters of a given MERV. The assumption in this analysis represents a conservative approach as a higher efficiency filter with lower pressure drop would require less energy for installation and thus have greater benefits to those calculated.

The operation time to minimize the annual operation cost can be determined by setting the time derivative of Equation 5.6 to zero and solving for time to changeout. All system costs calculated by this model are additional costs beyond the provision of the base ventilation requirements including costs of filters, added flow circulation, and conditioning of added ventilation. Added flow costs are calculated based on an increase in fan energy, assuming a system external flow resistance of 375Pa. Costs of conditioning additional ventilation air are estimated using heating-degree-days (HDD) and cooling-degree-days (CDD) [93] and assuming system operation times as described for the filtration calculations. For constant flow rate the cost of conditioning ventilation air can be calculated by:

$$C_{heat} = \$_g Q_{OA} \rho_{air} C_{p,air} HDD \eta_o \frac{\delta}{\eta_{heat}} \qquad \text{Equation 5.7}$$

$$C_{cool} = \$_E Q_{OA} \rho_{air} C_{p,air} CDD \eta_o \frac{\delta}{COP} \qquad \text{Equation 5.8}$$

where C_{heat} is the annual cost of heating increased ventilation air (USD/yr); C_{cool} is the annual cost of cooling increased ventilation air (USD/yr); $\$_g$ is the price of natural gas (0.0416 USD/kWh in the UK); $\$_E$ is the price of electricity; ρ_{air} is the density of air (1.2 kg/m^3); $C_{p,air}$ is the specific heat of air (1000 J/(kg·K)); HDD is the heating-degree-days (day K/yr); CDD is the cooling-degree-days (day K/yr); η_o is the operation fraction of the system per year (0.31); δ is a conversion factor (86,400 s/day x 0.277 kWh/MJ x 10^{-6} MJ/J); η_{heat} is the efficiency of a natural gas boiler; and COP is the coefficient of performance of the cooling system (assumed 3.0).

5.2.3 Occupant Health Model

The economic benefits of improved occupant health can be determined by the avoided morbidity and mortality from improved air quality, when compared to a baseline case. The baseline case chosen in this model is the indoor air quality determined when the system operates without an air filter. Net benefits are calculated based on the difference between indoor particle concentrations for the model building operating with a given filtration system versus the base case. A separate baseline indoor concentration was determined for scenarios when indoor generation is present to account for the increase in particle concentration. The health benefits are determined from the reduction in particulate matter concentration based on Change – Response (C-R) relations for each health endpoint. The C-R functions are determined for specific health endpoints based on a variety of epidemiological studies. The health endpoints included in this study are those identified to have the greatest impact on employees in an age range typical for an office building (age 20-65 years). An extensive review of the implications of air pollution and methods for valuation is provided by the USEPA [90]. The change in endpoint with change in aerosol concentration and the associated monetary benefit can be determined by:

$$\Delta y_i = -[y_0(exp(-B_i \Delta PM_i) - 1)] \qquad \text{Equation 5.9}$$

$$A_i = \Delta y_i N \$_i \eta_t \qquad \text{Equation 5.10}$$

where A_i is the value of avoided morbidity or mortality endpoint (USD/yr); Δy_i is the change in annual health endpoint per person; y_0 is the annual baseline rate per person; B_i is the endpoint effect estimate; ΔPM_i is the change in relevant particulate matter concentration (μg/m^3); N is the number of occupants; $\$_i$ is the monetary value of each health incident (USD/incident); and η_t is a correction factor (0.228) for time spent in the building.

The valuation of morbidity endpoints follows the procedure utilized by the USEPA [90] with the subpopulation limited to 20-65 years of age (the assumed age range of office workers). A summary of the values used in calculations is provided in Table 5.1. These values are subject to significant variability between studies and are generally developed with a limited population base, which will add to uncertainty in the results when applied across a global population. Greater detail is provided in : Supplemental Information – Chapter 5.

Table 5.1: Summary of morbidity and mortality endpoint variables

Effect, y_i	Related PM	Effect Estimate, B_i (% per μg/m^3)	Standard error of Effect Estimate, σ_B (-)	Annual Baseline rate, y_0 (per person)	Monetary Value per Incidence (2010 dollars)
Mortality	$PM_{2.5}$	1.06[a]	0.287[f]	0.003375[a]	2,304,450[a,g]
Respiratory Related Hospital Admissions	$PM_{2.5}$	0.17[b]	0.051[b]	0.01369[b]	17,900[a,h]
Asthma Related ER Visits	PM_{10}	0.367[c]	0.126[c]	0.0028[c]	415[a,h]
Minor Restricted Activity Days (MRAD)	$PM_{2.5}$	0.741[d]	0.07[d]	7.8[d]	70[a,h]
Work Loss Days (WLD)	$PM_{2.5}$	0.46[e]	0.036[e]	2.37[e]	204[a]

a - Source: [90]

b - Based on COPD [92]. Source: [147]

c - Source: [10]

d - Source: [8]

e - Source: [146]

f – Source: [90]

g – Willingness to pay method

h - Cost of incident

5.2.4 Conversion to Other Regions

The valuation of filters, labour, morbidity and mortality will vary between regions based on economic circumstances. The relative Gross National Income (GNI) and Price Level Index (PLI) for the countries in this study have been used to convert between locations [91]. A description of the conversion is provided in the : Supplemental Information – Chapter 5. While calculations have been performed with input variables to reflect local conditions, the results are presented in USD and the relative impact of these results or availability of funds to do the work may be different between locations.

5.2.5 Model Application

The models above have been used to determine the impact of filter installation characteristics on system operation costs and potential health benefits due to associated changes in indoor particle concentration. The comparison has been performed for a number of cities to develop an understanding of the impact of air quality standards and guidelines on building operations. The average annual outdoor particulate matter concentrations, local electricity prices, GNI per capita, and PLI for each city in the study is shown in Table 5.2. The values shown in Table 5.2 are representative values for the cities in question. Variability is inherent in these parameters such as the potential variation of outdoor particle concentration both spatially and temporally within a city or difference in electricity costs due to demand pricing. The potential exists for significant reductions in operation costs depending on time of use and power reduction incentives from the local utility. The actual cost calculations in a real building should consider these nuances and the results here should be used as a guide. Analysis of all potential variations is outside the scope of this work.

Table 5.2: Study city parameters

City	$PM_{2.5}$ ($\mu g/m^3$)[a]	PM_{10} ($\mu g/m^3$)[a]	Electricity Price (USD/kWh)	GNI per capita (USD/person)[l]	Price Level Index[m]
Beijing	72.6	121	0.09[b]	4,940	42
Berlin	20.8	26	0.14[c]	43,980	111
Delhi	118.8	198	0.06[d]	1,410	33

City	$PM_{2.5}$ (μg/m³)[a]	PM_{10} (μg/m³)[a]	Electricity Price (USD/kWh)	GNI per capita (USD/person)[l]	Price Level Index[m]
Johannesburg	39.6	66	0.12[e]	6,960	61
Kraków	35.5	64	0.11[c]	12,480	59
London	13.5	29	0.12f	37,780	118
Madrid	13.1	26	0.12[c]	30,990	95
Mexico	24.4	52	0.11[f]	9,240	65
Moscow	19.8	33	0.09[g]	10,400	45
New York City	12.7	21	0.15[h]	48,450	100
Paris	22.9	38	0.09[c]	42,420	115
Sao Paulo	15.0	38	0.34[i]	10,720	56
Singapore	19.0	29	0.22[j]	42,930	65
Stockholm	10.6	28	0.10[c]	53,230	124
Tokyo	13.8	23	0.17[f]	45,180	118
Vancouver	4.6	12	0.08[k]	45,560	100
Zürich	14.7	21	0.12[f]	76,380	140

a – Source: [143]
b – Source: [150]
c – Source: [153]
d – Source: [156]
e – Source: [158]
f – Source: [148]
g – Source: [151]
h – Source: [154]
i – Source: [157]
j – Source: [159]
k – Source: [149]
l – Source: [152]
m – Source: [155]

The model was also used to compare the impact of changes to filtration system components. A comparison of the impact of increases in supply air filter efficiency in cities described in Table 5.2 was performed to develop an understanding of relative financial impacts. Specific system changes have been investigated by using London as a test case. Net benefits of system operation were compared for systems with increased outdoor, recirculated, or return airflow along with improvements in installed filter efficiency. System changes have been investigated from the viewpoint of three major stakeholders – policy makers, building designers, and building operators – to develop an understanding of how benefits of system changes can be interpreted differently using modified points of reference.

5.3 Results

The results are discussed with respect to filter costs and benefits for numerous system operation locations and designs. Net benefits are calculated by adding financial benefits from reduced morbidity and mortality and subtracting increased operation costs due to system changes. The results are discussed primarily for the model without indoor particle generation. A similar analysis assuming the presence of indoor sources is available in : Supplemental Information – Chapter 5 and referred to where relevant below.

5.3.1 Operation Costs and Air Quality Guidelines

5.3.1.1 Costs of Filter Operation in Different Regions

Figure 5.2 compares the total annual operating cost and optimal changeout period for the theoretical building located in different cities. The comparison assumes that the building ventilation system is the 100% outdoor air base case scenario with MERV 13 filters installed. The area of a bubble represents the annual average $PM_{2.5}$ concentration and the shading represents electricity price in the city.

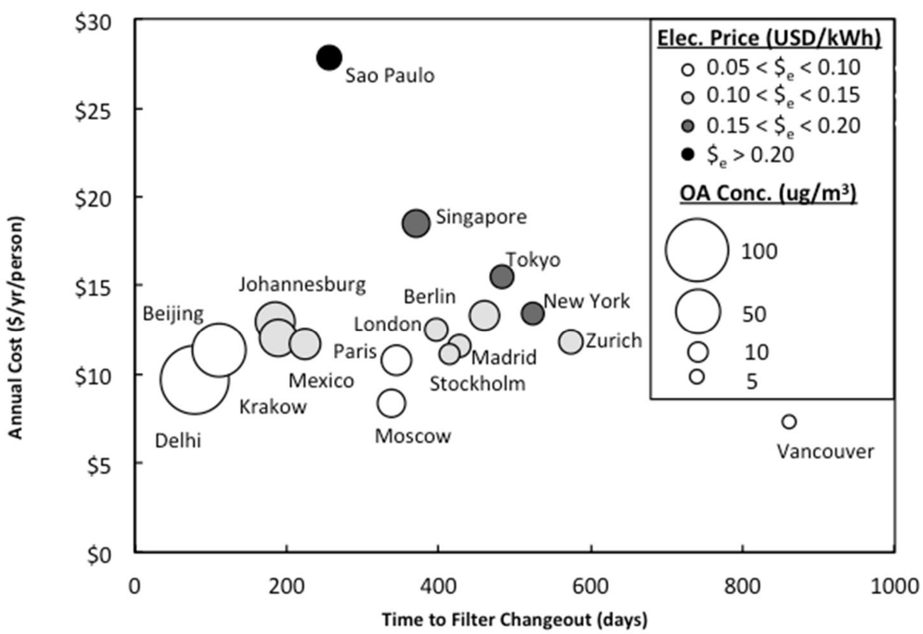

Figure 5.2: Cost of operation versus Time to Filter Changeout for the filtration system with MERV 13 filters. Operation time has been optimized such that the annual operation cost is minimized in

each city. Bubble area represents average annual outdoor $PM_{2.5}$ concentration. Bubbles are shaded in relation to the local cost of electricity, $\$_e$, in USD/kWh.

The results from Figure 5.2 show that air filter operation cost can vary by over 300% when the systems are changed at optimum times. The least costly city in which to operate a filtration system with MERV 13 filters from this study is Vancouver (7.34 USD/yr/person) and the most costly is Sao Paulo (27.83 USD/yr/person). The minimum annual cost of operating MERV 13 filters in Figure 5.2 is most strongly correlated with electricity price (r^2=0.978). The time to optimum changeout is influenced by a wider array of parameters with the most important being GNI (r^2=0.781), PM_{10} (r^2=-0.720), and PLI (r^2=0.704). The annual operation cost of a filter installation in a given city has been shown previously to be a strong function of the time to filter changeout [129]. The time to minimum changeout (and thus minimum annual cost) determined in Figure 5.2 will therefore be indirectly affected by GNI, PM_{10}, and PLI.

5.3.1.2 Cost of Achieving Air Quality Standards

Figure 5.3 compares the cost of operating the filtration system in the study cities using the minimum filter MERV required to meet WHO air quality guidelines ($PM_{2.5}$=10μg/m^3) given the different outdoor particle concentrations and represents the impact of existing guidelines on system costs. Also shown is the cost of operating the system with MERV 13 filters (to achieve LEED IEQ points). The other system parameters are identical to those used for Figure 5.2.

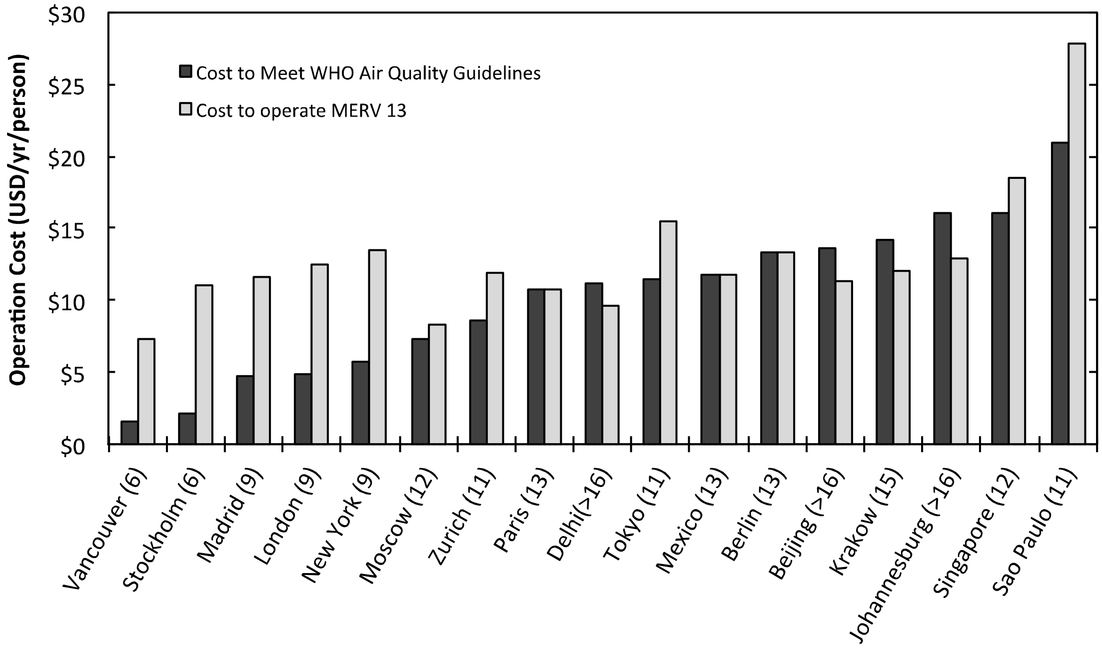

Figure 5.3: Cost to meet WHO Air Quality Guidelines by city (dark bars) and cost of operating the same building with MERV 13 filters (light bars). Required filter MERV to meet air quality guidelines is indicated in parentheses by city name.

The results of Figure 5.3 show a large variation in the cost and required filter efficiency, with higher required efficiency associated with higher outdoor concentrations, to meet WHO air quality guidelines. The 10% filter bypass air carries a large amount of particulate matter, and therefore the model building operating in Beijing, Delhi, and Johannesburg cannot meet IAQ guidelines even with a MERV 16 filter installed. For these cities the comparison has been performed using the results for a MERV 16 filter. Vancouver and Stockholm have outdoor particle concentrations low enough to meet the WHO guidelines without filtration and only require the baseline MERV 6 filter for protection of mechanical components. Typical filtration costs to meet guidelines in the test building are approximately ~10.3 USD/yr/person though a large variation is present. The highest cost, associated with Sao Paulo (21.0 USD/yr/person), is 13x greater than the lowest operation cost in Vancouver (1.6 USD/yr/person).

If the goal of the filtration system is to meet WHO air quality guidelines within the building then a potential for cost savings exists for building operation in cities that can meet the required air quality with a filter MERV lower than the MERV 13 suggested by

LEED. The savings in operation cost while meeting WHO guidelines with a filter efficiency of less than MERV 13 is apparent from a comparison of the bars in Figure 5.3. The city with the greatest potential for savings compared to operation with MERV 13 filters is Stockholm (80% reduction). The cities that require filters with MERV higher than MERV 13 would incur additional costs to meet IAQ standards but would be able to provide a level of indoor air quality that meets international guidelines. The city with the greatest additional expense incurred would be Johannesburg (24% increase).

The results presented in Figure 5.3 and the discussion regarding filter requirements thus far has focused on 100% OA systems. Systems with return air added in addition to the baseline outdoor air required show similar trends as presented in Figure 5.3 but with generally higher cost due to increased filter bank size and lower required MERV (assuming filters in supply air only) due to added total airflow. The precise change in costs is a function of the volume of additional return air assumed. For systems with additional return air flow of $Q_{RA}=Q_{OA}$ a building in Johannesburg requires MERV 14 filters with 58% cost increase over a 100% outdoor air system. Similarly, the same building would require a MERV 7 filter with 14.5% cost increase to operate in London.

5.3.2 Benefits of Changes to 100% Outdoor Air Systems

5.3.2.1 Impact of Increased MERV

Research has shown that there is no lower threshold to PM exposure and improved human health [160,161]. Therefore, there may be benefits from achieving indoor particle concentrations *below* the WHO guidelines. An understanding of the relative economic impacts of increased operation cost versus reduced health impacts can provide guidelines for the optimal MERV of filter to be installed in an air-handling system.

Figure 5.4a shows the monetized annual net benefits of installing air filters of increasing efficiency from MERV 6 to MERV 16 as compared to a system operating without air filters in the theoretical building. The system is assumed to operate with 100% OA and to provide baseline ventilation. The comparison assumes that no indoor generation is present within the model building.

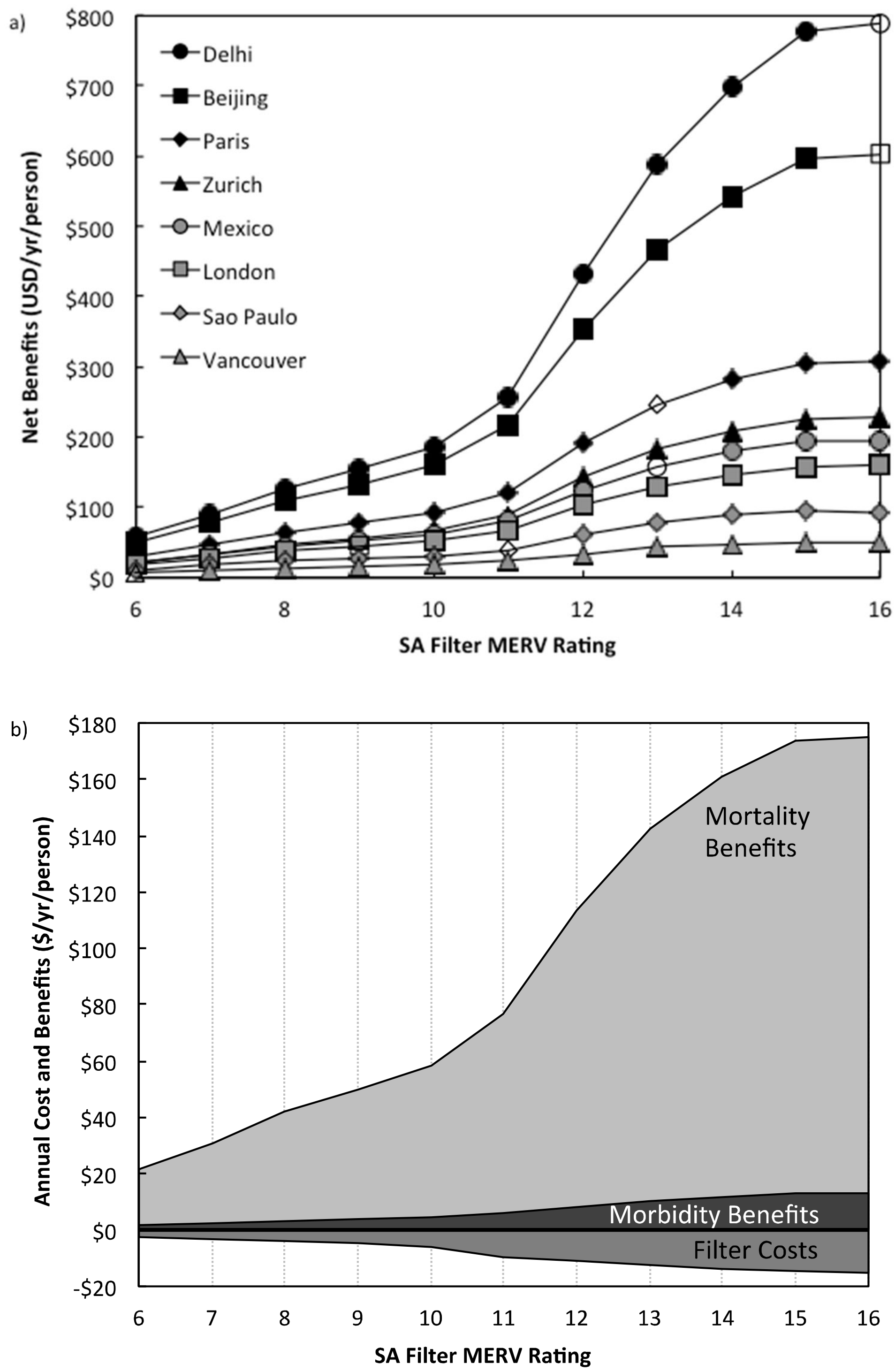

Figure 5.4: Net benefits in select cities (a) and breakdown of costs and benefits for London (b) of improved filter efficiency for operation with 100% outdoor air and no indoor generation sources. Open symbols in (a) refer to filter required to meet WHO air quality guidelines.

The results in Figure 5.4a show a general trend of increasing net benefits with increased filter efficiency. This implies that the added cost of increasing the efficiency of the filters is outweighed by the increase in health benefits to the occupants by reduced exposure to airborne particles. The greatest benefits are seen in locations with high outdoor PM concentrations such as Delhi and Beijing. For MERV 16 filter installations the net benefit in Delhi is 14x greater than in Vancouver. Net benefits are also increased for locations with a high GNI per capita such as Zurich. The magnitude of net benefits is tempered in locations characterized by high electricity prices such as Sao Paulo due to the high cost of filter operation.

The reduction in the slope of the curves in Figure 5.4a between MERV 13 and MERV 16 is due to the small increases in filter efficiency. These marginal increases in efficiency result in marginal reductions in indoor $PM_{2.5}$ and PM_{10} when MERV 16 filters replace MERV 13 filters. For all cases investigated in this study the net benefit versus MERV slope is always positive though not within the margin of uncertainty of the model results, which indicates that the increased benefits of installing higher efficiency filters may not always outweigh the added costs. Conversely, the slope of the net benefit curves may be increased if future epidemiological studies show that the correlation of morbidity and mortality is more strongly linked with smaller particles.

Another approach to investigate the usefulness of air quality guidelines is to compare the net benefits of installing the highest available MERV in comparison with the MERV 13 filter required to achieve LEED points or the minimum MERV required to meet WHO air quality guidelines. In this study MERV 16 filters have been used as the highest MERV for standard HVAC operation. The greatest benefits of replacing MERV 13 filters with MERV 16 filters are seen in cities with high outdoor particle concentrations such as Beijing and Delhi, where the net benefits increase by 29% and 34%, respectively. A smaller increase in net benefits is seen for a city with low levels of ambient pollution, such as Vancouver (19%).

Figure 5.4b shows the relative value of cost and benefit increases as a function of filter efficiency for a 100% outdoor air system in the model building operating in London. The benefits of reduced morbidity are approximately equal to the increased cost of operating the filtration system with higher MERV. The net benefits of increasing filter efficiency are dominated by the monetized reduction in occupant mortality due to reduced exposure to $PM_{2.5}$ which is approximately 10x the value of the added cost of filter improvements.

5.3.2.2 Impacts of Filter Bypass

An important aspect of achieving the benefits from a filter installation is to limit the amount of air that bypasses the filters [144]. Figure 5.5 compares the net benefits of air filter installations in Delhi, London, and Vancouver for varying levels of filter bypass from 0-25%. The comparison has been performed for MERV ratings of installed filters from 6 to 16. The modeled building assumes 100% outdoor air and no internal particle generation.

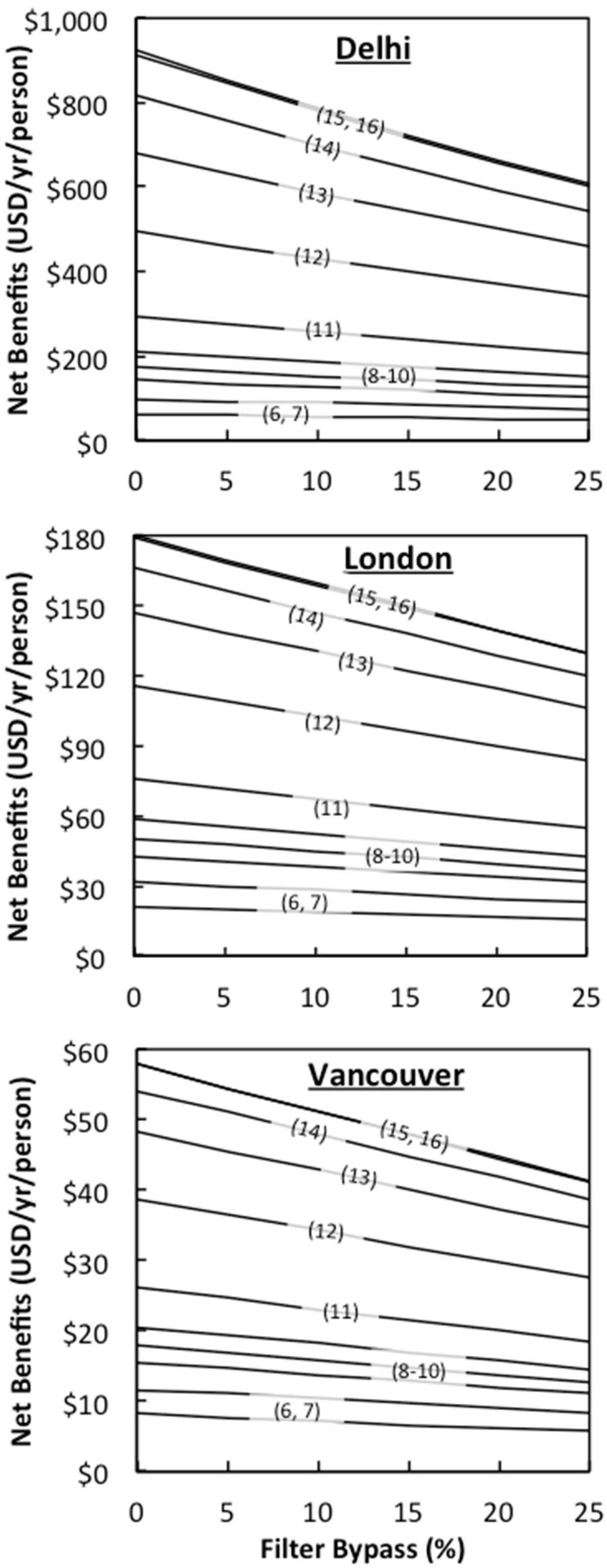

Figure 5.5: Net benefits of filter installations with varying levels of filter bypass for buildings in Delhi, London, and Vancouver. Net benefit scales vary between cities. Filter MERV is indicated in parentheses.

The added costs of filter operation with reduced bypass are outweighed by the increases in benefits due to occupant health. A comparison of the results between cities in Figure 5.5 shows that filter bypass can have a significant impact on the relative net benefits of installed filter ratings for all levels of outdoor particle concentration investigated in this study. The impact is significantly higher for locations with high levels of ambient particle concentrations such as Delhi. Filter bypass also has a significantly larger impact on the performance of high efficiency filters than it does on installations with low MERV filters. The average slope of the net benefit versus filter bypass relations between 0-25% bypass for MERV 16 filter installations in Delhi, London, and Vancouver are -12.7, -2.0, and -0.7, respectively. The slopes of the same relations for a MERV 6 installation are -0.7, -0.2, and -0.1, respectively.

Controlling filter bypass can increase the potential for net benefits of a filtration system, or conversely, if left unchecked, can significantly limit the benefits seen from installing high efficiency filters. The net benefit curves for MERV 16 and MERV 15 filters are almost identical for all cities shown in Figure 5.5. The relative control of filter bypass is critical in achieving any substantial increase in net benefits when increasing from MERV 15 to MERV 16 filters as even a 1 percentage point increase in the bypass with MERV 16 filters would negate any gains in the net benefits. Filter bypass can play a critical role in the comparative net benefits of systems operating with even larger differences in filter efficiency. The installation of MERV 13 filters will provide the same level of net benefits as a MERV 14 system with an additional 10 percentage points of bypass or a MERV 16 installation with an additional 15 percentage points of bypass to within ±5% for all cities in this study. Filter bypass does not have a significant impact on the relative performance of low efficiency filters (MERV <11); a MERV 6 filter with 0% bypass has a lower net benefit than does a MERV 7 filter with 25% bypass.

5.3.3 Return Air Systems

5.3.3.1 Comparison of Increased Outdoor Air or Return Air Flow

An important characteristic of the air-handling system design is the amount and type of additional airflow beyond the base required to properly ventilate a space. Additional airflow can impact the indoor air quality by increasing dilution using outdoor air or increasing filtration of indoor particles through return air. Figure 5.6 compares the net benefits of increased outdoor air and return airflow. In all cases the baseline outdoor airflow is maintained and added to with additional airflow as indicated. The evaluation has been performed for MERV 7, 11 and 15 filters installed in the supply air stream with no indoor generation.

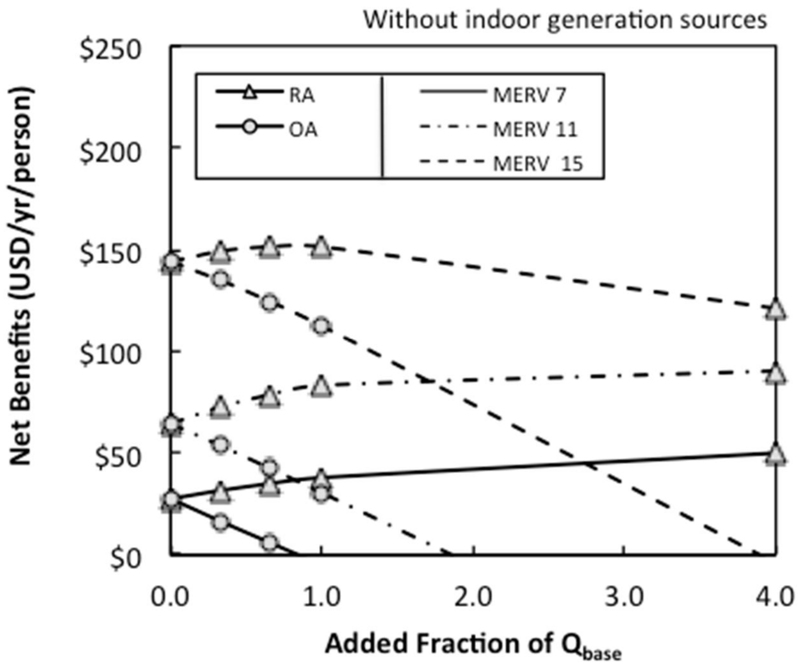

Figure 5.6: Comparison of the effect of increasing flow rate in the return air or outdoor air stream on net benefits for a range of MERV without indoor generation for operation in London. The airstream in which the flow is increased above the base case outdoor airflow is denoted by symbol type. The different line types denote the MERV of filters installed in the supply air stream.

Without indoor sources of particle generation, increases in outdoor airflow to provide dilution to the space shows declining net benefits as the ventilation rate increases. For all installed filtration efficiencies investigated the added cost of conditioning the air and operating the filters eventually surpasses the increased benefits. This occurs at ~0.8, ~1.8, and ~3.8 for MERV 7, 11, and 15 installations, respectively. Beyond these increases in flowrate the system is better off operating with the minimum ventilation required for the occupants without an installed filter.

The net benefits generally increase with added airflow in a return air system when no indoor source of particles is present. Net benefits continue to grow with increased flow when MERV 7 and MERV 11 filters are installed for the range of values investigated in this study. The change in net benefit from Q_{RA}=0 to Q_{RA}=4Q_{base} for a MERV 7 installation is 81%. The change in net benefit from Q_{RA}=0 to Q_{RA}=4$_{base}$ for a MERV 15 installation is -15% indicating that a limit exists for increased benefits with added flow. In Figure 5.6 this limit is reached for the system with MERV 15 filters after $Q_{RA} \approx Q_{base}$.

The general trend is that additional return airflow has only a modest impact for buildings without indoor generation sources and is slightly more beneficial when indoor sources are present. If changes in both filter MERV and airflow rate are unrestricted by other system requirements (such as heating provision using return air flow) then the potential for increased net benefits may exist. Limitations to the benefits of increased return air flow are encountered for systems with both high MERV filters and high return air flow (Q_{RA}>4Q_{base}).

5.3.3.2 Impact of Increased Filter Efficiency

Figure 5.7 compares the benefits to costs of modifying the supply air filter MERV or return air flowrate for a building operating in London without indoor generation sources. The comparison provides an indication of options available for improving benefits to occupants through modifications to building operation when the air handling system has been designed with return air branches.

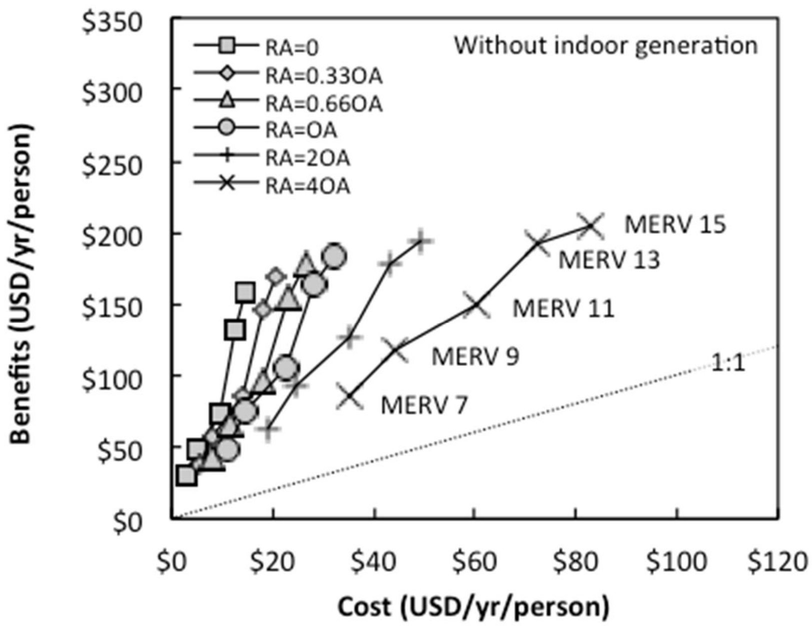

Figure 5.7: Comparison of the benefits and costs of installing SA filters with increased efficiency in systems with varying return air flowrates for the model building operating in London without indoor particle generation. Each symbol type denotes a different return air flowrate. The sequence of points for a particular return air flowrate denotes different SA filter MERV (from left to right: MERV 7, 9, 11, 13, 15).

The benefit to cost relationship in Figure 5.7 shows larger slope for MERV than it does for increases in return air flowrate. An increase in efficiency of installed filters with an accompanying reduction in return air can result in increases in benefits to the occupant without an increase in operation cost. The general trends are similar for systems operating with indoor generation sources as they are for systems without indoor generation sources, though the magnitude of potential benefits are greater. An extreme example of this from Figure 5.7 is to modify the operation of a system with MERV 7 filters and $Q_{RA}=4Q_{OA}$ to utilize MERV 15 filters and reduce the return air flow to $Q_{RA}=Q_{OA}$. This change would approximately double the net benefits of system operation without an increase in operation cost.

5.3.4 Recirculation Air Systems

5.3.4.1 Impact of Airflow and Filter Efficiency

Adding recirculated air within a space served by a 100% outdoor air system is a common method of providing localized heating/cooling through a fan coil unit (with or without a filter) or as a method of reducing particle concentration by use of a portable air cleaner. Figure 5.8 compares the net benefits of increasing the recirculated airstream filter efficiency or flow rate for the theoretical building in London with outdoor airflow to meet baseline ventilation and MERV 7 or 15 filters without indoor generation. The comparison has been performed for $Q_{RCL}=0.33Q_{OA}$ and $Q_{RCL}=Q_{OA}$.

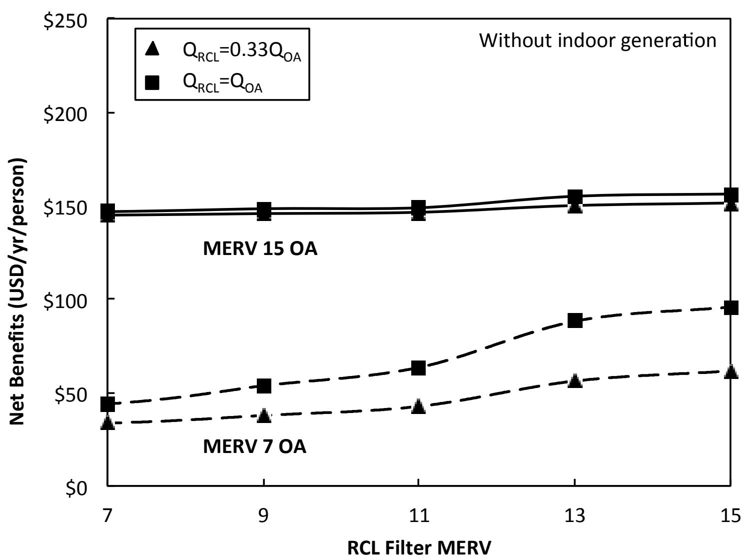

Figure 5.8: Net benefits of increasing recirculated filter efficiency for the theoretical building without indoor generation operating in London with MERV 7 or 15 filters installed in the outdoor air stream. Triangles represent a system where $Q_{RCL}=0.33Q_{OA}$. Squares represent a system where $Q_{RCL}=Q_{OA}$.

The slope of the net benefits versus MERV curve is positive for all filters investigated in this study indicating that it is beneficial to install a high efficiency filter in the recirculating air stream. The benefits are marginal for improvements in recirculated air filter when the outdoor air filter has a high efficiency (MERV 15). For all cases investigated the net benefits are higher for operation when a high efficiency filter is installed in the outdoor air stream. This indicates that for cities with outdoor particle concentrations equal to or greater than London increasing the outdoor air filter efficiency provides a greater benefit than increasing the associated recirculating air filter efficiency when $Q_{RCL} \leq Q_{OA}$.

Figure 5.9 compares the benefits and costs of filter selection in 100% outdoor air systems with varying levels of recirculated air for the model building located in London. The effect of varying outdoor air and recirculated air filter MERV and recirculated air flow rate is studied without indoor generation. In all cases the baseline outdoor airflow is maintained and recirculated air is added as indicated.

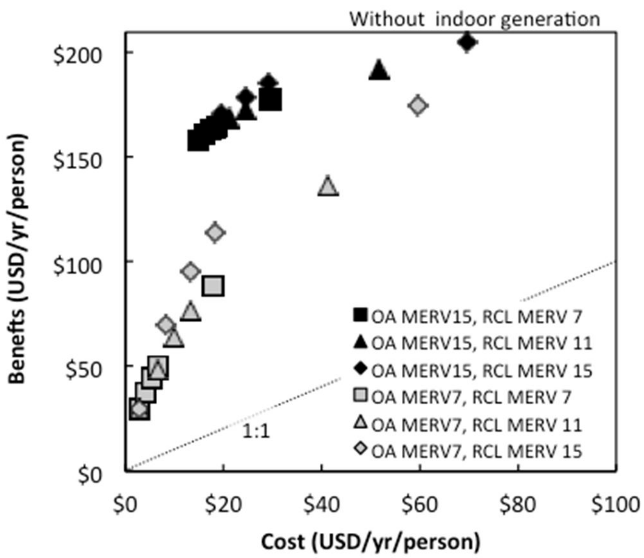

Figure 5.9: Comparison of the benefits and costs of installing different combinations of outdoor air and recirculated air filters in a 100% outdoor air system operating without indoor generation for a building in London. Each symbol type denotes a different recirculated air filter MERV and each colour indicates a different supply air filter MERV. The subsequent points in each series denote airflow increases in recirculated airflow rate (from left to right: $Q_{RCL}=0$, $Q_{RCL}=0.33Q_{OA}$, $Q_{RCL}=0.66Q_{OA}$, $Q_{RCL}=Q_{OA}$, $Q_{RCL}=4Q_{OA}$).

A comparison of the cost to benefit relation of increasing recirculation airflow rate shows that all variations of recirculation filter MERV with a constant outdoor air MERV fall approximately on the same curve. This indicates that no substantial gains are possible in system benefit through modification to the recirculated flow system without incurring an additional cost.

The use of high efficiency (MERV 15) outdoor air filters can provide a substantial additional benefit to the system for a given cost over the use of low efficiency (MERV 7) filters when no sources of indoor generation are present. For systems operating with costs greater than 20 USD/yr/person in Figure 5.9 substantial benefits can be realized without additional costs if the outdoor air filter is upgraded while simultaneously reducing the recirculated air flow rate. If a building operator is willing to pay the cost threshold associated with high efficiency outdoor air filters then filter efficiency upgrades are preferable to the use of increased recirculation airflow rate or improved recirculation filter efficiency.

5.3.4.2 Impact of Recirculation Air Filters in a Return Air System

The impact of recirculation air filters on net benefits was determined for systems with return air. The impact of recirculation air filters was found to be similar to the findings for 100% outdoor air systems. Increasing the efficiency of recirculation air filters increases net benefits when low efficiency supply air filters are installed but has little impact with high efficiency supply air filters. Increasing the airflow of the recirculation air has little impact on the system performance. The greatest benefits are possible with high efficiency supply air filters. Additional details are provided in : Supplemental Information – Chapter 5.

5.3.5 Sensitivity Analysis

Figure 5.10 shows the results of a sensitivity analysis to model input parameter values. The net benefit of filter installation was determined for variations of model input parameters of ±10% (box) or the maximum variability expected from the primary literature (whiskers). The fractional change in input parameters from the base case for maximum variability is shown in the accompanying table. The base case investigated assumes MERV 13 filters installed in a 100% outdoor air system providing the baseline ventilation requirements in London. The maximum change values for Morbidity and Mortality effect estimates used are $\pm\sigma_B$ as indicated by the USEPA [90]. The maximum change in Morbidity endpoint values are the maximum variability identified by the USEPA [90]. The maximum change in Mortality endpoint values are the range identified to contain most reasonable data by the USEPA [90]. The maximum range for the indoor aerosol dynamics model parameters are found in the primary literature indicated in Figure

5.10. Most model parameters that impact only filter cost calculations have been excluded from the presented sensitivity analysis as the change was found to have negligible impact on the net benefit calculation. An investigation of the impact of these parameters is shown in Chapter 4. The comparison was performed without indoor generation sources as this will result in higher sensitivity to model parameters.

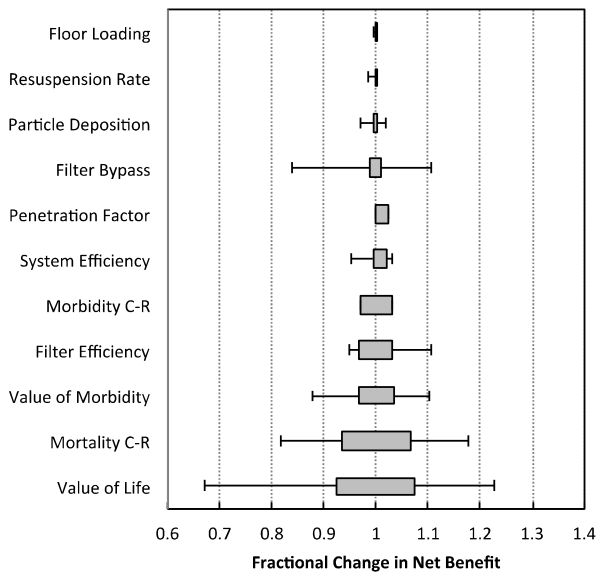

Parameter	Fraction of Base Value Lower Bound	Fraction of Base Value Upper Bound
Floor Loading	0[a]	3.6[a]
Resuspension Rate	0.1[a]	10[a]
Particle Deposition	0.33[b]	1.5[b]
Filter Bypass	0[c]	2.5[c]
Penetration Factor	0.83[d]	1.08[d]
System Efficiency	0.55	1.45
Morbidity C-R	Varies by endpoint[e]	
Filter Efficiency	0.95[f]	1.05[f]
Value of Morbidity	Varies by endpoint[e]	
Mortality C-R	0.73[e]	1.27[e]
Value of Life	0.56[e]	1.30[e]

a - Source: [160]
b - Source: [161]
c - Source: [142]
d - Source: [162]
e - Source: [88]
f - Typical filter

Figure 5.10: Model sensitivity to input parameters. The boxed regions indicate the fractional change in net benefits for a ±10% change in the parameter value from the base case. Whiskers indicate the fractional change in net benefits for the maximum change in the parameter value. Maximum changes are determined based on variability from primary sources [90,144,162-164] and are shown in the accompanying table.

The results in Figure 5.10 show that the model is most sensitive to the Morbidity and Mortality costs and C-R relations, and the efficiency of the installed filters. The model results are not sensitive to input parameters of the filter cost or indoor aerosols dynamic models. The model parameter subject to the largest variation in probable values is resuspension rate, which can vary by an order of magnitude [162]. The effect on model outputs due to a change in resuspension rate of a factor of ten is 1.4%. Particle resuspension has the greatest impact on indoor concentration of particles with a diameter >1μm. These particles do not have a significant effect on $PM_{2.5}$, which is primarily responsible for changes in health endpoints. Fan system efficiency was varied by up to 25 percentage points from the base of 55% to highlight the potential variation for systems with large differences from the model building. The significant variation in fan system efficiency changes the net benefits by up to 5%. If all input parameters are assigned their maximum/minimum values the variability in the net benefit calculation from the base case would be +106%/-73%.

5.4 Discussion

The model results will be discussed from the viewpoint of three different stakeholders: building designers, building owner/operators, and policy/guideline makers. By examining the benefits of changing operation conditions for air filtration systems from the viewpoint of different decision-making stakeholders, it is possible to develop a more nuanced understanding of the financial implications of modifications to the filtration system. The viewpoint of the building designer is likely to focus on how modifications to the physical system will impact indoor air quality and system operation while avoiding the need for significant changes to system components. The building owner/operator is largely restricted to controlling the system, within the constraints of the existing building and HVAC design, and has an interest in the benefits to the occupants that do not prevent minimizing operational cost. Policy/guideline writers have an interest in the gains to society as a whole and focus more heavily on the impacts of large-scale system decisions.

5.4.1 Recommendations for Building Designers

The provision of outdoor air is required to control the buildup of gas phase pollutants and is typically designed around control of CO_2. Adding additional outdoor air is expensive due to the need to condition air and will not provide significant reductions to indoor particle concentrations. Benefits to particle removal are only seen for small increases above the base ventilation. Increases in outdoor air should not be provided solely as a means of controlling particulate matter.

Increasing the return air flow has limited financial benefits for low flow rates when there is no indoor particle source. Increasing the airflow in systems with high levels of return air (Q_{RA}>4Q_{OA}) can cause reductions in net benefit when high efficiency filters are installed. Modest increases in return air are beneficial for particle control but are less effective than increases in supply air filter efficiency and are not recommended solely for the purpose of reducing indoor PM concentrations.

The addition of recirculated flow to provide additional filtration can be effective for reducing indoor particle concentrations for 100% outdoor air systems. The added benefit of increased recirculated airflow and filter efficiency is limited for systems that utilize return air, especially when high efficiency supply air filters are already employed. Benefits of recirculation air filters are increased for systems with indoor generation sources.

5.4.2 Recommendations for Building Operators

The optimum filter operation characteristics are not obvious for a given building or air handling system type. Calculations to determine system costs and benefits can show methods of improving indoor air quality (and occupant health) without incurring additional operation costs through changes to filtration practices.

Increasing the recirculation airflow and filter efficiency is a means of improving benefits to building occupants but has an associated increase in operation cost. If the IAQ must be improved in a building through the use of recirculation air then it is preferable to add high efficiency filters rather than adding large volumes of airflow through low efficiency filters. If the building operators are willing to pay the minimum cost associated with high efficiency supply air filters in 100% outdoor air systems, a higher benefit can be realized by the building occupant than is provided by the use of low efficiency supply air filters with added recirculation air. In general, higher benefits can also be achieved at a given cost in return air systems by increasing the supply air filter MERV while reducing the volume of return air.

5.4.3 Recommendations for Policy/Guideline Writers

The results in Figures 5.3 and 5.4 highlight inconsistencies with WHO and USEPA air quality guidelines, and LEED indoor air credit requirements (and thus ASHRAE guidelines and local building code requirements). The single prescriptive filter efficiency (MERV 13) set forth by LEED does not account for variable conditions between cities, resulting in significant variations in IAQ. A framework such as LEED, focused on energy and indoor environmental quality, would benefit from specifying a target level of indoor particle concentration such as that set forth by WHO and allow for energy efficiency to be optimized in meeting that target with specific regard to site conditions such as air handling system design and outdoor particle concentration. In contrast, if a standard MERV is to be used it would be beneficial to society as a whole to encourage the use of higher efficiency filters, such as MERV 16, as these show an increase in net benefit over MERV 13 installations. A compromise between the two methods would be regionally specific filter MERV to account for global variations in annual average outdoor particle concentrations rather than city or building specific calculations. This would allow for lower MERV requirements in regions with low annual average particle concentrations (such as rural environments) while more polluted locations (dense urban populations) could benefit from more stringent filter requirements. A filter bypass limitation is important to stipulate in conjunction with any required MERV of installed filters, to ensure that the desired indoor air quality is achieved.

It is clear that installing high efficiency filters provides a financial benefit when morbidity and mortality endpoints are considered, for the majority of aerosol and electricity price scenarios. However, the financial benefits of reduced morbidity and mortality due to improved filter efficiency are not always realized by the same party that bears the cost. This represents a roadblock for voluntary implementation of increased efficiency standards. The benefits of reduced Mortality are generally of most importance to the occupants. The cost of installing higher efficiency filters is borne by the building owner or operator. The benefits of reduced Morbidity are directly realized by the occupants but are potentially beneficial to the employer through reduced Work Lost Days or improved productivity (not explored). The financial benefits of reduced Morbidity and the added cost of improved filtration are of approximately equal magnitude, which may be motivation enough to warrant the improved systems. Policy makers are interested in benefits to society as a whole and must weigh the impacts of requiring improvements to IAQ on building operation cost and occupant health.

5.4.4 Model Limitations

The utilization of models in this work adds limitations to the predicted results. The filter efficiency is assumed to be constant as the filter loads with dust and has not been investigated for nominal filter face velocities other than 2.5 m/s. This limits the flow rates that can be tested and introduces error in the results that are highest for low efficiency filters. Additionally, it is assumed that the existing HVAC equipment has sufficient capacity to meet any increases in flow rate or resistance for the scenarios investigated. The possible interventions to existing systems will be limited if they are currently operating at flow capacity. The comparison was also limited to the use of mechanical filters (those without an electric charge). This limitation is due to available ASHRAE 52.2 test data for electret filters and can be expanded in the future. Reliance on ASHRAE 52.2 testing for model development introduces the potential for significant error in the filter models. The results of ASHRAE 52.2 testing performed in a laboratory have been shown to result in discrepancies when compared to real filter performance. One significant limitation to the procedure is the use of a test dust. This dust has been designed with the intention of simulating accumulation during service life but inevitably results in discrepancies when compared to real dust. Future improvements to ASHRAE testing methods to more accurately predict real world operations will improve the accuracy of the models used in this work. Another limitation of the model is the use of a single constant annual average outdoor particle concentration, necessitated by the lack of available short term monitoring data in cities around the world. This limitation does not allow the model to capture short-term variations in particle concentrations and how these would impact occupant exposure. Additionally, the model cannot currently be used to determine the efficacy of filtration scenarios in meeting WHO guidelines for 24-hr particle exposure limits.

The use of a limited number of epidemiological studies for effect estimates can introduce errors due to geographical and population differences. The values used in this investigation have been chosen after review of numerous studies by the USEPA [90] and can be used to provide an estimate of the relative effects of improved air quality within buildings. The model calculations have also been performed with effect estimates of plus/minus one standard deviation (as indicated in Table 5.1) to capture the uncertainty amongst leading models. These data are not shown as the trends are similar to those in this work. The use of different effect estimates changes the magnitude of calculated benefits but does not impact the trends and conclusions found in this study. If future epidemiological studies find geographical variations in effect estimate the relative results between cities in Figure 5.4 will vary but the trends of filter impact on net benefits within a given city will remain unchanged. Standard C-R functions are derived from outdoor PM concentrations and used to describe impact on occupants in the indoor environment. This will result in errors in the prediction of monetized health benefits but is currently the best available practice.

5.5 Conclusions

Indoor aerosol dynamics, filter cost, and epidemiology models have been combined to allow for a detailed investigation of the impact of filtration and air system changes on indoor air quality, monetized health benefits of occupant exposure, and system operation costs. The model has been used to investigate the impact of system changes from the perspective of building designers, building operators and policy/guideline writers accounting for differences in stakeholder objectives and level of control over system characteristics. The combined model introduced in this work can be used as a tool to inform high-level decisions or to optimize designs and existing installations.

Building designers have an interest in meeting existing indoor air quality policy and guidelines while maintaining efficient system operation. Increases in outdoor air are not effective in controlling particle concentrations and add significantly to the system operation cost. Increasing supply air filter efficiency was found to be beneficial over the range of MERV 6 to MERV 16 for 100% outdoor air systems in all cities studied and provide improvements for return air systems up to the maximum level of this study (return air equal to 4x outdoor air flow). Benefits may be seen for higher levels of return air beyond those evaluated herein. Increases in return air and recirculation air are beneficial for 100% outdoor air systems but have limitations to upper levels of flow rate that are specific to building location and system design.

Building operators are limited in the changes available to provide improvements to air quality and are generally restricted to the existing air system design. The installation of high efficiency supply air filters can improve system benefits without increases in operation costs in return air systems when the return airflow rate is simultaneously reduced. Recirculation airflow and filters can increase the benefits to occupants but typically have an associated increase in system operation cost.

The purpose of air quality design guidelines is to protect population health through control of system operation and indoor environmental conditions. This work has shown that control of indoor particulate matter is too complicated to be addressed by specifying a single minimum filter efficiency to cover all installations. The resulting indoor particle concentration is complicated by local conditions and system design. Policy decisions are better suited to mandate maximum indoor particle concentrations, not specific filter MERV, and allowing freedom of design to optimize operation cost and energy use in meeting these conditions within the restriction of the building operations. As an alternative to the current practice of setting a required MERV to cover large regions (e.g., North American or European standards) an umbrella MERV would be better suited to smaller geographic regions that captures variations in global outdoor PM concentrations and the differences between urban and rural concentrations. If specific MERVs are to be required an accompanying limit to filter bypass is critical to ensure that the desired indoor air quality is achieved by the use of the installed filters.

Future work using these models to guide policy, design, and operation would benefit from reduction in the uncertainty identified in this study. The model can also be used to develop an understanding of the impacts of other system design variables by expansion of the indoor aerosol dynamics model through the use of compartment models, stratified air systems, or personal ventilation systems. Finally, understanding the impacts of system designs could be improved by expanding the model to account for temporal variations in particle concentrations in place of the current use of the annual average concentration.

6 Impact of Relative Humidity on HVAC Filters Loaded with Hygroscopic and Non-Hygroscopic Particles[4]

6.1 Introduction

Filter performance changes throughout the lifetime of the filter as particles are captured within the media. The flow resistance of air filters increases with dust loading but follows different profiles depending on the loading characteristic of the filter type. HVAC filters typically operate as depth loading filters – those that capture particles throughout the depth of the media – and are characterized by a loading profile approximated by an exponential curve [120,129]. HEPA filters exhibit a very short depth loading stage that then transitions to surface loading where the dust forms a cake layer on the surface [108,110,165]. The cake continues to grow as incident particles are captured at the surface. The relation between flow resistance and dust loading follows a linear profile with a slope determined by the particle characteristics. Previous experiments studying the impact of relative humidity on filter behavior have focused on HEPA filters [107,115,116]. The previous work shows that RH influences loading behavior and can change resistance of loaded HEPA filters. The focus was on surface loading filters and operation at flow resistance higher than those seen for HVAC systems. Particles captured throughout the depth of HVAC filters are dispersed and characterized by dendrite growth instead of the densely packed particles in surface loaded HEPA filters [27].

At high relative humidity salt particles will deliquesce. Changes in properties of hygroscopic particles are impacted by particle size and have been shown to occur at relative humidity far below the deliquescence relative humidity (DRH) for nano-sized particles [166,167]. The Growth Factor (GF) represents the change in particle size from the dry diameter and is a function of particle size, relative humidity, and salt studied. For

[4] A version of this chapter has been published. Montgomery, J. F., Green, S. I. & Rogak, S. N., (2015). Impact of relative humidity on HVAC filters loaded with hygroscopic and non-hygroscopic particles. Aerosol Science and Technology 49(5), 322-331.

low relative humidity (<70%) and nano-sized particles (diameter <200nm) the GF is larger for smaller particles and higher RH [168]. Sodium chloride has also been shown to have a reversible uptake of liquid water on the surface for RH below deliquescence that can impact particle shape [167] and potentially, particle-particle interactions. These mechanisms could be responsible for structural changes in particles with relative humidity that results in changes to loaded filter performance [117].

The purpose of this study is to evaluate the impact of changes in RH on properties of loaded HVAC filters. Filter loading is performed for hygroscopic and non-hygroscopic particles to compare the impact of particle properties. This work provides insight into the importance of relative humidity for operation of real HVAC air filters, which are subject to variations of relative humidity throughout the loading cycle. The results will provide potential explanation for discrepancies seen between laboratory and field-testing of filter performance changes with particle loading.

6.2 Experiment and Methods

The experiments were performed in a laboratory test bench (Figure 6.1) that allows for control of flow rate, aerosol size and concentration, and relative humidity. The flow in the circuit is controlled at a constant flow rate throughout the experiment using a vacuum pump with a critical orifice on the inlet side. The aerosol source is a TSI 3076 constant output atomizer connected to cleaned and dried compressed air. The aerosol is passed through a desiccant drier to remove all moisture within the airstream. A TSI 3077 aerosol neutralizer is used to achieve a Boltzmann charge distribution. A make-up air stream ensures flow balance in the system and is used to control the relative humidity by modulating the proportion of make-up air that passes through a humidifier or desiccant drier.

The samples tested are 50mm diameter flat sheets of media from commercial filters. The flow velocity on the filter face is maintained at a constant 11cm/s during testing by means of a critical orifice. This velocity was selected as it is representative of the flow velocity through the media of typical pleated filters during normal operation. The flow resistance is measured throughout the experiment using a pressure transducer (Omega Model PX274) connected to a data acquisition system (LabJack U3-HV). The size-resolved aerosol number concentration is determined using a TSI 3936 Scanning Mobility Particle Sizer (SMPS). Continuously alternating measurements upstream and downstream of the filter were taken throughout the experiment and later used to determine the filter efficiency at any time during loading.

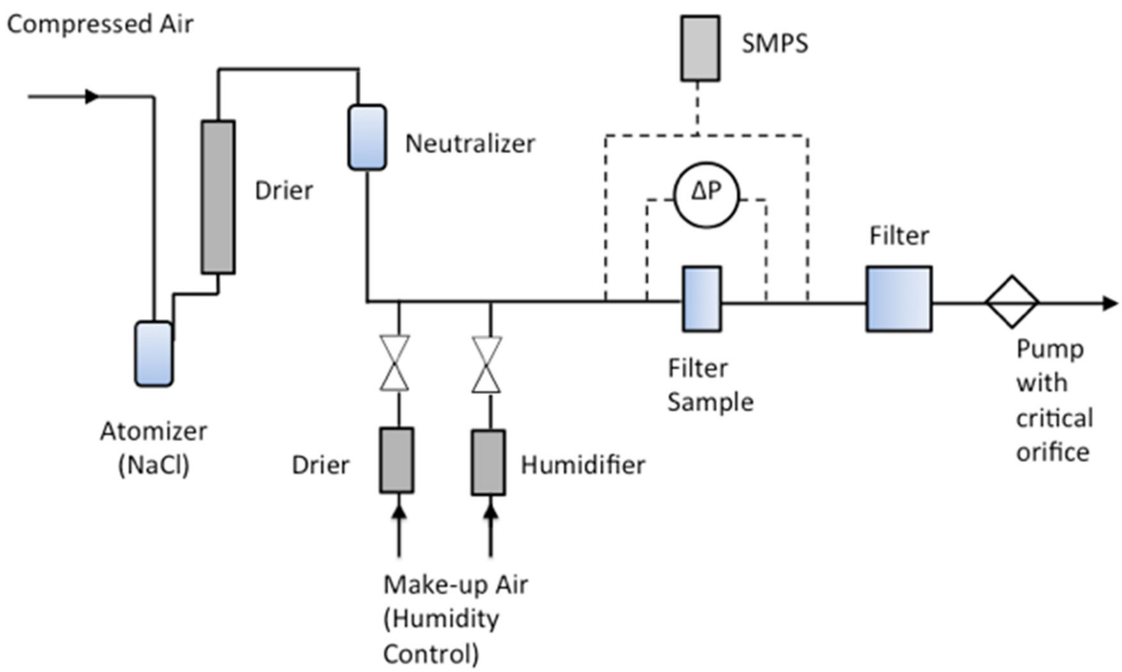

Figure 6.1: Schematic of filter loading test bench

The filter is loaded with hygroscopic (NaCl), non-hygroscopic (Al_2O_3), or a mixture of particles. The normalized particle number size distributions are shown in Figure 6.2 for particles during testing of hygroscopic or non-hygroscopic loading only. For loading with mixtures of particles the particles are atomized and dried separately to ensure consistency of size distributions before mixing and an additional vacuum pump and critical orifice are used to maintain the same total particle concentration and filter face velocity as that of the single particle-type experiments.

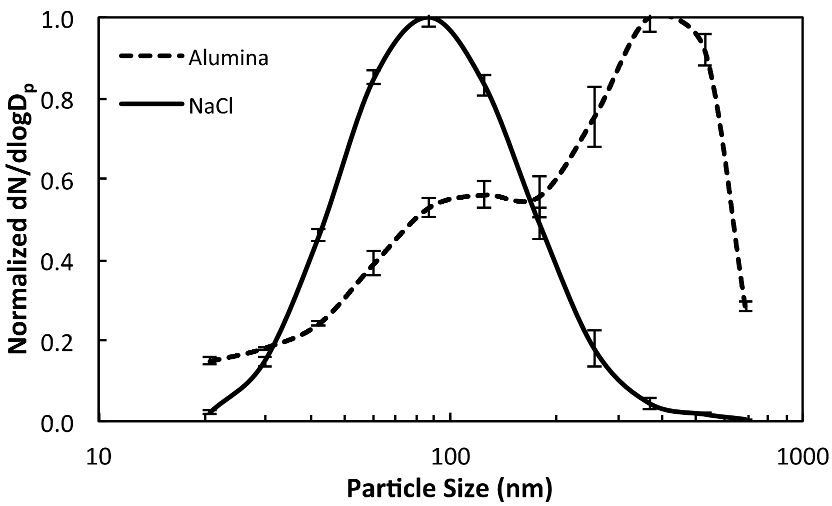

Figure 6.2: Normalized size distribution of alumina and sodium chloride particles used for filter loading

The filter media properties are shown in Table 6.1. The initial flow resistance of each filter was determined by averaging the initial flow resistance for all samples tested in this work. The range reported indicates the standard deviation. The average fiber diameter was determined by calculating the length-weighted mean fiber diameter from scanning electron microscope (SEM) images of the filter media samples. The media thickness was determined by measuring the cross section of the media from SEM images.

Media from two different commercial HVAC filters were tested; one electret and one mechanical. The mechanical filter (Filter 2) is rated as MERV 14 by ASHRAE 52.2-2012 testing [67]. The electret filter (Filter 1) is rated as MERV 14 by ASHRAE 52.2-2012 and A13 by ASHRAE 52.2-2012 Appendix J for discharged performance. The charged samples are designated as Filter 1c and the discharged samples as Filter 1d. The charge was removed from the electret filter by submerging the media in isopropyl alcohol for 30 minutes and letting dry for 24hrs. Submersion in the isopropyl alcohol does not change the physical properties of the filter and acts only to remove the electric charge [64] as is confirmed by comparing the initial pressure drop of the charged and discharged filter samples in Table 6.1. The 30-minute submersion was chosen after comparing the filter efficiency of media samples submerged for 5-120 minutes and finding no difference for submersion times greater than 15 minutes. This is in line with a previous review of electret filter discharge by submersion that found a variety of procedures between 2 minutes and 2 hours with no clearly developed standard [169]. Tests with samples of Filter 2 with and without submersion in isopropyl alcohol were performed to confirm that there was no impact and justify the decision to include testing only with samples without treatment.

Table 6.1: Filter properties

Filter	MERV	Type	Initial Flow Resistance (Pa) at V=11cm/s	Average Fiber Dia. (μm)	Media Thickness (μm)
1c	14	Charged	25.6 ±1.1	34	800
1d	A13	Discharged	25.5 ±2.1	34	800
2	14	Mechanical	77.3 ±3.1	1.9	430

The purpose of this work is to investigate the impact of relative humidity changes on the flow resistance and filtration efficiency of loaded HVAC air filters. The air filters are loaded under a range of relative humidity between 0-60% to represent low to medium RH conditions in real filter operations. The relative humidity during loading remains below the deliquescence relative humidity of NaCl, ~75%, [168,170] for all experiments in this work. Filters may experience relative humidity between 0-100% during real operating conditions. The results above deliquescence are expected to vary from those below and are the topic of potential future investigations.

After the end of the loading process (determined by a desired flow resistance) the atomizers were switched to a low concentration (resulting in a total number concentration of ~4x10^5 particles per m^3 of air) to ensure that the relative humidity conditions were maintained but no significant change in filter performance (resistance or efficiency) resulted from the continuous flow of particles. The loaded filter efficiency was determined under these steady state airflow conditions with the relative humidity equal to that during loading. The relative humidity of the airstream is then modified by adjusting the make-up air control valves to allow for exposure to relative humidity of a predetermined level. After the system reaches equilibrium the filter efficiency is once again measured.

6.3 Results

6.3.1 Impact of Relative Humidity on Clean Filter Properties

The initial filter conditions were tested for three levels of relative humidity with hygroscopic particles (NaCl). The filter sample was placed in the apparatus with clean air and the flow resistance recorded for 1hr at each of 0%, 20%, and 40% RH. No difference in flow resistance, nor filtration efficiency, of clean filter samples was observed for either the electret (charged or discharged) or mechanical filters. This finding is in line with previous experiments [116].

6.3.2 Hygroscopic Particles

Filters were loaded with hygroscopic particles to a final normalized flow resistance, $P^*=(P-P_i)/P_i$, equal to 4, where P is the flow resistance (Pa) and P_i is the flow resistance of the clean filter sample (Pa). The loaded filter samples were then exposed to a clean air stream controlled to a predetermined relative humidity. The system was allowed to come to equilibrium and the filter properties determined in the new state.

6.3.2.1 Charged Electret Filter

Figure 6.3 shows curves of normalized flow resistance versus time for Filter 1c samples loaded with NaCl. Time, *t*, equal to zero indicates the time at which the relative humidity was changed from the RH at loading to the RH of exposure. The curves are labeled A%->B% where A is the relative humidity during loading ($t<0$) and B indicates the relative humidity that the loaded filter is exposed to for $t>0$. The filter loading stage ($t<0$) to achieve $P_f*=4$ occurs over approximately 2.5hrs.

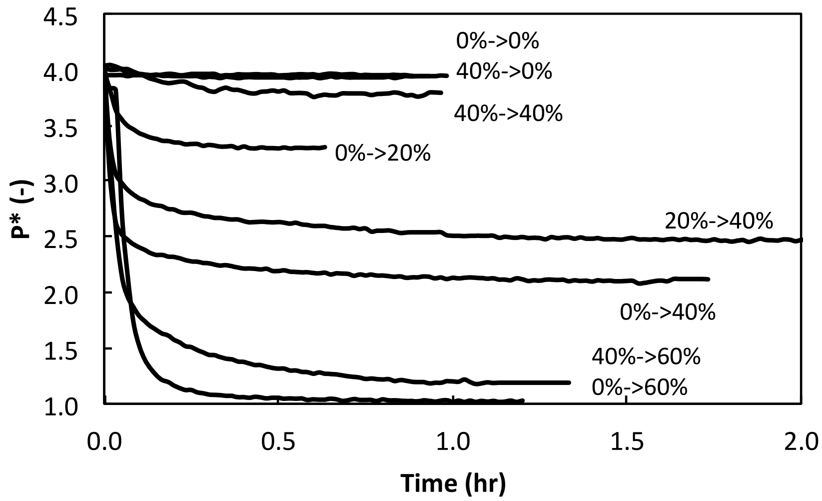

Figure 6.3: Change in resistance of Filter 1c when exposed to clean air with RH=B% after loading with NaCl at RH=A%. Curves are labeled as A%->B%.

When filters loaded with hygroscopic particles at 0% relative humidity are exposed to a higher RH there is an associated reduction in flow resistance. The reduction in flow resistance increases with increased exposure RH. The average reductions in normalized flow resistance after exposure for Filter 1c were 0.65±0.08, 1.74±0.20, and 2.86±0.08 for 0%->20%, 0%->40%, and 0%->60%, respectively. When filters are exposed to relative humidity lower than or equal to that during loading (ie. 40%->0% and 0%->0%) there is no change in associated flow resistance. Additionally, the reductions in flow resistance when exposing the loaded filters to a higher RH are not reversed if the RH is then lowered to 0% indicating that an irreversible physical change has occurred. This trend of reduced flow resistance with exposure to high relative humidity was seen for all filters tested. A sub-set of the results are shown in this work and are in agreement with the existing literature [116].

The changes in flow resistance are not limited to experiments with loading at 0% RH. When filters are loaded at 20% RH and then exposed to 40% RH the reduction in normalized flow resistance was found to be 1.49±0.03; greater than that from the 0%->20% (0.65±0.08) and less than the 40%->60% (2.50±0.01) experiments. The 40%->60% experiment results in a greater loss of flow resistance than the 0%->40% experiment but less than the 0%->60% experiment, which has the largest reduction in resistance of all scenarios tested. These comparisons indicate that the change in flow characteristics is a function of both the RH during loading and the exposure RH.

When a filter is loaded at 40% RH and exposed to clean air at 40% RH a small reduction in flow resistance is seen with time. This could be due to the particles requiring more time to achieve equilibrium than is provided between generation and deposition in the media. The particles are generated from liquid solution, dried to 0% RH in a desiccant drier and then mixed with moist air to adjust the RH. The slight decline in RH between t=0, when the relative humidity changes, and the equilibrium point of constant P* could be a result of changes in particle size as the last particles deposited come into equilibrium. Joubert et al. [117] noted a similar phenomenon when dust cakes were formed at 46% RH and left to come to equilibrium with 46% RH air.

Figure 6.4 shows the change in filtration efficiency (for 130nm particles) versus change in normalized flow resistance of filter samples loaded and exposed to the range of relative humidity tested in this work.

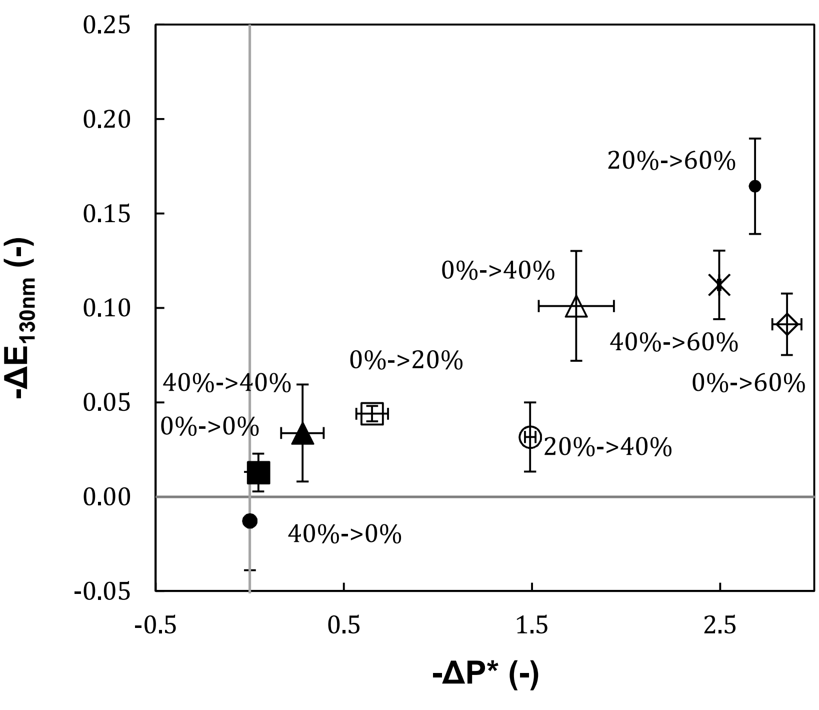

Figure 6.4: Change in efficiency (D_p=130nm) and normalized flow resistance of Filter 1c when loaded with NaCl at RH=A% and then exposed to clean air with RH=B% (A%->B%). The error bars represent the standard deviation of all experiments performed at the indicated condition (min. of 4).

The results in Figure 6.4 show that the changes in flow resistance due to exposure of loaded filters to varying levels of RH are accompanied by changes in the filtration efficiency. Filters exposed to a RH equal to or less than that during loading show little change in either filtration efficiency or flow resistance. The general trend shows that larger changes in normalized flow resistance after exposure are accompanied by larger changes in efficiency as would be expected from filtration theory. Filters loaded at 0% RH and then exposed to 20% RH or 40% RH show a reduction in filter efficiency of approximately 5 and 15 percentage points, respectively. Filters loaded at 20% RH and exposed to 40% RH show a smaller decrease in efficiency and flow resistance than do those loaded at 0% RH and exposed to 40% RH. The filters loaded at 20% RH and exposed to 40% RH show a similar change in filtration efficiency as the 0%->20% experiments but have a significantly greater change in flow resistance. Exposure of filters to 60% RH after loading at 0%, 20% or 40% RH show the highest changes in flow resistance and a change in efficiency approximately equal to the 0%->40% tests.

6.3.2.2 Discharged and Mechanical Filters

Similar experiments were performed for the discharged electret filter and the mechanical filter. The results follow a similar trend as those discussed in detail for experiments with charged electret filters, indicating that the impact of RH is not unique to electret filters. Figure 6.5 shows the change in filtration efficiency for 130nm particles versus the change in normalized flow resistance for Filter 1d and Filter 2 after loading with sodium chloride. Exposure of the loaded filter to a relative humidity lower than or equal to that during loading produces little to no change in either flow resistance or filtration efficiency. Filter 1d shows a reduction in filtration efficiency of approximately 15 percentage points and a drop in normalized flow resistance of approximately 1.9 when exposed to 40% RH after loading at 0% RH.

In contrast, Filter 2 shows no change in filtration efficiency when exposed to 40% RH after loading at 0% RH but has an associated reduction of normalized flow resistance equal to approximately 0.68. The lack of efficiency change may be explained by the high efficiency of the filter, which reaches a plateau of approximately 0.95 before reaching P*=4 (fully loaded). Just as it is possible for a filter to have increasing flow resistance with no increase in efficiency during loading, it is plausible that the restructuring of the particles present in the filter can impact flow resistance without an appreciable change in efficiency.

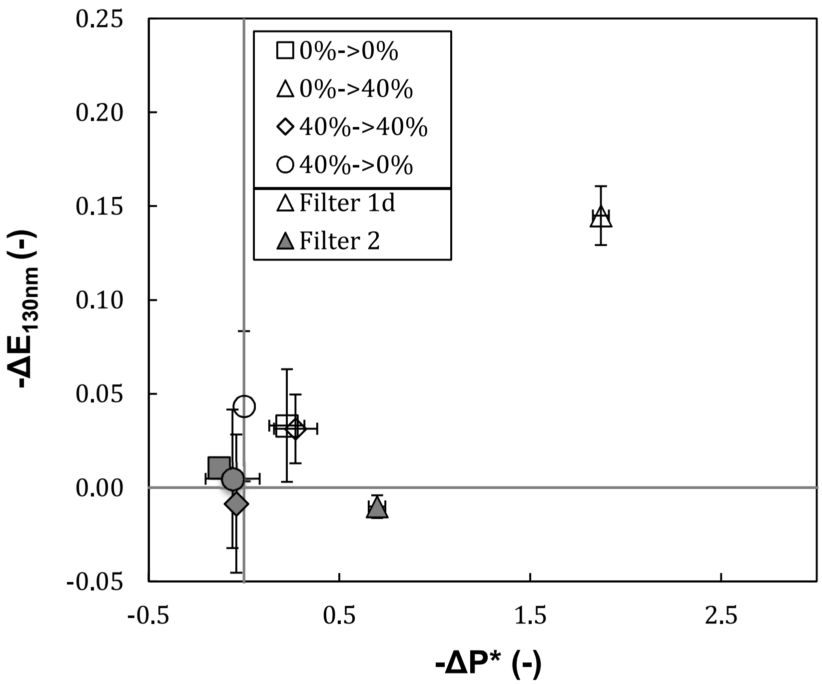

Figure 6.5: Change in efficiency (D_p=130nm) and normalized flow resistance of Filter 1d and Filter 2 when loaded with NaCl at RH=A% and then exposed to clean air with RH=B% (A%->B%). The error bars represent the standard deviation of all experiments performed at the indicated condition (min. of 4).

6.3.2.3 Impact of Filter Loading

Figure 6.6 shows the change in normalized resistance and efficiency (D_p=130 nm) of filters loaded and exposed to different relative humidity for final loaded normalized resistances (P_f*) up to 5. The loading is performed with NaCl particles. This allows for a comparison of the impact of different filter loading levels on the importance of relative humidity during filter operation. Each of the three filters are presented in the figure; a) Filter 1c, 0%->40%, b) Filter 1c, 40%->60%, c) Filter 1d, 0%->40%, and d) Filter 2, 0%->40%.

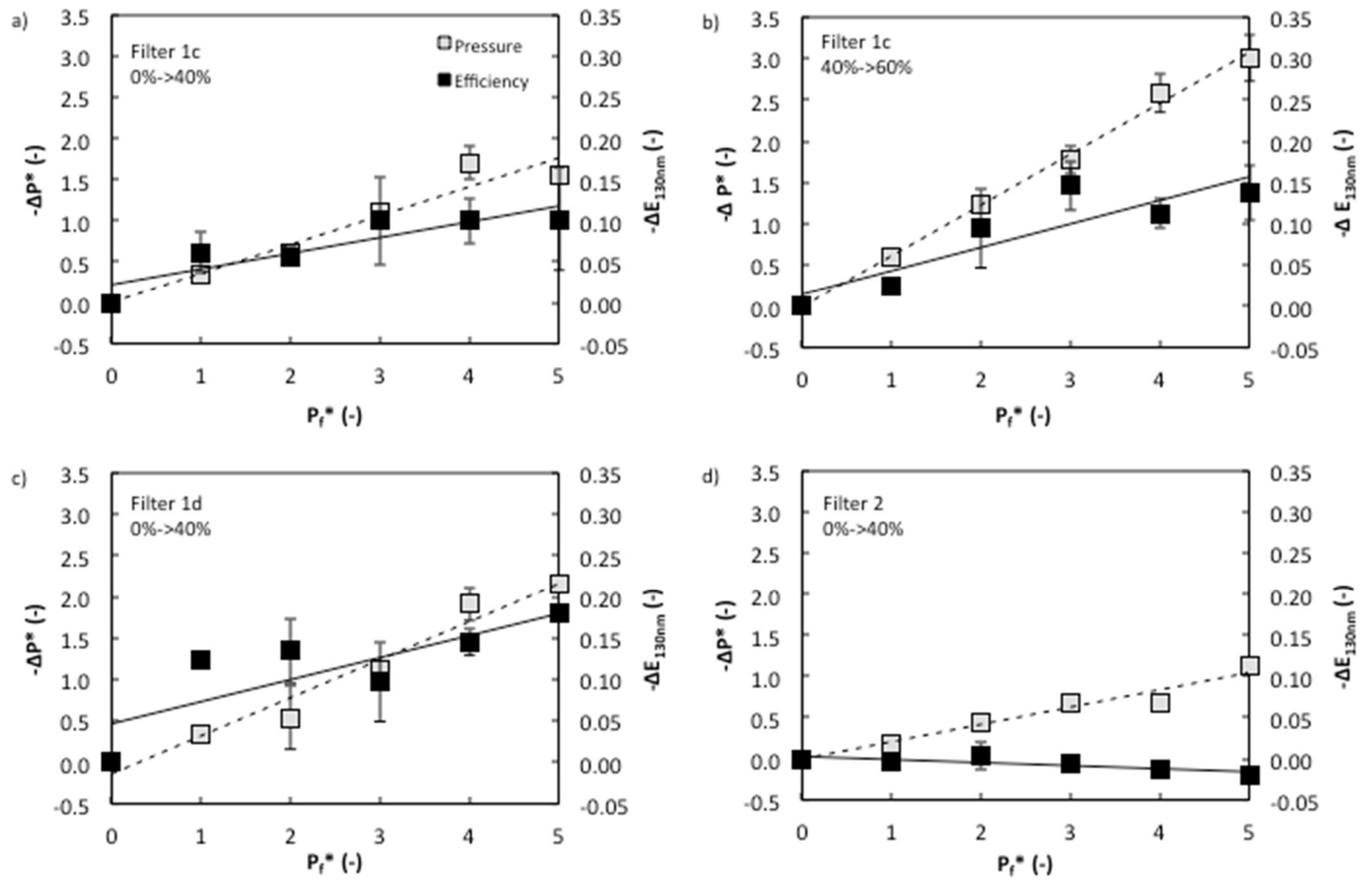

Figure 6.6: Change in normalized flow resistance and filtration efficiency (D_p=130nm) for varying levels of loading with NaCl; a) Filter 1c, 0%->40%, b) Filter 1c, 40%->60%, c) Filter 1d, 0%->40%, and d) Filter 2, 0%->40%. The error bars represent the standard deviation of all experiments performed at the indicated condition (min. of 4).

The change in normalized flow resistance after exposure shows a linear dependence on the final normalized resistance due to dust loading in the filter. When the filters are loaded with more salt (higher P_f^*) a larger drop in resistance occurs after exposure to elevated RH. The slope of the linear regression lines for each filter tested for 0%->40% are statistically significantly different (within a 95% confidence interval) indicating that the dust load is a factor in final flow resistance and captured dust is impacted by relative humidity in different ways depending on the filter properties. The slope of the $-\Delta P^*$ versus P_f^* regression lines are 0.35±0.04 and 0.46±0.04 for the Filter 1c and 1d, respectively. Filter 2 has a lower slope (0.21±0.02) than Filter 1, indicating that it is not as heavily influenced by the degree of salt loading. Potential reasons for this may be the salt aggregate structures, distribution, or density. The regression lines shown have an intercept of ~0 as expected because the filter structure itself is not impacted by relative humidity in the absence of particle loading.

The change in efficiency for 130 nm particles ($-\Delta E_{130nm}$) after exposure to 40% RH is also best described by a linear relation with the final normalized resistance due to dust loading in the filter, although the data show significantly greater variability. This is in part due to the uncertainty in efficiency measurements from comparisons of upstream and downstream particle number concentrations. Both the charged and discharged variations of Filter 1 show a general trend of greater changes in efficiency after exposure to 40% RH when they are loaded to higher levels of dust loading. Filter 2 shows essentially no change in efficiency due to exposure to 40% RH regardless of the level of salt loading. This could be explained by the high efficiency of the mechanical media and rapid increase in efficiency during loading. There is only a small difference in efficiency of Filter 2 loaded to $P_f^*=2$ and $P_f^*=5$ (0.94 and 0.97, respectively, a difference of 0.03) indicating that the dust is not adding appreciably to the efficiency of the filter and will therefore not impact the efficiency if it undergoes morphological changes. In contrast, the efficiency of Filter 1d loaded to $P_f^*=2$ and $P_f^*=5$ is 0.68 and 0.79, respectively, a difference of 0.11, which shows that the salt continues to add significantly to the efficiency of the filter throughout all levels of loading investigated.

A comparison of Figure 6.6a and 6.6b shows the impact of different loading and exposure RH on changes to loaded filter characteristics. The slope of the linear regression lines are statistically significantly different (within a 95% confidence interval) with a larger slope for 40%->60% tests (0.62±0.02) than for 0%->40% tests (0.35±0.04) even though the humidity range is smaller. This supports the previous evidence showing that the change in loaded filter properties is a function of both loading and exposure RH and is seen over the entire range of loading tested in this work. The filtration efficiency shows greater variability than the changes in normalized flow resistance but the slope of the 40%->60% tests (0.029±0.007) is greater than that of the 0%->40% tests (0.019±0.004). This comparison indicates that the particles captured within the filter media are more sensitive to changes in RH for exposure closer to the deliquescence relative humidity.

6.3.3 Non-Hygroscopic Particles

Similar experiments were performed using Filter 1 and loading with alumina to determine the impact of relative humidity changes on non-hygroscopic particles. Figure 6.7 shows the results of filtration efficiency changes for 130nm particles versus changes in normalized flow resistance for the combination of experiments with relative humidity of 0% and 40%. Similar to the experiments with hygroscopic particles there is no substantial change in properties when a loaded filter is exposed to a relative humidity less than or equal to that during loading. A small change in normalized flow resistance (<0.4) is seen when filters loaded at 0% RH with alumina are exposed to 40% RH. This result differs slightly from the findings for surface loaded filters, which showed no change in flow resistance of filters loaded with alumina in dry air and exposed to a higher relative humidity [117]. This may be the result of small impurities in the alumina powder used in the experiments. The change for Filter 1c loaded with NaCl at 0%->40% RH conditions is shown in the figure for reference.

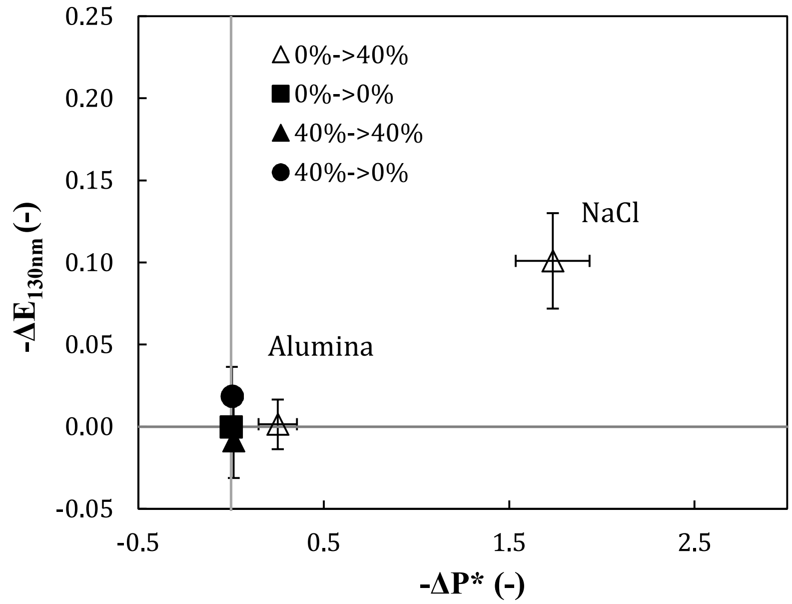

Figure 6.7: Change in filtration efficiency (D_p=130nm) and normalized flow resistance of Filter 1c loaded with alumina at RH=A% and then exposed to clean air with RH=B% (A%->B%). The error bars represent the standard deviation of all experiments performed at the indicated condition (min. of 4).

6.3.4 Mixtures of Hygroscopic and Non-Hygroscopic Particles

Experiments were also conducted with mixtures of hygroscopic and non-hygroscopic particles to more closely approximate real air systems. The composition of atmospheric aerosols is a complex function of time and location. Atmospheric aerosols include organic and inorganic, hygroscopic and non-hygroscopic particles that cannot be truly simulated within the lab environment. As a general approximation the fraction of hygroscopic particles can be taken as 0.5±0.3 [171].

Figure 6.8 shows the change in normalized flow resistance (a) and filtration efficiency (b) when Filter 1c samples are loaded with a mixture of hygroscopic (NaCl) and non-hygroscopic (Al_2O_3) particles at 0% RH and exposed to 40% RH. The experiments have been performed for aerosol mixtures between 0-100% alumina particles to provide an indication of the importance of aerosol mixture composition and allow for a comparison with real operations over a range of conditions.

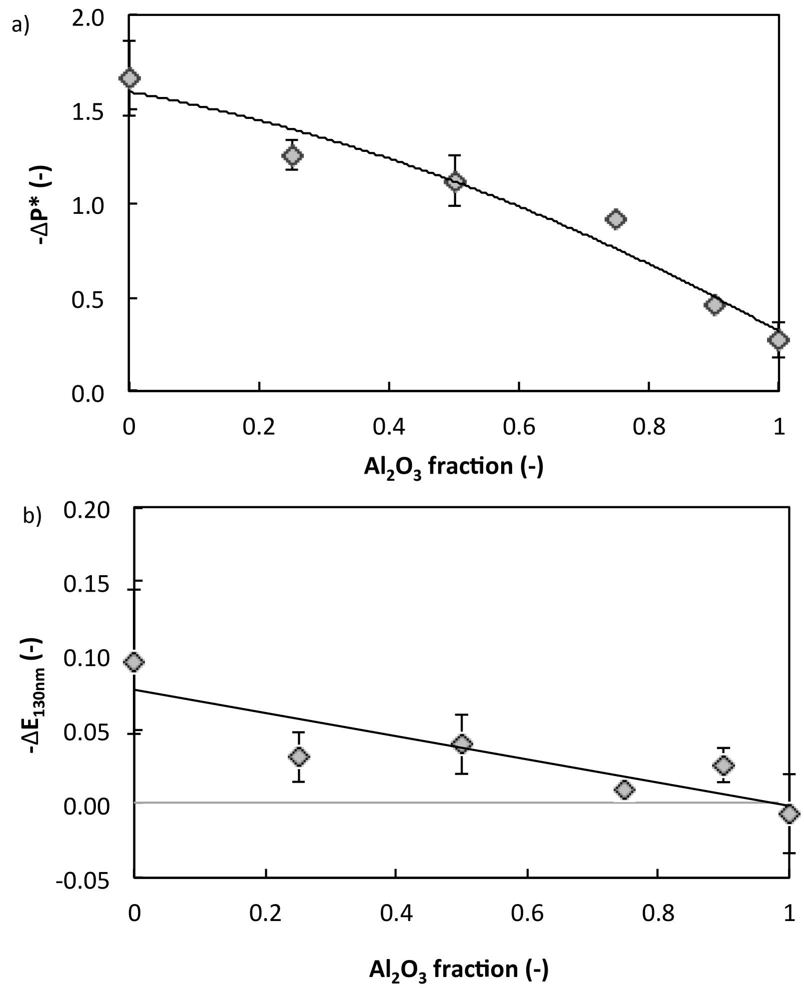

Figure 6.8: Change in normalized pressure (a) and filtration efficiency (b) for Filter 1c exposed to 40% RH, after loading with a mixture of NaCl and Al_2O_3 aerosols in varying proportions at 0% RH. The error bars represent the standard deviation of all experiments performed at the indicated condition (min. of 4).

The impact of exposure to elevated relative humidity is a function of the aerosol mixture present during the loading process. The change in filter performance characteristics is greater for higher fractions of hygroscopic particles. The change in normalized flow resistance due to exposure to elevated RH is lowest for 100% alumina particles and is potentially present as a result of hygroscopic impurities in the alumina powder as discussed in Section 6.3.3. The change in normalized flow resistance after exposing the loaded filter to 40% RH decreases as the ratio of alumina particles to sodium chloride particles increases. The increased change in normalized flow resistance is non-linear with the greatest rise seen for initial addition of NaCl to 10% and 25% of the total aerosols.

The change in normalized flow resistance after exposure to 40% RH when loaded with a 50:50 particle mixture at 0% RH is approximately half that found for 100% NaCl particles in Figure 6.4.

The impact of exposure to elevated RH on filtration efficiency is also increased as the fraction of alumina particles decreases. The relation is best described by a linear fit but has a higher degree of variability than the normalized flow resistance. The change in filtration efficiency for exposure to 40% RH is ~0 for an aerosol of 100% alumina particles and rises to ~0.1 for 100% NaCl. A filter loaded with a 50:50 particle mixture shows a loss of efficiency equal to somewhat less than half that found for the same filter loaded only with NaCl particles. As the non-hygroscopic particles have shown no response to changes in relative humidity any changes are a result of the fraction of loaded particles represented by NaCl. The NaCl particles can have an impact on the non-hygroscopic alumina particles as they are mixed in the flow and will deposit as mixed aggregates on the filter media.

Similar to the experiments with either hygroscopic or non-hygroscopic particles, exposing a filter loaded with a mixture of particles to a relative humidity less than or equal to the RH during loading results in insignificant changes in the normalized flow resistance and efficiency (results not shown).

6.4 Discussion

The results from this work show that relative humidity during loading and exposure of air filters with hygroscopic particles can significantly impact the filter properties. Reductions in filtration efficiency and/or flow resistance were seen for all tests where a filter loaded with hygroscopic particles was exposed to a relative humidity higher than that during loading. No changes in properties were seen with relative humidity changes when the filter was loaded with non-hygroscopic (alumina) particles. Filters loaded with mixtures of hygroscopic and non-hygroscopic particles showed a response to humidity changes indicating that relative humidity can be an important factor in real filter operation. The changes in filter properties after exposure to an elevated relative humidity were found to be irreversible when the filter was exposed again to a reduced RH but further changes were seen upon subsequent exposure to even higher RH. The irreversible nature of the process along with the constant properties of a clean filter at varying levels of relative humidity indicates that the particles captured in the filter media are undergoing a morphological or structural change. Measurements of downstream particle concentration during the testing shows that the loss of flow resistance due to exposure is not accompanied by an increase in downstream particle concentration and that all of the particle mass remains within the filter media during the changes.

Joubert et al. [117] have proposed that similar changes seen in the filtration characteristics when HEPA filters are exposed to elevated RH are a result of swelling of individual particles in the filter cake. The work of Hu et al. [168] shows that hygroscopic particles exhibit a Growth Factor of between 0-10% for particles 20-200nm over a relative humidity range of 0-70%. The HVAC filters investigated in this study do not form dust cakes but rather capture the particles throughout the depth of the media. Captured particles grow as aggregates into dendrite structures [112]. A potential explanation for the change in loaded filter properties with relative humidity is a change in the physical structure of these aggregates and dendrites.

Figure 6.9 shows a schematic of a possible structural change of a dendrite of captured particles when exposed to elevated relative humidity. The initial dendrite structure is formed as particles are captured within the media at low RH (Figure 6.9a). If air at an elevated RH then passes through the filter the hygroscopic particles will absorb moisture and grow in size (Figure 6.9b). This growth of the individual particles can impose forces on the dendrite structure if they are constrained, resulting in potential damage or reshaping of the aggregates (Figure 6.9c). A change in shape would result in changes of flow resistance and filtration efficiency which are both functions of particle arrangement within the filter media [110].

As the non-hygroscopic particles have shown no response to changes in relative humidity any changes are a result of the fraction of loading represented by hygroscopic particles. The hygroscopic particles can have an impact on the non-hygroscopic particles as they are mixed in the flow and will deposit as mixed aggregates on the filter media. Therefore the possibility exists for a dendrite to contain hygroscopic particles at the base that can cause the entire structure of mixed particles to collapse.

Another potential cause of changes in aggregate shape along with growth of the particles could be uptake of water on the particle surface. Nano-sized NaCl particles have been shown to uptake liquid water films when exposed to high relative humidity below the deliquescence point [167]. Water uptake has been shown at a relative humidity as low as 65% [172]. The potential exists for this mechanism at lower RH, though it has not been observed experimentally. The uptake of liquid water would result in surface tension being imposed on adjacent particles in the aggregate structures, which could add to the change or collapse of the aggregate morphology.

The general trends of flow resistance changes in this work were also seen for filters loaded with Na_2SO_4 particles and carbon soot particles generated from a PALAS GFG 1000. The similar response of both Na_2SO_4 and NaCl particles indicates that the structural change is not a result of the specific hygroscopic particle used. Weingartner et al. [173] has shown that suspended carbon soot agglomerates show reductions in mobility size when exposed to airstreams with increasing RH. This lends support to the potential for collapse of aggregates of hygroscopic particles when exposed to RH well below deliquescence.

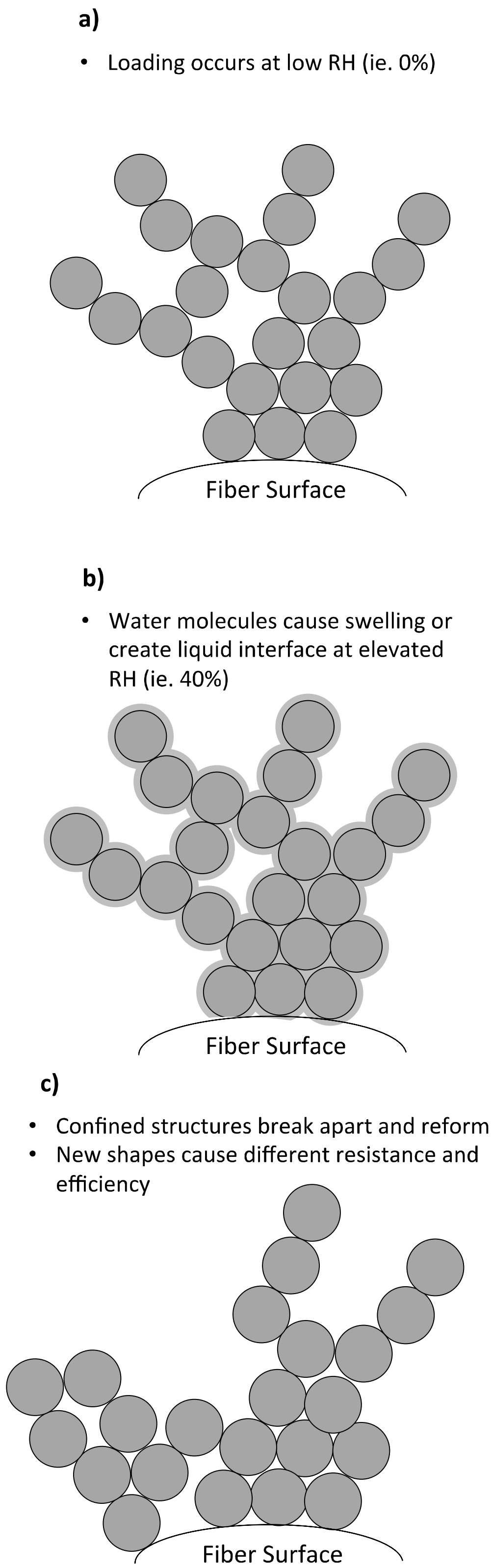

Figure 6.9: Schematic of potential particle aggregate changes due to growth of individual particles constrained in the structure when exposed to elevated relative humidity

The changes in loaded filter characteristics seen in this study will also be present in filters loaded under similar conditions in real installations. The range of relative humidity tested (0%-60%) is common in many HVAC systems. For example, cities in Arizona and other desert locations experience long periods with outdoor relative humidity of less than 20% in the summer months and increasing humidity through the winter. Under these conditions the flow resistance and filtration efficiency resulting from loading under dry conditions could be dramatically altered after exposure to the elevated RH.

The response of loaded filters to changes in RH presented in this work shows that a change or cycling from low to high RH will result in a different filter performance than would be seen for a filter operating under constant RH conditions. Changes in filter properties due to changes in relative humidity can result in variations in performance characteristics between installations in different locations or at different times and present a barrier for even comparison of in situ filter operation. The existing ASHRAE 52.2-2012 test methods do not account for variations in relative humidity during loading. The significant impact of relative humidity on loaded filter properties is a potential explanation for the differences seen between real and laboratory filter operations [95]. These discrepancies are likely to be greater for filters operating in locations with higher fractions of hygroscopic particles and will be difficult to predict from the existing knowledge on this topic.

6.5 Conclusions

This study investigated the influence of relative humidity on properties of air filters loaded with hygroscopic and non-hygroscopic particles. Flat sheets of commercial filter media were loaded with sodium chloride and alumina particles in a laboratory test apparatus. After loading at a specified relative humidity the filters were then exposed to clean air. A reduction in flow resistance and filtration efficiency were seen when the relative humidity of the clean air for exposure was higher than that during loading for filter media loaded with hygroscopic particles. The changes observed were found to be irreversible in nature, indicating an underlying physical change in the structure of the captured dust. No changes were observed for the bare filter or for filters with adhering non-hygroscopic particles.

The impact of the exposure to relative humidity was found to be a function of the filter media, the level of dust loading and both the loading and exposure relative humidity. The changes were greater with increased levels of dust loading and for filters loaded with higher proportions of hygroscopic particles. The greatest changes were seen when the loaded filter was exposed to the highest level of relative humidity in the study (RH=60%). The relative humidity range tested was limited to 60% to ensure no deliquescence of hygroscopic particles but is still relevant for many real world HVAC installations.

A hypothesis for the underlying physical change in particle properties responsible for the change in filter characteristics was presented. It is postulated that the aggregates of particles captured within the filter media while loading at low relative humidity undergo a growth in the primary particle size when exposed to elevated RH. This increase in particle size could impose stresses on the structure resulting in physical restructuring of the captured dust, which would explain the irreversible changes. Further research to identify and quantify changes in particle aggregate structures with relative humidity is required to confirm this hypothesis.

The results from this work have shown that relative humidity can be an important factor in determining the operation characteristics of an HVAC air filter. This can result in modifications in effectiveness or energy costs to operate a filter between installations that has not previously been considered. Future iterations of the standardized test method should be developed that account for humidity variations to ensure that the filter performance during standardized testing more closely resembles the performance in real installations.

7 Structural Change of Aerosol Particle Aggregates with Exposure to Elevated Relative Humidity[5]

7.1 Introduction

Experiments in the previous chapter compared performance of loaded HVAC filters after exposure to changes in relative humidity. Changes to the relative humidity of the airstream incident on the loaded filter were found to cause substantial changes in flow resistance and filtration efficiency which is consistent with experiments on HEPA filters [117]. These changes result only when the filters are exposed to increases in relative humidity and are found to be irreversible with reductions in incident RH. The changes in filter performance are greater for higher degrees of filter loading and greater fractions of hygroscopic versus non-hygroscopic particles. The results are consistent with the hypothesis that a physical restructuring of the captured hygroscopic particles occurs but further physical evidence is required.

The tandem differential mobility analyzer (TDMA) has been used to study growth of hygroscopic particles over a range of relative humidity from 0% to 100% [168,174,175]. Hygroscopic particles show significant growth at the deliquescence relative humidity and moderate growth for nano-sized particles when exposed to relative humidity far below deliquescence. Weingartner et al. [173,176] utilized the TDMA setup to show the restructuring of spark generated and engine soot. The change in agglomerate size was attributed to a restructuring of the particles due to surface tension of localized condensation. The degree of change was attributed to primary particle size and surface chemistry from engine operation. The potential for restructuring of aggregates of hygroscopic particles has not been studied.

Relative humidity (RH) plays a key role in the morphology and state of hygroscopic particles. A detailed review of H_2O-NaCl interactions has been provided by Ewing [177].

[5] A version of this chapter will be submitted to a peer-reviewed journal.

Numerous studies have investigated the interactions of water molecules with salt crystal structures. Atomic force microscopy and scanning polarization force microscopy have shown that water adsorbs preferentially at steps and non-uniformities in the crystal surface at relative humidity as low as 30% [178-180]. Infrared spectroscopy has shown that at room temperature H_2O adsorbs on to surface defects at low RH and forms water adlayers and thin films on the crystal surface [181,182]. The water interaction with salt crystals leads to changes in microscopic morphology such as rounding of edges and restructuring of steps that can have implications for particle interaction.

The purpose of this work is to investigate the impact of relative humidity on the structure of particle aggregates formed by coagulation while airborne or after deposition on fibrous media. The aim is to provide supporting evidence for the hypothesis that structural changes in deposited aggregates within the filter media is the mechanism responsible for changes of filter performance.

7.2 Experiment and Methods

Structural changes of aggregates were investigated using two methods. Airborne aggregates formed by Brownian coagulation were investigated using a TDMA setup with humidity control. Aggregates formed due to deposition and particle growth on fibrous media were investigated using fluorescence microscopy and a humidity controlled flow cell.

7.2.1 TDMA Analysis

In the TDMA setup (Figure 7.1), aerosol samples were generated using a TSI 3076 constant output atomizer connected to clean, dry compressed air. The aerosol passed through a diffusion drier containing $CaSO_4$ to remove all moisture within the airstream. A TSI 3077 aerosol neutralizer was used to achieve a Boltzmann charge distribution on the primary particles. The airstream was then humidified to the desired RH by controlling the volume fraction of air bypassing a tube with a wetted fabric lining. Aggregation occurs within the aging loop with a residence time of 30 minutes. The particle aggregate size studied was determined by controlling the voltage on the DMA column used for size selection. The airstream containing size-selected aggregates was then mixed with air of a controlled relative humidity and the size distribution measured using a TSI 3936 Scanning Mobility Particle Sizer (SMPS).

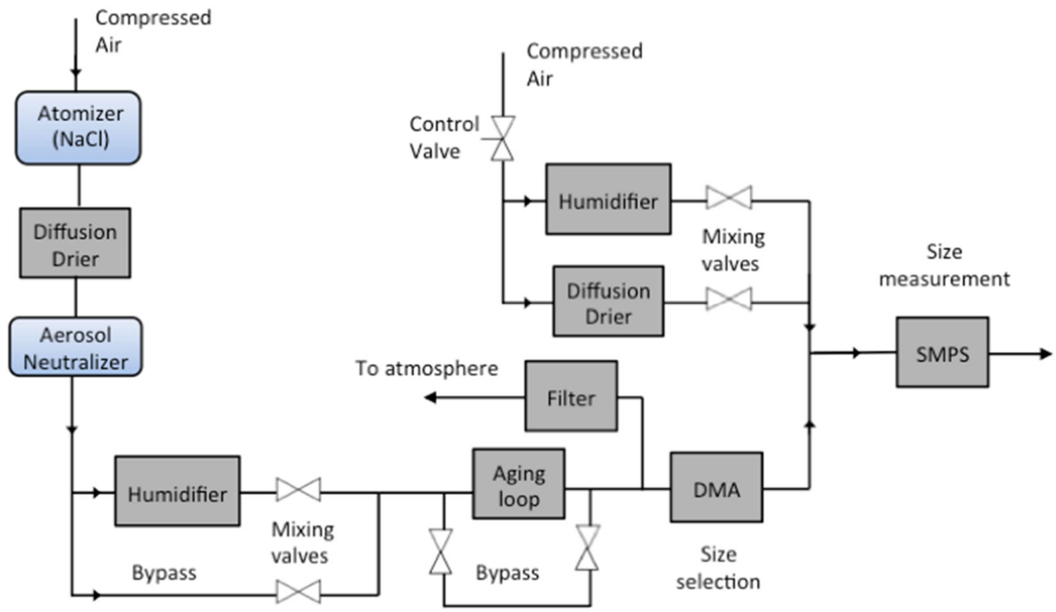

Figure 7.1: Schematic of TDMA experiment

The size distributions of hygroscopic aerosols before and after the coagulation loop is shown in Figure 7.2 for 0% RH conditions. These distributions are normalized by the peak concentration, which is naturally much reduced in the aging chamber. The distribution before coagulation is similar for all inlet RH tested in this work (0%-60%). Three types of atmospherically relevant hygroscopic particles were chosen; NaCl, Na_2SO_4, and $(NH_4)_2SO_4$, with deliquescence relative humidity of 75.3%, 84.2% and 80.2%, respectively, at 298 K [183]. Tests were also performed with aggregates of non-hygroscopic Al_2O_3 particles.

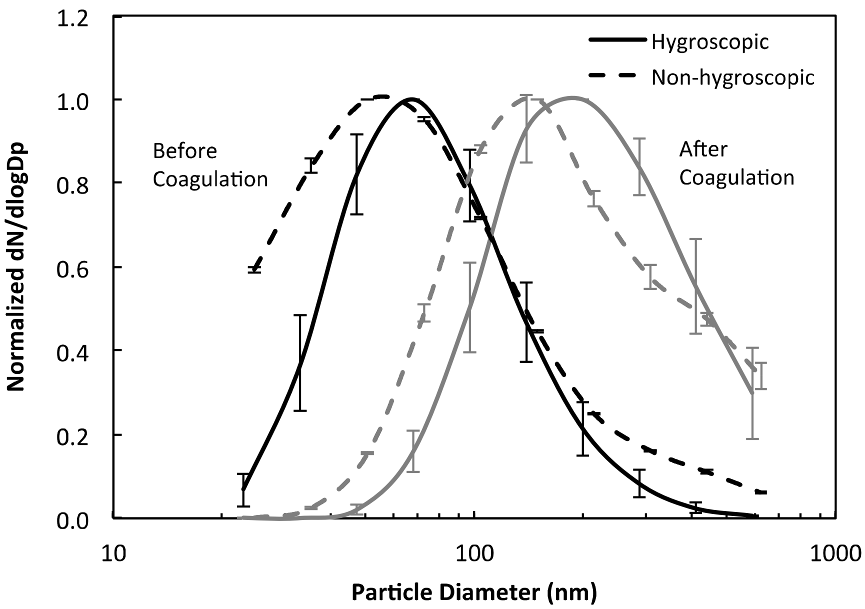

Figure 7.2: Size distribution of hygroscopic (NaCl, Na_2SO_4, $(NH_4)_2SO_4$) and non-hygroscopic (Al_2O_3) particles before and after coagulation at 0%RH. Error bars indicate the standard deviation of measurements.

7.2.2 Microscopy Analysis

The impact of RH on aerosol aggregate structures was analyzed using fluorescence microscopy imaging techniques. The visualization technique is a modified version of that used to determine phase change characteristics of single particles [184,185]. The aggregates analyzed in this work are formed from particles deposited on wire mesh from bulk aerosol flow using techniques similar to those of the filter loading experiments of Chapter 6. The loading and visualization apparatus are shown in Figure 7.3.

A 50mm diameter sample of 400x400 mesh, 25 μm diameter woven stainless steel mesh was used as a substrate to collect aerosol aggregates. A 2.5 g/L NaCl solution was atomized at 40psi using a TSI 3076 constant output atomizer to generate an aerosol that was then dried in a diffusion drier before passing through a TSI 3077 aerosol neutralizer (Figure 7.3a). Flow through the mesh is maintained at a constant superficial velocity of 11 cm/s by means of a critical orifice. The flow resistance of the clean mesh sample is 10.5 Pa at V=11cm/s. The aerosol flow is diluted by a 0% RH make-up airflow stream to ensure balanced flow in the system.

As the aerosol passes through the mesh, deposits of NaCl form aggregate structures [112]. The loading occurs until a desired normalized final flow resistance ($P_f^*=P_f/P_i-1$) is reached. The compressed air is then directed for 120s to the second atomizer containing a solution of Rhodamine that generates fluorescent seed particles (geometric mean diameter of 61.7 nm and geometric standard deviation of 1.79) that deposit on the NaCl aggregates. The Rhodamine particles are approximately two orders of magnitude smaller than the NaCl aggregates and act as point sources of light during fluorescent imaging that are used to quantify structural changes of the aggregates. The relative humidity was maintained at 0% throughout the coating operation and the addition of Rhodamine particles did not add measurably to the flow resistance of the loaded mesh sample. Alternative methods of marking the deposits, such as atomizing Rhodamine and NaCl together, were attempted but resulted in poorer images.

After coating the NaCl aggregates with Rhodamine the loading test cell was placed inside a glovebox maintained at RH <5%. The loaded mesh was removed, cut to size, and loaded into the flow cell as shown in Figure 7.3b. A 2.8 LPM (±0.1LPM) supply of 0% RH ultrahigh purity nitrogen (Praxair, 99.999%) flow was connected to the inlet side of the flow cell before removal from the glovebox to ensure that the loaded aggregates were not exposed to elevated relative humidity.

The mounting plate of the flow cell was connected to the stage of a fluorescent microscope (Zeiss LSM510; $\lambda_{excitation}$ = 543 nm, $\lambda_{emission}$ = 560-615 nm). The relative humidity of the airstream through the cell was controlled to either 0%RH by use of unconditioned N_2 or a controlled elevated RH by using gate valves to redirect the flow through a water bubbler inside a refrigerating circulator (Thermo Neslab, RTE-140) at a specified temperature. The relative humidity was calculated using the temperature surrounding the cell and the dewpoint reading from a hygrometer (General Eastern, Hygro M4) connected to the outlet flow. Images were captured at 10s intervals for a 15min experiment consisting of 5min exposure to 0% RH, 5min exposure to elevated RH, and 5min exposure to 0% RH. The images were then analyzed to determine changes in deposit geometry.

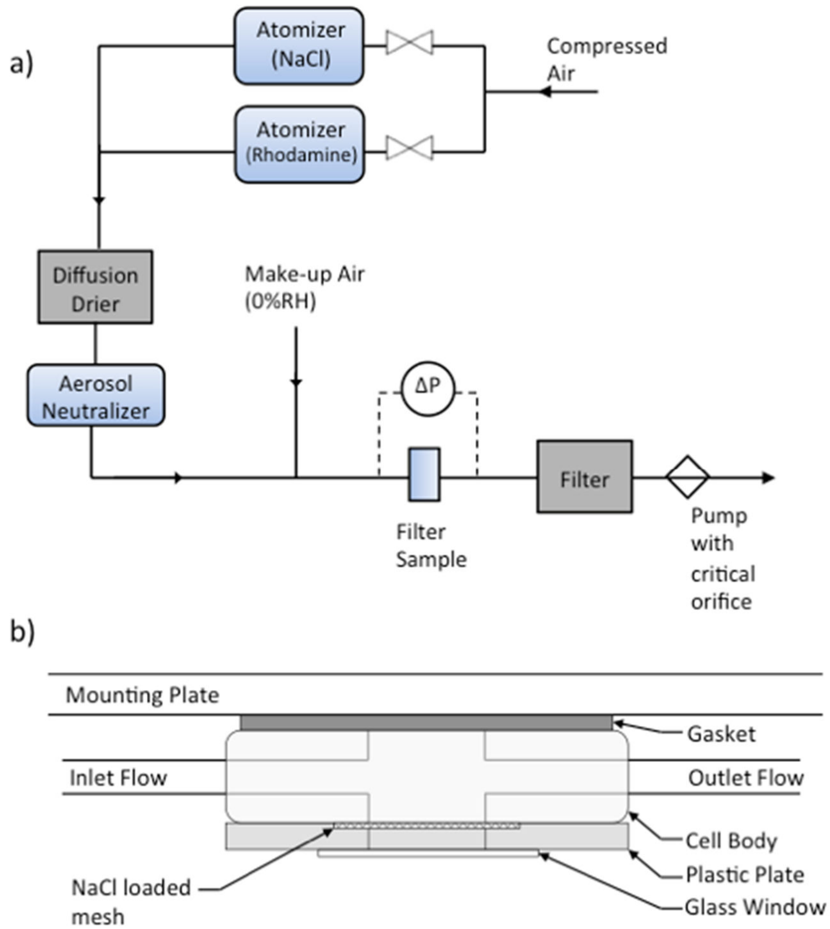

Figure 7.3: Schematic of the mesh loading (a) and visualization flow cell (b) apparatus.

7.3 Results

7.3.1 Tandem DMA Analysis of Airborne Aggregates

7.3.1.1 Sodium Chloride Aggregates

Figure 7.4 shows the size distributions of NaCl aerosols aged at 0% RH and then mixed with an air stream with the indicated relative humidity. Figure 7.4 plots the distribution determined using output from the TSI Aerosol Instrument Manager; for the peak locations reported later, a different inversion procedure was used. The 0%->0% distributions represent the base aggregate size whereas the distributions for elevated relative humidity represent changes in the aggregate structure. The base aggregate size is selected by controlling the DMA voltage for the given experiment over the range of relative humidity tested. Each set of distributions is determined from separate classifier voltage settings and represents distinct experiments. The series are labeled as A%->B% where A is the RH during coagulation and B is the RH after mixing downstream of the size selection.

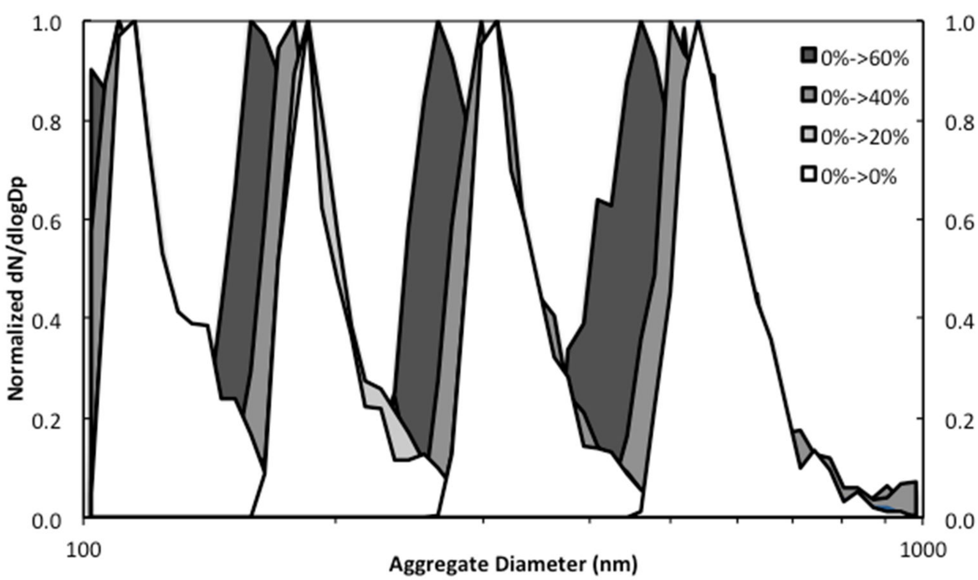

Figure 7.4: Change in size selected distributions for NaCl aggregates aged at 0% RH and exposed to varying RH. The series are labeled as A%->B% where A is the RH during aging and B is the RH after mixing downstream of size selection.

No appreciable change in distribution is observed in Figure 7.4 between 0%->0% and 0%->20% RH. The distributions show a distinct shift towards smaller diameter for both the peak and leading edge as relative humidity is increased above 20%. Elevating RH to 40% and 60% causes sequentially greater shifts in the size distribution. As the measurements are on aggregates (not single particles) this indicates a collapsing of the open structure to a more densely packed aggregate.

The degree of collapse can be quantified by comparing the Growth Factor of the peak particle diameter. The Growth Factor is defined as the ratio of the aggregate diameter after exposure to the specified relative humidity versus the aggregate diameter after coagulation; $GF=d_e/d_i$. A Growth Factor of less than 1 indicates a reduction in aggregate size. The raw particle count data extracted from the SMPS was used to determine the concentration in 248 size bins between 100 and 1000 nm using the equations and methodology outlined by Flagan [186] and similar to that of the default analysis with the

TSI software. A lognormal curve was fit to the concentration data to use for determining the location of the distribution peak. To eliminate the influence of noise on the curve fit only data for size bins with a concentration greater than 20% of the max were considered. The GF is then determined by comparing the peaks of relevant distributions. A sample of the measured and curve fit data for a 0%->60% experiment is shown in Figure 7.5.

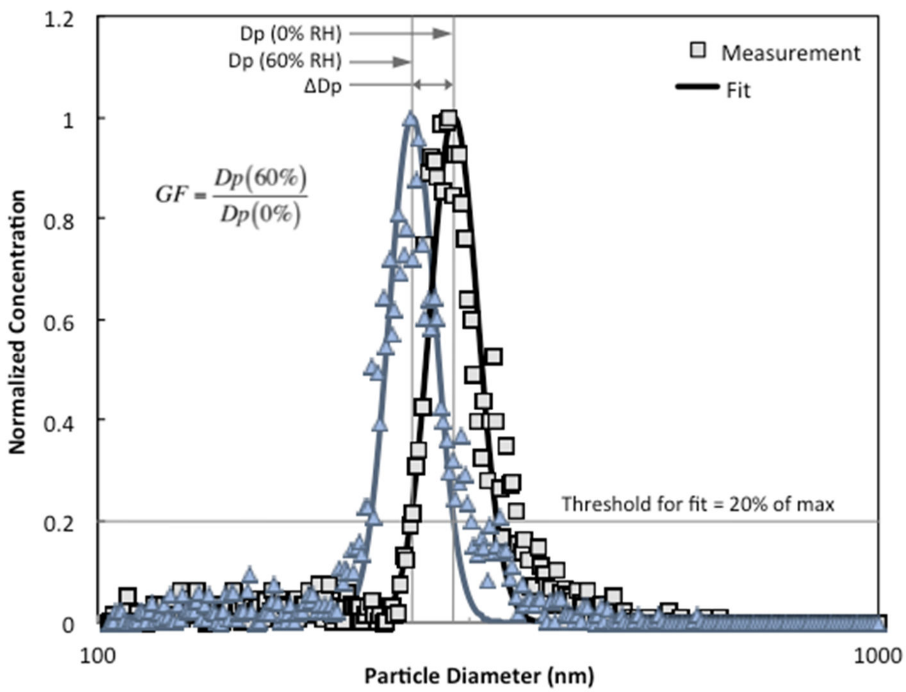

Figure 7.5: Sample lognormal curve fitting procedure to determine peak aggregate size from measured TDMA data for a sample 0%->60% experiment with NaCl.

A summary of the GF of the peak particle diameter versus initial diameter is shown in Figure 7.6 for combinations of initial and exposure relative humidity consisting of 0%, 20%, 40%, and 60% RH; all below the deliquescence relative humidity of sodium chloride. The data series are denoted by A%->B% where A is the relative humidity during coagulation and B is the relative humidity to which the airstream is raised through mixing after size selection.

Figure 7.6a shows the result of increasing the relative humidity from 0% to 20%, 40%, or 60%. The dashed line represents the uncertainty in the measurement technique and is calculated as one standard deviation of the Growth Factor calculated from 0%->0% tests (a sample of which are indicated by black X's). The Growth Factor of aggregates does not show a statistically significant change for exposure to 20% RH. Exposure to 40% RH shows an average Growth Factor of ~0.97 for 115nm particles and a slope of $-6.5\times10^{-5}\pm3.3\times10^{-5}$ for a linear regression fit to the GF versus dry aggregate size. Exposure to 60% RH shows a more significant response with a GF of ~0.95 for 110nm aggregates. The linear regression fit to the 0%->60% GF results has a slope of -2.6×10^{-4} $\pm3.3\times10^{-5}$ (within a 95% confidence interval). Thus tests show a decrease in Growth Factor with increasing initial aggregate size, indicating that aggregates comprised of more primary particles are more heavily influenced by changes in relative humidity.

The results for GF of peak diameter of aggregates formed at RH greater than 0% are shown in Figure 7.6b. All combinations of relative humidity in the figure show a GF of less than 1 for the large aggregates studied (>500nm) and decreasing Growth Factor with increasing aggregate size. The 20%->60% experiments show the lowest GF and the greatest reduction in GF as would be expected. The 20%->40% experiments also show a GF statistically smaller than 1 for aggregates ~200nm. The 20%->40% experiments show smaller GF than do the 0%->40% experiments presented in Figure 7.6a.

Figure 7.6c shows the Growth Factor for aggregates formed at relative humidity of 20%, 40%, or 60% that are then mixed with a 0%RH flow stream (reducing RH to less than 6% in each case). There is no statistically significant change in the diameter of the peak size. This indicates that the change in structure seen in Figure 7.6a&b is not a result of a *change* in RH but is specific to an *increase* in relative humidity. These results are in line with changes to the properties of filters loaded with hygroscopic particles in Chapter 6 [187].

Additional experiments from 0%RH to elevated RH were also conducted with Na_2SO_4 and $(NH_4)_2SO_4$ aerosols (results not shown). Those additional experiments similarly showed aggregate size reductions with exposure to elevated relative humidity. Aggregates formed from lower concentrations of NaCl showed similar responses to elevated RH.

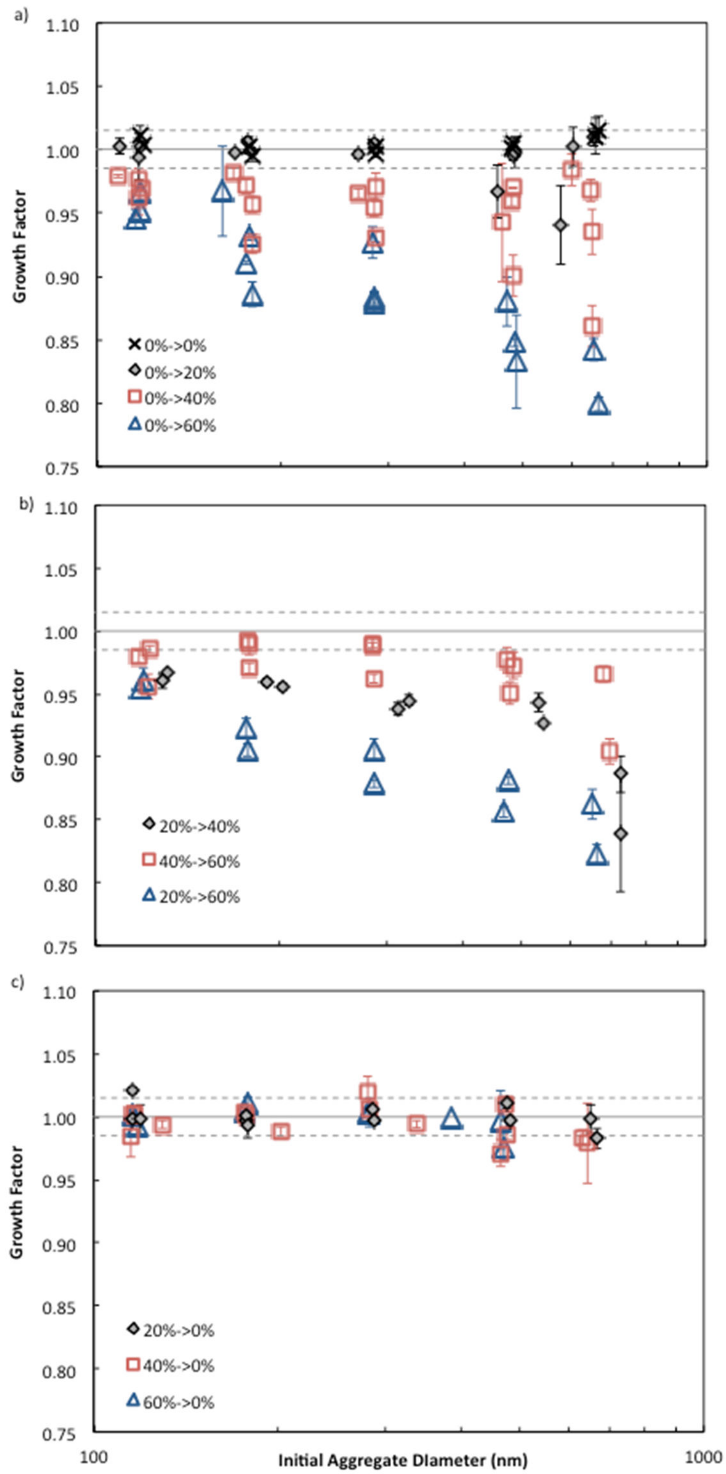

Figure 7.6: Impact of relative humidity changes on peak particle size of NaCl aggregates for (a) increases from 0%RH, (b) increases from intermediate RH, and (c) decreases to 0% RH. The dashed lines represent one standard deviation of the 0%->0% to indicate variability of the measurement method.

7.3.1.2 Alumina Aggregates

TDMA experiments were also performed using non-hygroscopic Al_2O_3 particles atomized from a liquid suspension and dried in a manner similar to that described for NaCl. Figure 7.7 shows the Growth Factor versus original aggregate size for Al_2O_3 aggregates formed in the coagulation chamber at 0%RH and then mixed with air to a final elevated RH of 20%, 40%, or 60%. The results show no statistically significant change in aggregate size for the range of experiments performed. These results are in line with experiments of filters loaded with Al_2O_3 which showed no change in flow resistance with exposure to high RH [115,116,187] and contrary to those loaded with hygroscopic particles. Weingartner et al. [173,176], however, showed that agglomerates of spark generated or diesel engine exhaust show a small restructuring when exposed to elevated RH. Image analysis of single particles have shown water uptake on hygroscopic particles below deliquescence but not on non-hygroscopic particles [167]. The discrepancy may be a result of differences in primary particle size between experiments. The soot agglomerates of Weingertner et al. [173,176] consisted of ~10nm primary particles compared to the ~100nm Al_2O_3 particles studied here. This would result in a significant difference in the wettability of the surface structure due to different contact angles between particles [188,189].

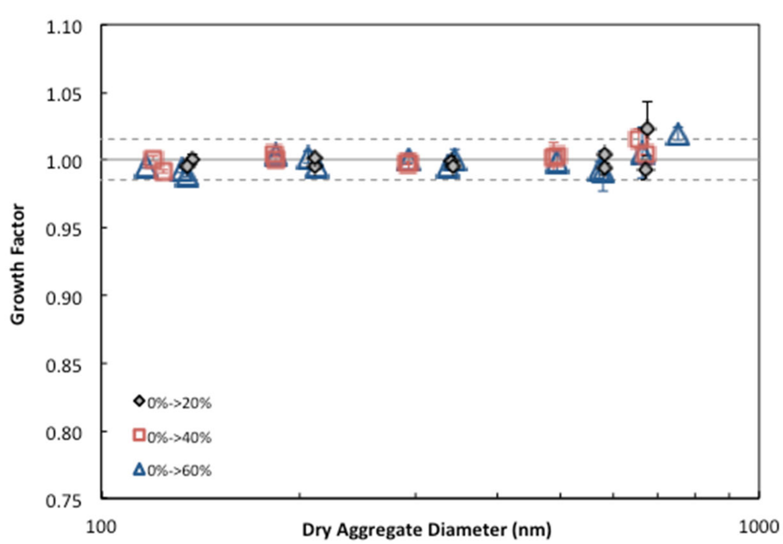

Figure 7.7: Impact of relative humidity changes on peak particle size of Al_2O_3 aggregates for increases from 0%RH.

7.3.1.3 Comparison of Hygroscopic Particle Aggregates

Figure 7.8 compares the Growth Factor of aggregates formed at 0% RH and then exposed to air streams with elevated relative humidity up to 82%. The experiments were conducted for aggregates of NaCl, Na_2SO_4 or $(NH_4)_2SO_4$. Similar experiments with primary particles (no coagulation) are shown for comparison. A direct comparison of the impact of salt type is not possible from this work due to the inability to ensure that aggregates of the same mobility size for different salts are comprised of the same primary particle size and structure.

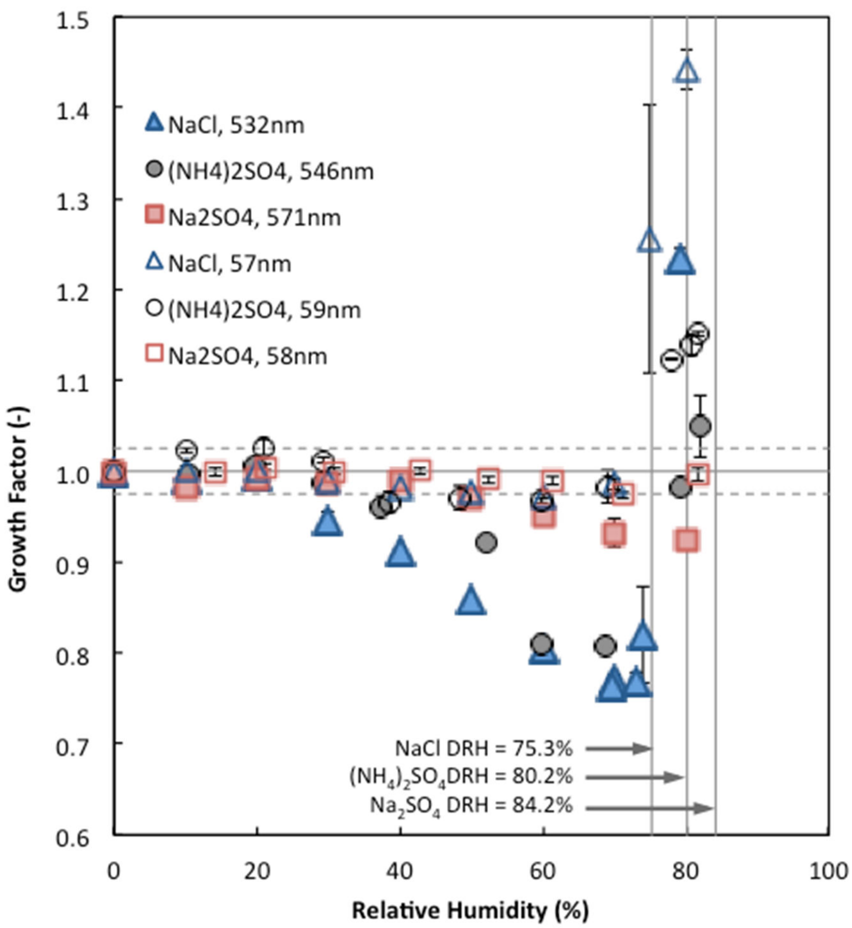

Figure 7.8: Growth factor of hygroscopic aggregates and primary particles formed at 0%RH and exposed to increasing relative humidity. The solid symbols represent data for aggregates. The open symbols represent data for single particles. The error bars are the standard deviation from multiple measurements during the same experiment.

All aggregates tested show a statistically significant GF <1 when the relative humidity is increased above 30%-40% RH. The Growth Factor decreases (indicating shrinking particle size) with increasing RH similar to the previous work studying agglomerates of carbon particles [176]. At the deliquescence relative humidity of the salt (~75% for NaCl, ~80% for $(NH_4)_2SO_4$) the trend reverses and the Growth Factor increases drastically to a GF>1 which indicates that the liquid droplet is larger than the initial aggregate structure. The results show that restructuring of aerosol aggregates occurs for a number of atmospherically relevant particle types when exposed to elevations in relative humidity prior to deliquescence.

Both NaCl and $(NH_4)_2SO_4$ show similar trends of reduced Growth Factor prior to deliquescence. The aggregates of Na_2SO_4 particles also show a continuous decline in GF to the final measurement at 80% RH. No increase in GF was seen for Na_2SO_4 as the apparatus was limited to a RH less than the DRH of ~84%. The Na_2SO_4 aggregates show less of a reduction in Growth Factor with increases in RH than the aggregates of other salts in this work. Potential reasons for this difference include the lower solubility of Na_2SO_4 and the potential formation of a thermodynamically stable hydrate ($Na_2SO_4 * 10H_2O$) at higher RH. Experiments with additional salt types are required to develop a better understanding of the impact of particle properties on aggregate restructuring.

The size of a collapsed aggregate can be approximated theoretically from aerosol fractal theory [190]. If the primary particles are assumed to have a diameter equal to the peak concentration diameter before coagulation (75 nm) and form aggregates of 532 nm (to match NaCl in Figure 7.8) with a fractal dimension of 1.8 and mass mobility exponent of 2.1, complete collapse to a sphere would result in a diameter of 296 nm. This represents a Growth Factor of 0.56, which is substantially lower than the minimum 0.77 shown in Figure 7.8. The real aggregate will not collapse to form a perfect sphere as the particles have a physical limit on packing fraction and the rearrangement is likely to maintain certain aspects of the geometry before collapse. This theoretical approach nonetheless provides a suitable lower bound for the potential collapse of aggregates.

The reduction in particle mobility diameter resulting from exposure to increased RH is consistent with a contraction of dendrite structures. Single hygroscopic aerosol particles show a restructuring or reformation of surface defect with increasing RH. [191-194] This is a result of the interaction of H_2O molecules with the salt surface, which results in adlayer formation of water at relative humidity far below deliquescence.[167,172,195] The formation of water layers on the surface of salt particles forming an aggregate provides an explanation for contraction of the aggregate structure. As water adsorption at the contact point between primary particles in the aggregates it will impose surface tension forces. [188,189] Force imbalances due to variations in geometry and surface properties could result in aggregate restructuring.

7.3.2 Image Analysis of Deposited Aggregates

Image analysis of aggregate structure on wire mesh samples can provide further insight into the physical changes that occur as aggregates formed at low relative humidity are exposed to airstreams with elevated RH. A sample optical image of a loaded mesh is shown in Figure 7.9 using a 63x objective. The long white cylindrical features are the steel wires of the woven mesh. Deposited on these wires are aggregates of NaCl nanoparticles. The aggregates range considerably in size but are often in the range of 10-30 μm; two orders of magnitude larger than the constituent primary particles from the original flow. They are also substantially larger than the aggregates measured in the TDMA experiments.

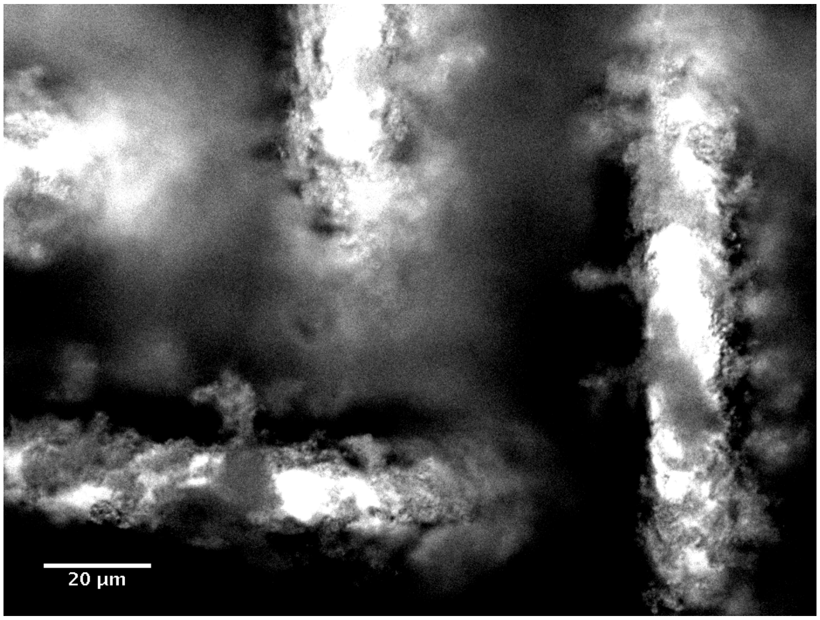

Figure 7.9: Sample optical image of NaCl aggregates formed on a wire mesh

Figure 7.10 shows two samples of image sequences obtained from the fluorescent imaging experiments. The fluorescent images are white where a Rhodamine particle is present in the field of view and black otherwise. The Rhodamine particles are deposited predominantly on the existing NaCl particles and provide an indication of the location and structure of the aggregates. The imaging area has been cropped to focus on a smaller region of interest resulting in different scales for each test. The images have been processed using ImageJ to automatically adjust the brightness and contrast and to add labels and indicators.

The two columns each represent a separate experiment. The left column focuses on aggregates that have formed within the wire mesh bounded by four wire strands represented by the black bounds in the corners of the image. The right column focuses on the tips of aggregate structures formed on top of a wire strand running vertically through the image. The five images in each column are spaced 2.5 min apart within the experimental procedure as described above. The second image represents time t=5min immediately before the flow was changed from 0% RH to the elevated value. The fourth image occurred immediately preceding the change back to 0%RH flow and the last image was 2.5 min after reverting back to 0% RH flow. The relative humidity at the time of each image is shown in the top left corner. The complete sequence of images captured at

10s intervals for these experiments and others are provided in video format in the Supplementary Materials and are used to inform the results in this section.

The particle structure was found to be stable when exposed to 0%RH flow for the 5min duration of these experiments and longer for other test cases (results not provided). After changing the valve positions to humidify the air (to 52% in the left column and 33% in the right) the aggregate structure starts to change within 20-30s. The aggregates in the left images separate to increase the open area between the wire mesh. The aggregate structures tend to collapse to more compact geometries as shown in comparison to the fixed lines overlayed on both images. There is considerable movement of aggregates between subsequent panels while exposed to elevated RH. When the flow is reverted back to 0% RH the aggregate motion ceases for the remainder of the experiment.

The changes shown in Figure 7.10 were repeatable for all other experiments with a variety of NaCl loading levels. These changes support the results of the TDMA analysis, which shows reduction in the mobility diameter of aggregates when exposed to elevated RH and no change when RH is lowered. They are also in line with the response of loaded filters, which show a reduction in the flow resistance (consistent with the opening of flow channels between the wire mesh) when exposed to an increase in RH above that during loading with hygroscopic particles [187].

Figure 7.11 shows the magnitude of displacement of a sample of 8 distinct Rhodamine particles on aggregates during the same microscopy experiment shown in the right column of Figure 7.10. This analysis is limited to 2D displacement of the structures, which is expected to be smaller than the actual three-dimensional change experienced. Little displacement is seen for the first 5min of the experiment while the RH is maintained at 0%, which provides an indication of the noise level in the results. After the airstream is conditioned to 33% RH (at t=5min) the particle displacement begins to rise. The magnitude and shape of the displacement curve varies for each particle tracked but generally increases until t=10min, at which time the airstream is reverted back to 0% RH. After this point there is again a period of only small variations in displacement until the end of the experiment. Twenty-five point sources were measured in each of the experiments for which video is provided in the Supplementary Materials. These point sources underwent an average displacement of 1.6μm between the first and last microscope image. This is a significant displacement when compared to the average diameter (100 nm) of primary particles deposited on the media. If the aggregates are assumed to be 10-30 μm the measured displacement represents 5-16% of the structure. These results are preliminary and a more robust analysis of magnitude and characteristics of structural change can be determined by modified experiments to produce 3D reconstructions of the aggregates before and after exposure for comparison.

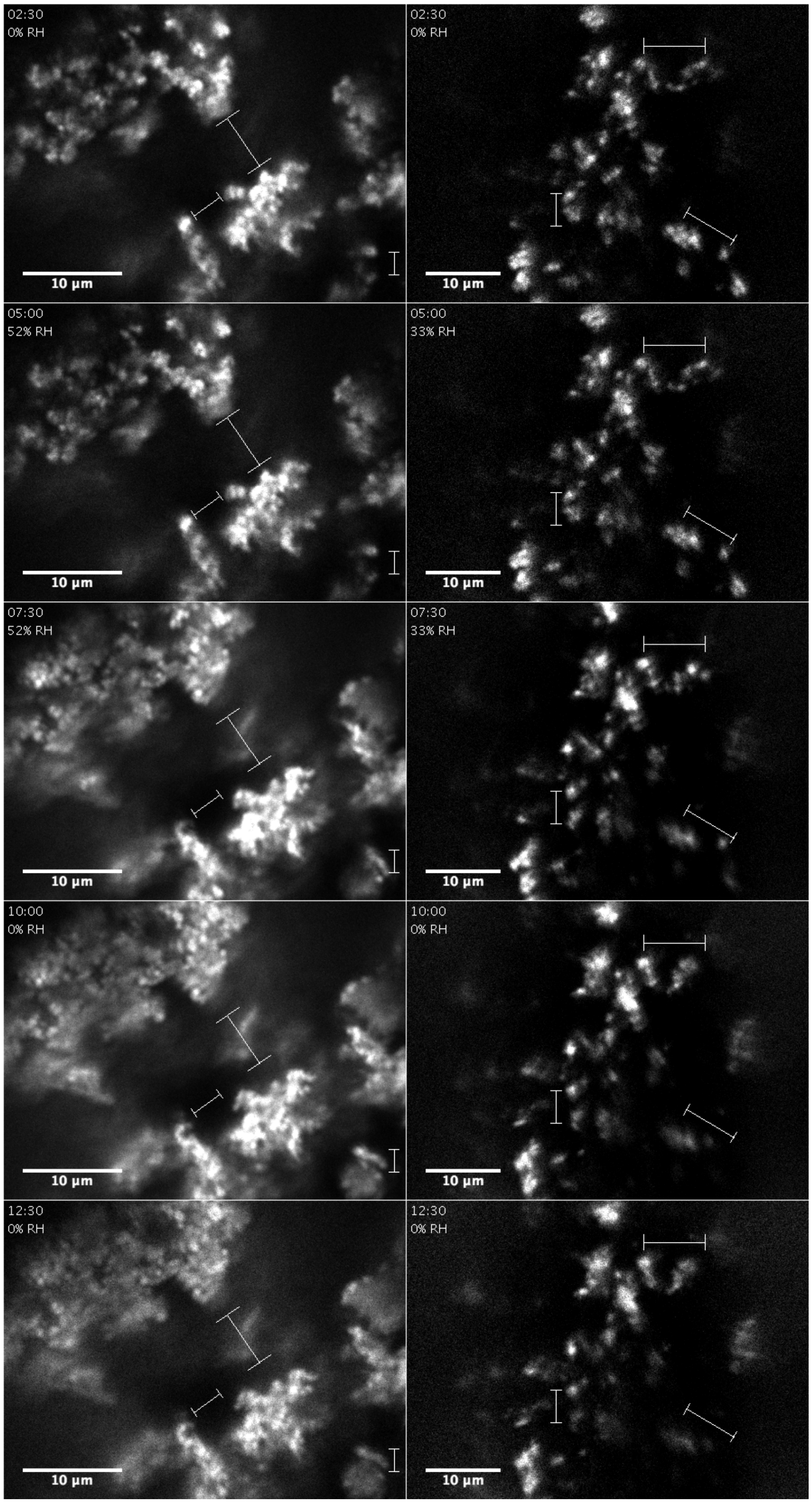

Figure 7.10: Sample fluorescent images used for analysis. The left column shows changes for exposure to 52% RH and the left for exposure to 33% RH. The grey bars are used to highlight specific areas of change.

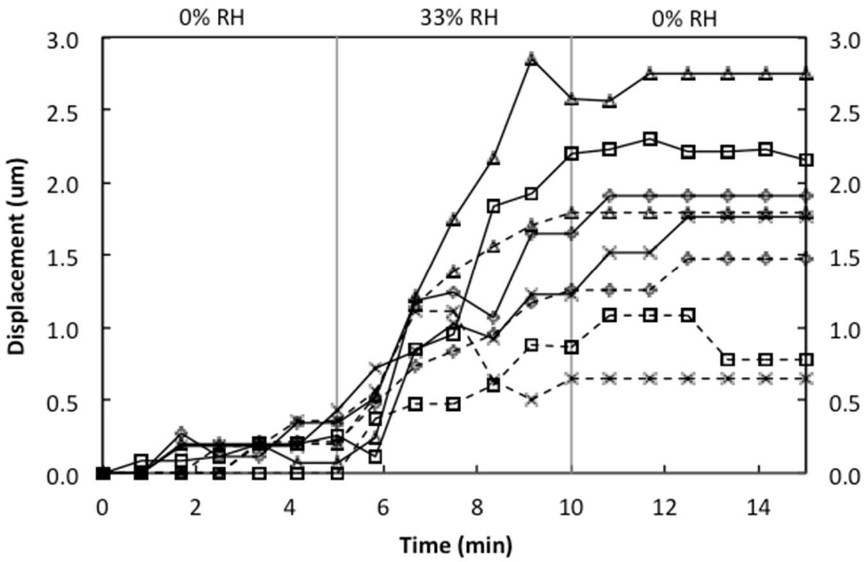

Figure 7.11: Displacement measurements for 8 sample Rhodamine particles deposited on aggregates during relative humidity exposure experiments. Each series represents measurements for a different random particle in one microscopy experiment.

7.4 Discussion

The reduction in particle mobility diameter resulting from exposure to increased RH is consistent with the contraction of dendrite structures seen in the fluorescence microscopy analysis. Single hygroscopic aerosol particles show an increase in Growth Factor with increasing RH [168]. This is a result of the interaction of H_2O molecules with the salt surface, which results in adlayer formation of water at relative humidity far below deliquescence [167,172,195]. The formation of water layers on the surface of salt particles forming an aggregate provides an explanation for contraction of the aggregate structure. If liquid water forms at the contact point between primary particles in the aggregates it will impose surface tension forces [188,189]. Force imbalances due to variations in geometry and surface properties could result in aggregate restructuring. Though these explanations are plausible for the changes seen, the current experimental methods do not provide direct evidence of liquid water formation within the aggregate structures and further investigation is required.

The behavior of particle aggregates has implications for particle control and measurement technology. The results of the current work emphasize the importance of relative humidity in characterization and operation of particle removal devices such as HVAC air filters or personal respirator equipment. A restructuring of particle aggregates explains the reduction in flow resistance seen in filters loaded with hygroscopic particles when exposed to elevated relative humidity in Chapter 6. A change in particle structure could also impact measurement technology that relies on flow (filters) or optical (aethalometer) properties of collected aerosol if hygroscopic particles are present and humidity variations are significant.

Generalizing the current work to broad conclusions regarding the changes of aggregates of hygroscopic particles with changes of relative humidity is challenging. The aggregate structures in the TDMA experiment are not constrained in a manner similar to aggregates captured on solid surfaces and therefore a direct comparison between the degrees of change may not be applicable, though the general trends should be aligned. Additionally, it should be noted that the TDMA and imaging within this work are performed on aggregates of substantially different sizes even though the primary particles are from the same aerosol source. The TDMA focuses on submicron aggregates with a maximum size of ~700 nm while the imaging analysis focuses on aggregates in the size range of 10-30 μm. Additionally, the wire mesh used for analysis is a simplified geometry of that for real air filters, which utilize random polymer fibers arrayed in a thick media. The changes in structure visualized in these experiments may be less than that in other operation modes as the set-up images the side of the mesh not directly exposed to the airflow. The airflow in the test cell is directed across the mesh structure rather than through it, as is the arrangement in real filters. The through-flow would be expected to add to the imposed forces on the aggregate structure.

7.5 Conclusions

The impact of relative humidity changes on aerosol aggregates has been investigated using a TDMA and fluorescence microscopy. These two methodologies provide independent verification that a physical change in the aggregate structures is occurring, which is consistent with changes in the pressure drop through loaded air filters under similar conditions. The imaging method developed has the potential for quantification of the relative structural changes under varying exposure conditions.

The TDMA analysis showed a shift towards smaller diameters of the size-selected aggregates of hygroscopic particles when exposed to relative humidity significantly below deliquescence. No change was seen for aggregates of similar size if exposed to an RH lower than that during formation, indicating that it is the increase in RH that causes a physical change in the aggregate structure. Non-hygroscopic Al_2O_3 particles did not show any response to similar increases in RH. The shift in particle distribution was quantified by the Growth Factor of the peak diameter of the aggregates. The GF decreased with increasing dry aggregate size as well as increasing relative humidity for aggregates formed under dry conditions. The trends were found for experiments performed with NaCl, Na_2SO_4, and $(NH_4)_2SO_4$ aggregates.

Image analysis using fluorescent microscopy of Rhodamine-seeded sodium chloride aggregates provides independent evidence of the change in aggregate structure with exposure to elevated relative humidity below deliquescence. Aggregate contraction was observed within the void space of the wire mesh as well as the aggregates projecting vertically from the wire surfaces. Analysis of the change in aggregate shape shows movement of 5-16% of the dry aggregate size. Tracking of single Rhodamine particles during the microscopy experiments showed that aggregate restructuring occurs only when exposed to elevated RH and ceases when the RH is subsequently lowered. Future analysis is required to develop a better understanding of the role that specific salt properties play in the magnitude of the aggregate restructuring.

The results of the TDMA and microscopy experiments provide evidence that a physical restructuring of aerosol aggregates occurs when exposed to elevated relative humidity. This supports the results shown in the previous chapter and supports the presented hypothesis that the particles captured on the filter media are undergoing a physical change as humidity is increased. Relative humidity changes are likely to occur in real filter operation resulting in variations from standardized filter tests. Future work will provide improved understanding of the role of relative humidity on real filter performance. Improvements in the microscopy methods will allow for quantitative analysis of the 3-dimensional changes of the aggregate structure to better predict the impact it may have on flow properties within loaded media samples.

8 Conclusions

8.1 Overview of Conclusions from Component Studies

This dissertation studied the energy consumption of air filtration systems and the impact that system changes have on performance parameters and indoor particle concentration. Previous studies of air filtration costs and benefits utilized simplified models that do not account for the transient nature of air filter operation including variations in flow rate, particle concentration, flow resistance, and filtration efficiency. Additional goals of the dissertation were to improve the understanding of potential modification to building system design and operation on occupant health. The absence of the dynamic filter behavior of older models prevented comparisons of the impact of filter performance with benefits of reduced exposure to indoor particle concentrations. The primary goal of this research was to improve the understanding and ability to predict the energy consumption of air filter operation. The research was successful through the development of an improved model used to predict performance based on information available from ASHRAE 52.2 testing. The dissertation also investigated the impact of relative humidity on performance parameters of loaded HVAC air filters. The experiments showed significant restructuring of particle aggregates resulting in reductions of flow resistance and filtration efficiency. The improved understanding of the role that relative humidity and filter loading plays in the evolution of filter performance will allow for better prediction of air filter performance and improvements to standardized test methods.

The research began with the development of an improved model relating flow resistance through filter media to flow rate and dust loading to characterize the filter operation for any system design throughout the entire life of the filter. During validation of the model against laboratory and field measurements it was found that the model prediction was accurate to ±15% compared to standardized tests but over-predicted the energy consumption compared to operation in real air handling systems at the Vancouver International Airport. The error associated with real operation was attributed to a combination of filter bypass and variations in particle properties. Accounting for an assumed 10% filter bypass in modeling of each installation reduced the error to ±15% but is not a realistic solution for widespread model application due to the unique characteristics of each installation. The results illuminated the need to further investigate the role of filter loading and variable system conditions on filter performance. Overall, the model was found to be adequate for predicting and comparing air filter performance.

The research continued with a case study to showcase the practical application of the new air filter model to compare energy efficiency of specific filter selections and installations at YVR. The model was used to inform modifications to the filters installed at the airport by comparing the annual operation cost and energy efficiency of Box, Bag, and V-type filters. The comparison found that V-type filters were the most energy efficient and Bag filters the least costly. A comparison of the impact of changes to system and filter parameters revealed that electricity cost and particle concentration are the most significant drivers of cost and that initial pressure drop is the most important parameter of the air filter when determining the cost of operation. The use of the model also showed that filter systems could be revised in locations with low outdoor particle concentrations so as to forego the installation of prefilters, with concomitant reduced energy consumption and operation cost. Removal of the prefilter would be contrary to standard practice. The success of the model use to reduce system cost at YVR led to similar applications at UBC and allows for future application by building owners and operators to improve system efficiency.

The air filter energy model from this work was then combined with existing indoor particle dynamics, and epidemiology models in a novel manner to allow comparisons of the financial impacts of filter and system changes on operation costs and health benefits to occupants. The benefits of increasing air filter installations from MERV 6 up to MERV 16 was found to outweigh the costs in all cities investigated. The financial benefits of reduced mortality outweighed the added cost by an order of magnitude. Changes to system operation such as outdoor air, return air and recirculated airflow were performed to determine methods of reducing cost and increasing benefits to occupants. Examples of potential improvements include increases to outdoor air and supply air filter efficiency with associated reductions in return and recirculated airflow rates resulting in lower indoor particle concentrations. The model used for comparison was made available as Supplemental Information to the publication [139].

Laboratory experiments were performed to determine the impact of relative humidity changes on loaded air filters to improve the understanding of the role that system parameters have on filter performance and the limitations these may pose to the accuracy of existing standardized tests used for model development. Relative humidity was found to play a significant role in determining the flow resistance and filtration efficiency of filter samples loaded with hygroscopic particles. Tests that increased relative humidity from 0% to 40% after loading resulted in a reduction of flow resistance of almost 50%. Filters loaded with non-hygroscopic particles (such as those used during standardized tests) did not respond to changes in RH. The proposed mechanism causing changes in loaded filter performance was a restructuring of particle aggregates within the media due to increases in individual particle diameter. Relative humidity can have a substantial impact on the performance of air filters that is not captured in existing tests used to create the filter energy model, and explains a portion of the discrepancy between modeled and experimental results.

The final component of this dissertation was an experiment to develop support for the hypothesis that aggregates of hygroscopic particles undergo physical changes when exposed to relative humidity below deliquescence. Experiments using a TDMA were performed to analyze aggregate sizes before and after mixing with elevated RH air. These experiments showed reductions in aggregate size up to the deliquescence relative humidity, after which there was a substantial increase in size associated with deliquescence. A fluorescent microscopy technique was developed to image structural changes in real time and showed that restructuring occurs when aggregates of hygroscopic particles are exposed to increases in relative humidity, but no restructuring was apparent when the relative humidity decreases. These changes are likely to occur throughout the operation of a real filter system and will have significant impacts on the properties of loaded filter media.

Additional conclusions drawn from each component of this dissertation can be found in the conclusion sections of each associated chapter. A brief synthesis of the conclusion from the dissertation as a whole is provided below.

8.2 Conclusions from Synthesis of Studies

The chapters of this dissertation are largely stand-alone research projects. When taken together the results of these studies can provide further insight into air filter performance. The implications of the dissertation as a whole are discussed below.

The modeling undertaken in this dissertation shows that air filter operation cost and energy efficiency vary widely even for a given specified filtration performance or MERV. The dynamic behavior of filter operation (including efficiency, flow, resistance, etc.) is important to consider for any modeling effort. The cost models developed in this work allow for optimization of the filter system with respect to selection criteria and operation time and build upon the previous steady state models in the literature. The results show that operation time is important when considering system performance and varies from manufacturer-recommended changeout times.

Adding indoor particle concentration and health impact modeling to the filter cost models has provided a more holistic interpretation of the value of filtration systems. The health benefits of improved filtration far outweigh the increased operation costs but may find resistance for implementation due to the benefits and costs being born by disparate parties. The high degree of variability in regional outdoor particulate matter concentration necessitates a specific indoor particle concentration guideline rather than existing practice of specifying filter MERV. This will allow system design variations to meet the IAQ guideline while minimizing energy. If specific indoor particle concentrations are not adopted a less stringent approach would be regionally specific MERV requirements based on typical outdoor particle concentration that account for system design and filter bypass to improve occupant health. The ability to monetize health benefits of system changes is garnering increased interest within the industry as occupant health considerations are being included in sustainable building design characterization. The combination of models allows for the monetized health benefits to be considered in analyzes of building design and retrofit strategies. The results from this model and future extensions will allow for calculation of relative exposure for varying system designs to ensure optimized occupant health while ensuring increasingly stringent energy efficiency standards are reached.

The model for filter performance developed in this dissertation has been shown to provide good agreement with standardized test results such as ASHRAE 52.2. The model performs less well in comparison with real filter installations. This indicates that the standardized test methods do not adequately represent the real world applications they are trying to simulate. Improved modeling and improved filter classification metrics can only be developed by bridging the gap between laboratory and real filter operation. The experiments exploring relative humidity have provided further insight into parameters that can have substantial influence on filter performance and are not currently captured in standardized test methods. Modifications to ASHRAE 52.2 are required that consider changes in relative humidity and challenge particles that better represent real conditions as well as a variety of conditions to better characterize air filter performance. Additional considerations for variability of flow conditions during loading should also be considered.

Microscale characteristics of filter media design are important in determining the macroscale filter performance. The dust loading adds considerably to the flow resistance and can alter filtration efficiency. The relative magnitude of these changes is a result of the design of the filter media and how it shapes captured particle aggregates. Throughout the operation life of the filter the changes to deposited particle structure can result in modified performance of the whole building system. The potential exists for design of improved filters; an ideal filter would see little change in pressure drop or filtration efficiency as dust accumulates in the filter. Additional research is required to fully understand the role of microscale characteristics but the work to date highlights the critical importance of dust loading characteristics and the need to focus research away from clean filter testing.

9 Recommendations for Future Work

9.1 Dissertation Strengths and Weaknesses

The strength of this dissertation is the advancement of the modeling techniques to more closely approximate real filter operation by accounting for variations in operation parameters such as flow rate to flow resistance relations with respect to dust load. The use of results from existing test methods has allowed for simple, immediate application of the model by building owners and filter manufacturers. Additional strengths to the research are its focus on experimental validation and fundamental research to posit explanations for discrepancies between laboratory and field operations that will improve future standardized tests and general filter research. Relative humidity was previously overlooked as an important parameter to control during industrial and academic filter tests. This work shows that proper characterization and control of RH is critical for accurate experimental results.

The limitations of this dissertation remain the uncertainties in universal applicability of the model. The model is limited to application with filters without electrostatic capture mechanisms due to an uncertainty in the behavior of these filters with dust loading. Additionally, the exact magnitude of the influence of variation in aerosol particle make-up on loading behavior is still an active field of research that will limit the modeling potential but will allow for improvements with future research. Limitations for specific components of the thesis have been discussed in the previous chapters.

9.2 Potential Future Studies

This dissertation has elucidated numerous avenues for future research through improvements in air filter modeling, investigations of system operation, and fundamental experiments to further improve our understanding of filter performance. Potential for future research stemming from this work will be discussed in the following sections.

9.2.1 Air Filter Modeling

The air filter model developed in this work is fundamentally applicable to any type of air filter but was derived using information predominantly for filters with only mechanical capture mechanisms. The general profile of flow resistance versus dust loading is expected to be similar between the two filter types but the filtration efficiency versus dust load is expected to be markedly different. The most practically applicable version of the model uses a constant filtration efficiency equal to the MERV of the mechanical filter. This represents a conservative estimate for mechanical filters but the behavior of electret filters shows more variability. Expansion of the model and future testing and comparison with electret filters, specifically with a focus on the best relation for filtration efficiency is needed before the model can be comfortably applied to electret filters.

The air filter model has been used to explore the potential to compare energy efficiency and operation cost of filter selections and system changes. Further study is warranted using the available model in conjunction with indoor particle dynamics and epidemiological information to assess additional system configurations. The model can also be applied to policy analysis to inform future guidelines such as acceptable indoor exposure and specification of filter installations based on outdoor particle concentrations. The model should also be expanded to account for acute health impacts and the transient nature of outdoor particle concentrations that will result in continuous variations of indoor exposure concentrations.

Studies should also be performed to expand system-based analyses to include additional system components not investigated in this work. This will allow a more holistic analysis of the HVAC system operation to eventually be incorporated into proper building scale life cycle assessments of operation characteristics and human health impacts. Immediate expansions of the model should include the addition of heating and cooling system performance through coil fouling conditions and heat recovery ventilator protection.

9.2.2 Filter System Performance

The air filter model is used in this dissertation to study the impact of system changes on operation costs and health benefits. The experimental validation of the model was performed for a single building within the constraints of the existing system. Although the results show good agreement, numerous additional validation and experimental studies should be conducted to confirm the model applicability and investigate potential improvements.

The financial benefits of system changes are based on reductions in indoor particle concentrations and Change-Response functions for occupant exposure outcomes. The particle concentration is determined using a well-known particle dynamics model [83] that has been calibrated at the building scale [85]. There is still considerable variability in the model input parameters and uncertainty in the results. Additional research to improve our understanding of the dynamics of particles within the indoor environment, such as resuspension due to human behavior [196], is currently underway and much needed to improve modeling results.

Additional whole building studies of system intervention analyses are also required. Examples of possible studies include measuring the indoor particle concentration within a well-characterized building to determine the impact of filter improvements, with the goal of validating the modeling developed in this dissertation. Other intervention studies that could be conducted to determine model validity include changes in flow conditions (such as return air flowrate), installations in different pollution contexts (such as a comparison between buildings in Vancouver and Beijing), and the use of modified ventilation schemes such as displacement versus mixing ventilation, or the use of personal ventilators.

Further research is required to determine the differences in filter performance between laboratory tests, full-scale standardized tests, and field experiments. There have been few previous experiments directly comparing test methods [121,123] and though the results provide an indication that the performance varies with test method a detailed analysis to determine the causes have not been performed. One of the most critical issues to determine is whether the variability is a result of the loading rate, the particle properties, or both. This type of long term testing has been identified as a need for the field at the most recent Indoor Air conference [197]. Knowledge of the role that testing method plays in filter performance will lead to improvement in ability for standardized tests such as

ASHRAE 52.2 to accurately predict real world conditions, and thus the models developed using the results from these test methods to be more accurate.

9.2.3 Fundamental Filter Research

Advancements in the understanding of the impact of particle and system properties, in particular, particle material and relative humidity have been developed in this work. This knowledge supplements the existing data supporting the role that particle geometry, size, deposition velocity, and more play in filter operation. Though the focus of filter studies has shifted from limited clean filter analyses to loading studies there is still a lack of understanding of how these properties translate to real filter applications. The laboratory research initiated in this work has led to a number of additional questions and potential research avenues.

The laboratory experiments performed during this project have been limited to a small number of particle size distributions. The existing literature shows that particle size impacts the evolution of flow resistance within the filter media and is an important characteristic in determining the operation of a specific installation. Additional experiments are required to complement the existing literature. Specific uncertainties remaining to be investigated include the role of aerosol concentration on deposition characteristics and changing flow resistance and filtration efficiency, the change in filter performance when challenged with particle size distributions representative of different outdoor distributions such as specific cities or geographic criteria (rural vs urban), and the importance of variations and cyclic loading on filter performance. These experiments are best performed in a laboratory setting on filter media samples to ensure controlled conditions with potential for complementary field-testing.

The experiments performed in Chapter 6 show that the choice of filter media can impact the relative importance of particle restructuring when exposed to elevated relative humidity. Additional experiments are required to elucidate the specific attributes of the filter media that causes these different responses and how they can be modified to improve filter performance throughout operation. These experiments are best performed in the lab environment using a combination of well-characterized commercial filter media samples and woven wire meshes. Loaded samples can be analyzed using visualization techniques to determine variations in aggregate structures with different filter characteristics. Testing of responses of loaded filter samples to changes in relative humidity will allow for links to be made between filter properties, aggregate structures, and the degree of restructuring to be expected during operation. This knowledge will assist in designing filter media that considers the impact of fiber properties on loading characteristics as well as clean filter conditions.

The work in this dissertation has also shown that the properties of particles loaded into the filter will impact the response to relative humidity changes. Potential properties of importance could include the particle size, hygroscopicity, and wettability. The experiments in both Chapters 6 & 7 should be repeated with a range of particle sizes including those generated from aerosol atomizers and vibrating orifice generators to expand the range of particle sizes to >1μm. Testing of aggregate restructuring should also be performed with aggregates of fixed size and shape characteristics but comprised of varied salt types using the TDMA experiments. This should include single salt type and combination aggregates of hygroscopic and non-hygroscopic particles to improve the understanding of the degree of restructuring expected from a range of atmospherically relevant aggregates.

Filter loading experiments in this work, and the majority of the literature, focus on relative humidity below deliquescence. Studies focused on the behavior of filters exposed to elevated relative humidity are required. These should include loading at low RH and exposure to RH>DRH, similar to experiments in Chapter 6 as well as experiments with cyclic loading above and below the deliquescence relative humidity throughout the loading cycle. Experiments of this nature will more closely approximate the varied conditions in a real air-handling system and provide more accurate prediction of the expected changes in filter performance during real operation.

The quantitative analysis of aggregate movement in Chapter 7 was limited to motion in the plane of focus. An improved quantification of motion and better understanding of the aggregate structures formed from deposited particles can be developed if the three-dimensional structure of the aggregate is determined. The scanning mode of the fluorescent microscope allows for steps in the z-direction of the field and reconstruction of the aggregate geometry. Scanning before and after changes in humidity will allow for quantitative comparison of the overall structure change. Combining three-dimensional information before and after exposure with additional time series data for stepped relative humidity changes will provide a more nuanced understanding of the physical changes occurring within filter media. These results could be expanded to allow for quantification of expected flow resistance changes due to aggregate restructuring that can be compared to measured changes in flow resistance determined during loading and exposure of filter samples.

References

1 Pérez-Lombard L, Ortiz J, Pout C. A review on buildings energy consumption information. *Energy & Buildings* 2008; **40**:394–398.

2 NRCAN. Energy Efficiency Trends in Canada, 1990 to 2010. Natural Resources Canada; 2013.

3 COAG. Guide to Best Practice Maintenance & Operation of HVAC Systems for Energy Efficiency. Department of Climate Change and Energy Efficiency; 2012.

4 Fisk WJ, Rosenfeld AH. Estimates of improved productivity and health from better indoor environments. *Indoor Air* 1998; **8**:158–172.

5 Fisk WJ. Health and productivity gains from better indoor environments and their Relationship with Building Energy Efficiency. *Annual Review of Energy and the Environment* 2000; **25**:537–566.

6 Crouse DL, Peters PA, van Donkelaar A, Goldberg MS, Villeneuve PJ, Brion O, *et al.* Risk of Nonaccidental and Cardiovascular Mortality in Relation to Long-term Exposure to Low Concentrations of Fine Particulate Matter: A Canadian National-Level Cohort Study. *Environmental Health Perspectives* 2012; **120**:708–714.

7 Laden F, Schwartz J, Speizer FE, Dockery DW. Reduction in Fine Particulate Air Pollution and Mortality: Extended Follow-up of the Harvard Six Cities Study. *American Journal of Respiratory and Critical Care Medicine* 2006; **173**:667–672.

8 Ostro BD, Rothschild S. Air pollution and acute respiratory morbidity: An observational study of multiple pollutants. *Environmental Research* 2012; **50**:238–247.

9 Pope CA III, Burnett RT, Thun MJ, Calle EE, Krewski D, Ito K, *et al.* Lung Cancer, Cardiopulmonary Mortality, and Long-term Exposure to Fine Particulate Air Pollution. *JAMA* 2002; **287**:1132–1141.

10 Schwartz J, Slater D, Larson TV, Pierson WE, Koenig JQ. Particulate air pollution and hospital emergency room visits for asthma in Seattle. *American Review of Respiratory Disease* 1993; **147**:826–831.

11 Pope CA III, Dockery DW. Health Effects of Fine Particulate Air Pollution: Lines that Connect. *J Air Waste Manage* 2006; **56**:709–742.

12 Anderson JO, Thundiyil JG, Stolbach A. Clearing the Air: A Review of the Effects of Particulate Matter Air Pollution on Human Health. *Journal of Medical Toxicology* 2012; **8**:166–175.

13 Hystad P, Demers PA, Johnson KC, Carpiano RM, Brauer M. Long-term Residential Exposure to Air Pollution and Lung Cancer Risk. *Epidemiology* 2013; **24**:762–772.

14 Franck U, Odeh S, Wiedensohler A, Wehner B, Herbarth O. The effect of particle size on cardiovascular disorders — The smaller the worse. *Science of The Total Environment* 2011; **409**:4217–4221.

15 Janssen NAH, Hoek G, Simic-Lawson M, Fischer P, van Bree L, Brink ten H, *et al.* Black Carbon as an Additional Indicator of the Adverse Health Effects of Airborne Particles Compared with PM10 and PM2.5. *Environmental Health Perspectives* 2011; **119**:1691–1699.

16 WHO. Review of evidence on health aspects of air pollution – REVIHAAP. Regional Office for Europe: World Health Organization; 2013. http://www.euro.who.int/__data/assets/pdf_file/0004/193108/REVIHAAP-Final-technical-report-final-version.pdf

17 WHO. WHO Air Quality Guidelines for Particulate Matter, Ozone, Nitrogen Dioxide and Sulfur Dioxide. Global Update 2005, Summary of Risk Assessment. 2005.

18 Klepeis NE, Nelson WC, Ott WR, Robinson JP, Tsang AM, Switzer P, *et al.* The National Human Activity Pattern Survey (NHAPS): a resource for assessing exposure to environmental pollutants. *Journal of Exposure Analysis and Environmental Epidemiology* 2001; **11**:231–252.

19 Abt E, Suh HH, Catalano P, Koutrakis P. Relative Contribution of Outdoor and Indoor Particle Sources to Indoor Concentrations. *Environmental Science and Technology* 2000; **34**:3579–3587.

20 Yu BF, Hu ZB, Liu M, Yang HL, Kong QX, Liu YH. Review of research on air-conditioning systems and indoor air quality control for human health. *International Journal of Refrigeration* 2009; **32**:3–20.

21 Taleghani M, Tenpierik M, Kurvers S, van den Dobbelsteen A. A review into thermal comfort of buildings. *Renewable and Sustainable Energy Reviews* 2013; **26**:201–215.

22 ASHRAE. *HVAC Applications*. Atlanta, GA: American Society of Heating, Refrigeration and Air-Conditioning Engineers, Inc.; 2011.

23 ASHRAE. ANSI/ASHRAE Standard 62.1-2013, Ventilation for Acceptable Indoor Air Quality. Atlanta, GA: American Society of Heating, Refrigeration and Air-Conditioning Engineers, Inc.; 2013.

24 ASHRAE. ANSI/ASHRAE Standard 55 Thermal Environmental Conditions for Human Occupancy. Atlanta, GA: American Society for Heating, Refrigerating,

and Air-Conditioning Engineers; 2013.

25 ASHRAE. ANSI/ASHRAE Standard 90.1-2010, Energy Standard for Buildings Except Low-Rise Residential Buildings. Atlanta, GA: American Society of Heating, Refrigeration and Air-Conditioning Engineers, Inc.; 2010.

26 Tronville PM. Global standards for filter testing. *ASHRAE Journal* 2006; **48**:58–62.

27 Brown RC. *Air Filtration - An Integrated Approach to the Theory and Applications of Fibrous Filters*. New York: Pergaman Press; 1993.

28 Rivers RD, Murphy DJ. Determination of air filter performance under variable air volume (VAV) conditions. Atlanta, GA: ASHRAE; 1996.

29 Liu M, Claridge DE, Deng S. An air filter pressure loss model for fan energy calculation in air handling units. *International Journal of Energy Research* 2003; **27**:589–600.

30 Happel J. Viscous Flow Relative to Arrays of Cylinders. *AIChE J* 1959; **5**:174–177.

31 Kuwabara S. The forces experienced by randomly distributed parallel circular cylinders or spheres in a viscous flow at small Reynolds numbers. *Journal of the Physical Society of Japan* 1959; **14**:527.

32 Kirsch AA, Fuchs NA. The fluid flow in a system of parallel cylinders perpendicular to the flow direction at small Reynolds numbers. *Journal of the Physical Society of Japan* 1967; **22**:1251–1255.

33 Kirsch AA, IB S. Pressure-Drop and Diffusional Deposition of Aerosol in Polydisperse Model Filter. *Journal of Colloid and Interface Science* 1973; **43**:10–16.

34 Lebedev MN, Stechkina IB, Chernyakov AL. The two-component fiber row: Viscous drag and particle deposition in the regime with interception. *Colloid Journal* 2003; **65**:211–221.

35 Mattern KJ, Deen WM. "Mixing rules" for estimating the hydraulic permeability of fiber mixtures. *AIChE J* 2007; **54**:32–41.

36 Kirsch AA, Stechkina IB, Fuchs NA. Gas flow in aerosol filters made of polydisperse ultrafine fibres. *Journal of Aerosol Science* 1974; **5**:39–45.

37 Brown RC, Thorpe A. Glass-fibre filters with bimodal fibre size distributions. *Powder Technology* 2001; **118**:3–9.

38 Clague DS, Phillips RJ. A numerical calculation of the hydraulic permeability of

three-dimensional disordered fibrous media. *Physics of Fluids* 1997; **9**:1562–1572.

39 Vahedi Tafreshi H, A Rahman MS, Jaganathan S, Wang Q, Pourdeyhimi B. Analytical expressions for predicting permeability of bimodal fibrous porous media. *Chemical Engineering Science* 2009; **64**:1154–1159.

40 Pich J. Pressure Characteristics of Fibrous Aerosol Filters. *Journal of Colloid and Interface Science* 1971; **37**:912–917.

41 Kirsch AA, Stechkina IB, Fuchs NA. Effect of gas slip on the pressure drop in fibrous filters. *Journal of Aerosol Science* 1973; **4**:287–293.

42 Stern SC, Zeller HW, Schekman AI. The aerosol efficiency and pressure drop of a fibrous filter at reduced pressures. *Journal of Colloid Science* 1960; **15**:546–562.

43 Stenhouse JIT. Fibrous Filtration. In: *Physical & Chemical Properties of Aerosols*. Colbeck I (editor). London: Blackie Academic & Professional; 1998.

44 Pich J. Theory of gravitational deposition of particles in fibrous aerosol filters. *Journal of Aerosol Science* 1973; **4**:217–226.

45 Pich J, Spurny K. Direction of Fluid Flow and the Properties of Fibrous Filters. *Aerosol Science and Technology* 1991; **15**:179–183.

46 Kirsch AA, Chechuev PV. Diffusion Deposition of Aerosol in Fibrous Filters at Intermediate Peclet Numbers. *Aerosol Science and Technology* 1985; **4**:11–16.

47 Chen CY. Filtration of aerosols by fibrous media. *Chemical Reviews* 1955; **55**:595–623.

48 Lee KW, Liu BYH. Theoretical Study of Aerosol Filtration by Fibrous Filters. *Aerosol Science and Technology* 1982; **1**:147–161.

49 Stechkina IB, Fuchs NA. Studies on fibrous aerosol filters—I. Calculation of diffusional deposition of aerosols in fibrous filters. *Annals of Occupational Hygiene* 1966; **9**:59–64.

50 Spielman L, Goren SL. Model for predicting pressure drop and filtration efficiency in fibrous media. *Environmental Science and Technology* 1968; **2**:279–287.

51 Friedlander SK. Mass and heat transfer to single spheres and cylinders at low Reynolds numbers. *AIChE J* 1957; **3**:43–48.

52 Lee KW, Liu BYH. Experimental Study of Aerosol Filtration by Fibrous Filters. *Aerosol Science and Technology* 1981; **1**:35–46.

53 Cheng Y-S, Yamada Y, Yeh H-C. Diffusion Deposition on Model Fibrous Filters with Intermediate Porosity. *Aerosol Science and Technology* 1990; **12**:286–299.

54 Lee KW, Gieseke JA. Note on the Approximation of Interceptional Collection Efficiencies. *Journal of Aerosol Science* 1980; **11**:335–341.

55 Brown RC, Wake D. Air Filtration by Interception - Theory and Experiment. *Journal of Aerosol Science* 1991; **22**:181–186.

56 Stechkina IB, Kirsch AA, Fuchs NA. Studies on Fibrous Aerosol Filters—IV Calculation of Aerosol Deposition in Model Filters in the Range of Maximum Penetration. *Annals of Occupational Hygiene* 1969; **12**:1–8.

57 Harrop JA, Stenhouse J. The theoretical prediction of inertial impaction efficiencies in fibrous filters. *Chemical Engineering Science* 1969; **24**:1475–1481.

58 Nguyen X, Beeckmans JM. Single fibre capture efficiencies of aerosol particles in real and model filters in the inertial-interceptive domain. *Journal of Aerosol Science* 1975; **6**:205–212.

59 Stenhouse J, Harrop JA, Freshwater DC. The mechanisms of particle capture in gas filters. *Journal of Aerosol Science* 1970; **1**:41–52.

60 Suneja SK, Lee CH. Aerosol Filtration by Fibrous Filters at Intermediate Reynolds-Numbers (Less-Than-or-Equal-to 100). *Atmospheric Environment* 1974; **8**:1081–1094.

61 Pich J. Analytical method for calculation of deposition of particles from flowing fluids and central force fields in aerosol filters. *Environmental Science and Technology* 1977; **11**:608–612.

62 Pich J, Emi H, Kanaoka C. Coulombic deposition mechanism in electret filters. *Journal of Aerosol Science* 1987; **18**:29–35.

63 Grzybowski P, Gradon L. Analysis of Motion and Deposition of Fibrous Aerosol-Particles Flowing Around a Single Filter Element - the Electrostatic Effect. *Chemical Engineering Science* 1992; **47**:1453–1459.

64 Romay FJ, Liu BYH, Chae S-J. Experimental Study of Electrostatic Capture Mechanisms in Commercial Electret Filters. *Aerosol Science and Technology* 1998; **28**:224–234.

65 Brown RC. Capture of dust particles in filters by linedipole charged fibres. *Journal of Aerosol Science* 1981; **12**:349–356.

66 Brown RC. The Behavior of Electrostatic Filters Made of Fibers or Sheets Arranged Parallel to the Air-Flow. *Journal of Aerosol Science* 1982; **13**:249–257.

67 ASHRAE. ANSI/ASHRAE Standard 52.2-2012, Method of Testing General Ventilation Air-Cleaning Devices for Removal Efficiency by Particle Size. Atlanta, GA: American Society of Heating, Refrigerating, and Air Conditioning

Engineers; 2012.

68 Wang J, Kim SC, Pui DYH. Investigation of the figure of merit for filters with a single nanofiber layer on a substrate. *Journal of Aerosol Science* 2008; **39**:323–334.

69 Eninger RM, Honda T, Adhikari A, Heinonen-Tanski H, Reponen T, Grinshpun SA. Filter Performance of N99 and N95 Facepiece Respirators Against Viruses and Ultrafine Particles. *Annals of Occupational Hygiene* 2008; **52**:385–396.

70 Chen CC, Willeke K. Aerosol Penetration Through Surgical Masks. *American Journal of Infection Control* 1992; **20**:177–184.

71 Leung WW-F, Hung C-H, Yuen P-T. Experimental Investigation on Continuous Filtration of Sub-Micron Aerosol by Filter Composed of Dual-Layers Including a Nanofiber Layer. *Aerosol Science and Technology* 2009; **43**:1174–1183.

72 Yun KM, Hogan CJ Jr., Matsubayashi Y, Kawabe M, Iskandar F, Okuyama K. Nanoparticle filtration by electrospun polymer fibers. *Chemical Engineering Science* 2007; **62**:4751–4759.

73 Sun C. Delivering Sustainability Promise to Ventilation Air Filtration - Part II: Life Cycle Sustainability of Air Filters. *ASHRAE Transactions* 2010; **116**:25–32.

74 Arnold BD, Matela DM, Veeck AC. Life-cycle costing of air filtration. *ASHRAE Journal* 2005; **47**:30–32.

75 Kimberly-Clark. Filtration Products - Operating Cost Analysis Tool. <http://www.kcprofessional.com/resources/tools/filtration-cost-analysis.asp>. 2014.http://www.kcprofessional.com/resources/tools/filtration-cost-analysis.asp (accessed Feb2014).

76 Freudenberg. Saving Energy with Viledon Air Filters. www.freudenberg-filter.com. 2009.http://www.freudenberg-filter.com/fileadmin/templates/EN_downloads/Energieprospekt_E_4-09.pdf (accessed Feb2014).

77 3M. Total Cost of Ownership Tool from 3M. 2011.

78 Camfil-Farr. Energy Saving Software. www.camfil.com. 2014.http://www.camfil.com/Filter-technology/Camfil-Farr-Software/Energy-saving-software-/ (accessed Feb2014).

79 Vokes. Calculating the cost of HVAC air filters. 2010.

80 Eurovent. Recommendation concerning calculating of life cycle cost for air filters. 2005.

81 Fisk WJ, Faulkner D, Palonen J, Seppanen O. Performance and costs of particle air filtration technologies. *Indoor Air* 2002; **12**:223–234.

82 Jamriska M, Morawska L, Ensor DS. Control strategies for sub-micrometer particles indoors: model study of air filtration and ventilation. *Indoor Air* 2003; **13**:96–105.

83 Nazaroff WW. Indoor particle dynamics. *Indoor Air* 2004; **14**:175–183.

84 Nazaroff WW, Cass GR. Mathematical-Modeling of Indoor Aerosol Dynamics. *Environmental Science and Technology* 1989; **23**:157–166.

85 Jamriska M, Morawska L, Clark BA. Effect of ventilation and filtration on submicrometer particles in an indoor environment. *Indoor Air* 2000; **10**:19–26.

86 Noh KC, Hwang J. The Effect of Ventilation Rate and Filter Performance on Indoor Particle Concentration and Fan Power Consumption in a Residential Housing Unit. *Indoor and Built Environment* 2010; **19**:444–452.

87 Carlsson T, Johnsson M. PM Removal For Particle Air Filters For General Ventilation. 11th World Filtration Congress, Graz, Austria; 2012.

88 Quang TN, He C, Morawska L, Knibbs LD. Influence of ventilation and filtration on indoor particle concentrations in urban office buildings. *Atmospheric Environment* 2013; **79**:41–52.

89 Zaatari M, Novoselac A, Siegel J. The relationship between filter pressure drop, indoor air quality, and energy consumption in rooftop HVAC units. *Building and Environment* 2014; **73**:151–161.

90 USEPA. The Benefits and Costs of the Clean Air Act from 1990 to 2020. United States Environmental Protection Agency; 2011.

91 Sultan ZM. Estimates of associated outdoor particulate matter health risk and costs reductions from alternative building, ventilation and filtration scenarios. *Science of The Total Environment* 2007; **377**:1–11.

92 Bekö G, Clausen G, Weschler CJ. Is the use of particle air filtration justified? Costs and benefits of filtration with regard to health effects, building cleaning and occupant productivity. *Building and Environment* 2008; **43**:1647–1657.

93 Azimi P, Stephens B. HVAC filtration for controlling infectious airborne disease transmission in indoor environments: Predicting risk reductions and operational costs. *Building and Environment* 2013; **70**:150–160.

94 Fisk WJ. Health benefits of particle filtration. *Indoor Air* 2013; **23**:357–368.

95 Raynor PC, Chae S-J. Dust loading on electrostatically charged filters in a standard

test and a real HVAC system. *Filtration and Separation* 2003; **40**:35–39.

96 Billings CE. *Effects of particle accumulation in aerosol filtration*. 1966; :1–232.

97 Kanaoka C, Hiragi S. Pressure drop of air filter with dust load. *Journal of Aerosol Science* 1990; **21**:127–137.

98 Leibold H, Wilhelm JG. Investigation into the penetration and pressure drop of HEPA filter media during loading with submicron particle aerosols at high concentrations. *Journal of Aerosol Science* 1991; **22**:S773–S776.

99 Brown RC, Wake D, Gray R, Blackford DB, Bostock GJ. Effect of industrial aerosols on the performance of electrically charged filter material. *Annals of Occupational Hygiene* 1988; **32**:271–294.

100 Walsh DC, Stenhouse J. Clogging of an electrically active fibrous filter material: experimental results and two-dimensional simulations. *Powder Technology* 1997; **93**:63–75.

101 Walsh DC, Stenhouse JIT. Parameters Affecting the Loading Behavior and Degradation of Electrically Active Filter Materials. *Aerosol Science and Technology* 1998; **29**:419–432.

102 Walsh DC, Stenhouse J. The effect of particle size, charge, and composition on the loading characteristics of an electrically active fibrous filter material. *Journal of Aerosol Science* 1997; **28**:307–321.

103 Bémer D, Callé S. Evolution of the Efficiency and Pressure Drop of a Filter Media with Loading. *Aerosol Science and Technology* 2000; **33**:427–439.

104 Japuntich DA, Stenhouse J, Liu BYH. Experimental Results of Solid Monodisperse Particle Clogging of Fibrous Filters. *Journal of Aerosol Science* 1994; **25**:385–393.

105 Novick VJ, Klassen JF, Monson PR. Predicting mass loading as a function of pressure difference across prefilter/hepa filter systems. 22nd DOE/NRC Nuclear Air Cleaning and Treatment Conference, Denver, Colorado; 1992.

106 Song CB, Park HS, Lee KW. Experimental study of filter clogging with monodisperse PSL particles. *Powder Technology* 2006; **163**:152–159.

107 Miguel AF. Effect of air humidity on the evolution of permeability and performance of a fibrous filter during loading with hygroscopic and non-hygroscopic particles. *Journal of Aerosol Science* 2003; **34**:783–799.

108 Thomas D, Contal P, Renaudin V, Penicot P, Leclerc D, Vendel J. Modelling pressure drop in HEPA filters during dynamic filtration. *Journal of Aerosol Science* 1999; **30**:235–246.

109 Walsh DC, Stenhouse JIT, Scurrah KL, Graef A. The effect of solid and liquid aerosol particle loading on fibrous filter material performance. *Journal of Aerosol Science* 1996; **27**:S617–S618.

110 Thomas D, Penicot P, Contal P, Leclerc D, Vendel J. Clogging of fibrous filters by solid aerosol particles - Experimental and modelling study. *Chemical Engineering Science* 2001; **56**:3549–3561.

111 Hinds WC, Kadrichu NP. The Effect of Dust Loading on Penetration and Resistance of Glass Fiber Filters. *Aerosol Science and Technology* 1997; **27**:162–173.

112 Kasper G, Schollmeier S, Meyer J. Structure and density of deposits formed on filter fibers by inertial particle deposition and bounce. *Journal of Aerosol Science* 2010; **41**:1167–1182.

113 Kasper G, Schollmeier S, Meyer J, Hoferer J. The collection efficiency of a particle-loaded single filter fiber. *Journal of Aerosol Science* 2009; **40**:993–1009.

114 Kanaoka C, Emi H, Myojo T. Simulation of the growing process of a particle dendrite and evaluation of a single fiber collection efficiency with dust load. *Journal of Aerosol Science* 1980; **11**:377–389.

115 Gupta A, Novick VJ, Biswas P, Monson PR. Effect of Humidity and Particle Hygroscopicity on the Mass Loading Capacity of High Efficiency Particulate Air (HEPA) Filters. *Aerosol Science and Technology* 1993; **19**:94–107.

116 Joubert A, Laborde JC, Bouilloux L, Callé-Chazelet S, Thomas D. Influence of Humidity on Clogging of Flat and Pleated HEPA Filters. *Aerosol Science and Technology* 2010; **44**:1065–1076.

117 Joubert A, Laborde JC, Bouilloux L, Chazelet S, Thomas D. Modelling the pressure drop across HEPA filters during cake filtration in the presence of humidity. *Chemical Engineering Journal* 2011; **166**:616–623.

118 Hanley JT, Ensor DS, Smith DD, Sparks LE. Fractional Aerosol Filtration Efficiency of in-Duct Ventilation Air Cleaners. *Indoor Air* 1994; **4**:169–178.

119 Raynor PC, Kim BG, Ramachandran G, Strommen MR, Horns JH, Streifel AJ. Collection of biological and non-biological particles by new and used filters made from glass and electrostatically charged synthetic fibers. *Indoor Air* 2007; **18**:51–62.

120 Sun C, Woodman D. Delivering sustainability promise to HVAC air filtration - Part I: classification of energy efficiency for air filters. *ASHRAE Transactions* 2009; **115**:581.

121 Raynor PC, Chae S-J. The Long-Term Performance of Electrically Charged Filters

in a Ventilation System. *Journal of Occupational and Environmental Hygiene* 2004; **1**:463–471.

122 Moyer ES, Commodore MA, Hayes JL, Fotta SA, Berardinelli SP Jr. Real-Time Evaluation of Ventilation Filter-Bank Systems. *Journal of Occupational and Environmental Hygiene* 2007; **4**:58–69.

123 Meyers D, Arnold BD. Electrets and filtration: Lab testing and field performance head to head. *Filtration and Separation* 2005; **42**:44–49.

124 Stephens B, Siegel JA. Comparison of Test Methods for Determining the Particle Removal Efficiency of Filters in Residential and Light-Commercial Central HVAC Systems. *Aerosol Science and Technology* 2012; **46**:504–513.

125 Kowalski WJ, Bahnfleth WP, Whittam TS. Filtration of airborne microorganisms: modeling and prediction. *ASHRAE TRANS* 1999; **105**:4–17.

126 Boskovic L, Agranovski IE, Altman IS, Braddock RD. Filter efficiency as a function of nanoparticle velocity and shape. *Journal of Aerosol Science* 2008; **39**:635–644.

127 Dupoux J, Briand A. Air filter efficiency as a function of particle size and velocity. *Water, Air, & Soil Pollution* 1974; **3**:537–549.

128 Rudnick S. Optimizing the Design of Room Air Filters for the Removal of Submicrometer Particles. *Aerosol Science and Technology* 2004; **38**:861–869.

129 Montgomery JF, Green SI, Rogak SN, Bartlett K. Predicting the energy use and operation cost of HVAC air filters. *Energy & Buildings* 2012; **47**:643–650.

130 ASHRAE. *ASHRAE Handbook - Fundamentals*. Atlanta, GA: American Society of Heating, Refrigeration and Air-Conditioning Engineers, Inc.; 2009.

131 Ministry of Environment. BC Air Data Archive. BC Air Data Archive. 2014.http://envistaweb.env.gov.bc.ca (accessed 13 Dec2013).

132 Zaatari M, Siegel J. Particle characterization in retail environments: concentrations, sources, and removal mechanisms. *Indoor Air* 2014; **24**:350–361.

133 VerShaw J, Choinowski DB, Siegel JA, Nigro PJ. Implications of filter bypass. *ASHRAE Transactions* 2009; **115**:191–198.

134 Montgomery JF, Green SI, Rogak SN, Bartlett K. Predicting the energy use and operation cost of HVAC air filters under variable-air-volume operation. 11^{th} World Filtration Congress, Graz, Austria; 2012.

135 Stenhouse J, Trottier R. The Loading of Fibrous Filters with Submicron Particles. *Journal of Aerosol Science* 1991; **22**:S777–S780.

136 CEN. EN15251-2005, Criteria for the Indoor Environment including thermal, indoor air quality, light and noise. European Committee for Standardization; 2005.

137 Fisk WJ, Black D, Brunner G. Benefits and costs of improved IEQ in US offices. *Indoor Air* 2011; **21**:11.

138 Seppanen O, Fisk WJ. Association of ventilation system type with SBS symptoms in office workers. *Indoor Air* 2002; **12**:98–112.

139 Montgomery JF, Reynolds CC, Rogak SN, Green SI. Financial implications of modifications to building filtration systems. *Building and Environment* 2015; **85**:17–28.

140 EIA. Commercial Building Energy Consumption Survey - Overview of Commercial Buildings. 2008. http://www.eia.gov/consumption/commercial/data/2003/#b1

141 CEN. EN 13779 - 2007, Ventilation for non-residential buildings - Performance requirements for ventilation and room-conditioning systems. European Committee for Standardization; 2007.

142 Grot RA, Persily AK. Measured air infiltration and ventilation rates in eight large office buildings. In: *Measured air leakage of buildings*. Treschsel HR, Lagus PL (editors). ASTM International; 1986.

143 WHO. Urban Outdoor Air Pollution Database. World Health Organization; 2011.

144 Ward M, Siegel JA. Modeling filter bypass: Impact on filter efficiency. *ASHRAE Transactions* 2005; **111**:1091–1100.

145 Waring MS, Siegel JA. Particle loading rates for HVAC filters, heat exchangers, and ducts. *Indoor Air* 2008; **18**:209–224.

146 Ostro BD. Air pollution and morbidity revisited: a specification test. *Journal of Environmental Economics and Management* 1987; **14**:87–98.

147 Moolgavkar SH. Air pollution and hospital admissions for chronic obstructive pulmonary disease in three metropolitan areas in the United States. *Inhalation Toxicology* 2000; **12**:75–90.

148 OECD IEA. Electricity Information 2012. 2012:1–883.

149 Hydro Quebec. Comparison of electricity prices in major North American cities. 2012.

150 eBeijing. Guide to Heating, Electricity, Water, and Gas - Policies and Procedures. 2012. http://www.ebeijing.gov.cn/feature_2/GuideToHeatingElectricityWaterAndGas/

151 Enerdata. Russia Electricity Market. 2012. https://estore.enerdata.net/power-market/russia-electricity-report.html

152 World Bank. GNI per capita, Atlas method. data.worldbank.org. 2013.http://data.worldbank.org/indicator/NY.GNP.PCAP.CD (accessed 22 Jan2013).

153 Europe's Energy Portal. Europe's Energy Portal. energy.eu. 2013.http://www.energy.eu (accessed 22 Jan2013).

154 US IEA. Average Price by State by Provider. 2011.

155 World Bank. Global Purchasing Power Parities and Real Expenditures. 2008.

156 DERC. Delhi Electricity Price Commission. 2013.http://www.derc.gov.in (accessed 22 Jan2013).

157 ANEEL. Agencia Nacional de Energie Electrica. 2012. http://www.aneel.gov.br

158 City Power Johannesburg. Electricity Tariffs 2010/11. 2011.http://www.citypower.co.za/customer_tariff.html (accessed 22 Jan2013).

159 Government of Singapore. Electricity Tariff and You. ema.gov.sg. 2013.http://www.ema.gov.sg/Electricity/new/ (accessed 22 Jan2013).

160 Lepeule J, Laden F, Dockery D, Schwartz J. Chronic Exposure to Fine Particles and Mortality: An Extended Follow-up of the Harvard Six Cities Study from 1974 to 2009. *Environmental Health Perspectives* 2012; **120**:965–970.

161 Daniels MJ, Dominici F, Samet JM, Zeger SL. Estimating particulate matter-mortality dose-response curves and threshold levels: An analysis of daily time-series for the 20 largest US cities. *American Journal of Epidemiology* 2000; **152**:397–406.

162 Thatcher TL, Layton DW. Deposition, Resuspension, and Penetration of Particles Within a Residence. *Atmospheric Environment* 1995; **29**:1487–1497.

163 Riley WJ, McKone TE, Lai ACK, Nazaroff WW. Indoor Particulate Matter of Outdoor Origin: Importance of Size-Dependent Removal Mechanisms. *Environmental Science and Technology* 2002; **36**:200–207.

164 Liu D, Nazaroff WW. Modeling pollutant penetration across building envelopes. *Atmospheric Environment* 2001; **35**:4451–4462.

165 Endo Y, Chen DR, Pui D. Bimodal aerosol loading and dust cake formation on air filters. *Filtration and Separation* 1998; **35**:191–195.

166 Biskos G, Russell LM, Buseck PR, Martin ST. Nanosize effect on the hygroscopic

growth factor of aerosol particles. *Geophys Res Lett* 2006; **33**.

167 Wise ME, Martin ST, Russell LM, Buseck PR. Water Uptake by NaCl Particles Prior to Deliquescence and the Phase Rule. *Aerosol Science and Technology* 2008; **42**:281–294.

168 Hu D, Qiao L, Chen J, Ye X, Yang X, Cheng T, *et al.* Hygroscopicity of Inorganic Aerosols: Size and Relative Humidity Effects on the Growth Factor. *Aerosol Air Qual Res* 2010; **10**:255–264.

169 Sanchez AL, Hubbard JA, Dellinger JG, Servantes BL. Experimental Study of Electrostatic Aerosol Filtration at Moderate Filter Face Velocity. *Aerosol Science and Technology* 2013; **47**:606–615.

170 Langlet M, Nadaud F, Benali M, Pezron I, Saleh K, Guigon P, *et al.* Kinetics of dissolution and recrystallization of sodium chloride at controlled relative humidity. *KONA Powder and Particle Journa* 2011; **29**:168–179.

171 Pöschl U. Atmospheric Aerosols: Composition, Transformation, Climate and Health Effects. *Angew Chem Int Ed* 2005; **44**:7520–7540.

172 Bruzewicz DA, Checco A, Ocko BM, Lewis ER, McGraw RL, Schwartz SE. Reversible uptake of water on NaCl nanoparticles at relative humidity below deliquescence point observed by noncontact environmental atomic force microscopy. *J Chem Phys* 2011; **134**.

173 Weingartner E, Burtscher H, Baltensperger U. Hygroscopic properties of carbon and diesel soot particles. *Atmospheric Environment* 1997; **31**:2311–2327.

174 Biskos G, Malinowski A, Russell LM, Buseck PR, Martin ST. Nanosize Effect on the Deliquescence and the Efflorescence of Sodium Chloride Particles. *Aerosol Science and Technology* 2006; **40**:97–106.

175 Rader DJ, McMurry PH. Application of the Tandem Differential Mobility Analyzer to Studies of Droplet Growth or Evaporation. *Journal of Aerosol Science* 1986; **17**:771–787.

176 Weingartner E, Baltensperger U, Burtscher H. Growth and Structural Change of Combustion Aerosols at High Relative Humidity. *Environmental Science and Technology* 1995; **29**:2982–2986.

177 Ewing GE. H2O on NaCl: From Single Molecule, to Clusters, to Monolayer, to Thin Film, to Deliquescence. In: *Structure and Bonding*. Berlin/Heidelberg: Springer-Verlag; 2005. pp. 1–25.

178 Dai Q, Hu J, Salmeron M. Adsorption of water on NaCl (100) surfaces: Role of atomic steps. *Journal of Physical Chemistry B* 1997; **101**:1994–1998.

179 Shindo H, Ohashi M, Tateishi O, Seo A. Atomic force microscopic observation of step movements on NaCl(001) and NaF(001) with the help of adsorbed water. *Faraday Trans* 1997; **93**:1169–1174.

180 Verdaguer A, Sacha GM, Luna M, Frank Ogletree D, Salmeron M. Initial stages of water adsorption on NaCl (100) studied by scanning polarization force microscopy. *J Chem Phys* 2005; **123**:124703.

181 Dai DJ, Peters SJ, Ewing GE. Water-Adsorption and Dissociation on Nacl Surfaces. *Journal of Physical Chemistry* 1995; **99**:10299–10304.

182 Foster MC, Ewing GE. Adsorption of water on the NaCl(001) surface. II. An infrared study at ambient temperatures. *Journal of Chemical Physics* 2000; **112**:6817.

183 Kreidenweis SM, Petters MD, DeMott PJ. Single-parameter estimates of aerosol water content. *Environmental Research Letters* 2008; **3**:035002.

184 You Y, Renbaum-Wolff L, Carreras-Sospedra M, Hanna SJ, Hiranuma N, Kamal S, *et al.* Images reveal that atmospheric particles can undergo liquid-liquid phase separations. *Proceedings of the National Academy of Sciences of the United States of America* 2012; **109**:13188–13193.

185 Parsons MT. Deliquescence of malonic, succinic, glutaric, and adipic acid particles. *J Geophys Res* 2004; **109**:D06212.

186 Flagan RC. Differential mobility analysis of aerosols: a tutorial. *KONA Powder and Particle Journal* 2008; **26**:254.

187 Montgomery JF, Green SI, Rogak SN. Impact of Relative Humidity on HVAC Filters Loaded with Hygroscopic and Non-Hygroscopic Particles. *Aerosol Science and Technology* 2015; :00–00.

188 Butt H-J, Kappl M. Advances in Colloid and Interface Science. *Advances in Colloid and Interface Science* 2009; **146**:48–60.

189 Rabinovich YI, Esayanur MS, Moudgil BM. Capillary Forces between Two Spheres with a Fixed Volume Liquid Bridge: Theory and Experiment. *Langmuir* 2005; **21**:10992–10997.

190 Nyeki S, Colbeck I. Fractal Dimension Analysis of Single, In-Situ, Restructured Carbonaceous Aggregates. *Aerosol Science and Technology* 1995; **23**:109–120.

191 Mikhailov E, Vlasenko S, Martin ST, Koop T, Poeschl U. Amorphous and crystalline aerosol particles interacting with water vapor: conceptual framework and experimental evidence for restructuring, phase transitions and kinetic limitations. *Atmospheric Chemistry and Physics* 2009; **9**:9491–9522.

192 Swietlicki E, Hansson HC, Hameri K, Svenningsson B, Massling A, McFiggans G, *et al.* Hygroscopic properties of submicrometer atmospheric aerosol particles measured with H-TDMA instruments in various environments—a review. *Tellus B* 2008; **60B**, 432-469.

193 Gysel M, Weingartner E, Baltensperger U. Hygroscopicity of Aerosol Particles at Low Temperatures. 2. Theoretical and Experimental Hygroscopic Properties of Laboratory Generated Aerosols. *Environmental Science and Technology* 2002; **36**:63–68.

194 Biskos G, Paulsen D, Russell LM, Buseck PR, Martin ST. Prompt deliquescence and efflorescence of aerosol nanoparticles. *Atmospheric Chemistry and Physics* 2006; **6**:4633–4642.

195 Darr JP, Davis SQ, Kohno Y, McKenna K, Morales P. Morphological effects on the hygroscopic properties of sodium chloride–sodium sulfate aerosols. *Journal of Aerosol Science* 2014; **77**:158–167.

196 Qian J, Peccia J, Ferro AR. Walking-induced particle resuspension in indoor environments. *Atmospheric Environment* 2014; **89**:464–481.

197 Siegel J. Primary and Secondary Consequences of Indoor Air Cleaners. *Indoor Air* 2015; doi: 10.1111/ina.12194.

198 Jaenicke R. Tropospheric Aerosols. In: *Aerosol-Cloud-Climate Interactions*. Hobbs PV (editor). San Diego: Academic Press; 1993.

199 Wallace LA, Emmerich SJ, Howard-Reed C. Source Strengths of Ultrafine and Fine Particles Due to Cooking with a Gas Stove. *Environmental Science and Technology* 2004; **38**:2304–2311.

200 Census. Accessed by CDC Wonder, US Center for Disease Control and Prevention. 2010.http://wonder.cdc.gov (accessed 22 Jan2013).

201 CDC. CDC WONDER. 2010.http://wonder.cdc.gov (accessed 22 Jan2013).

202 Aunan K, Pan X-C. Exposure-response functions for health effects of ambient air pollution applicable for China – a meta-analysis. *Science of The Total Environment* 2004; **329**:3–16.

203 Kunzli N, Kaiser R, Medina S, Studnicka M, Chanel O, Filliger P, *et al.* Public-health impact of outdoor and traffic-related air pollution: a European assessment. *Lancet* 2000; **356**:795–801.

204 WHO. The World Health Report 2002. 2002.

205 Wyon DP. The effects of indoor air quality on performance and productivity. *Indoor Air* 2004; **14**:92–101.

206 Quah E, Boon TL. The economic cost of particulate air pollution on health in Singapore. *Journal of Asian Economics* 2003; **14**:73–90.

Appendix A: Supplemental Information – Chapter 5

Introduction

This Appendix contains additional results not provided within the body of Chapter 5 with specific emphasis on the building operation with an indoor generation source.

Model and Methodology

Indoor Aerosol Dynamics Model Parameters

A description of the indoor aerosol dynamics model parameters has been provided by Nazaroff [83] and extended by Waring and Siegel [145]. The ambient outdoor particle concentration is assumed to be the sum of three log-normally distributed modes [198]. The modal distribution was assumed to be that of an urban environment and the total concentration was scaled to provide PM_{10} and $PM_{2.5}$ concentrations to match those of the WHO database [143] for annual average PM in the cities of interest (see Table 5.2). The particle density was assumed to be 1 g/cm^3 for particles with diameter less than 2.5μm and 2.5g/cm^3 for particles greater than 2.5μm [145]. The dust loading of the floor was estimated by Waring and Siegel [145], based on the work of Thatcher and Layton [162], to be the sum of two log-normally distributed modes. The model assumes a total floor loading of 59.8 μg/m^2 based on a weighted average of 60% hard surface and 40% carpeting and equal areas of tracked and untracked surface [162]. When generation is present the source term is assumed to be lognormal with a geometric mean diameter of 0.06 μm. The generation term is modeled as a cooking source averaged over the entire day with an average emission rate of 5.79 mg/h with an assumed particle density of 1 g/cm^3 [145,199]. Though a cooking source may not be representative of activities within all commercial office buildings it provides an indication of the impact of generation of particles in a size bin typical for many indoor generation activities for many building types such as the use of candles, incense, or cleaning supplies.

The particle deposition rate, λ_d, resuspension rate, R, and building penetration factor, P_{Bldg}, are shown in Figure A.1. The estimated deposition rate [163] function includes the effects of both deposition on surfaces and loss of small particles due to coagulation [82]. The resuspension rate has been estimated based on average indoor activity levels [162] and has been used previously by Waring and Siegel [145]. The penetration factor is the fraction of particles in the infiltration air that penetrate into the building. The estimate assumes a uniform distribution of building crack sizes from 0.5-2.0mm and a pressure differential of 4Pa across the cracks [164].

Air Filtration Model Parameters

Filter properties used in the model are shown in Table A.2. Filter price, $\$_F$, was determined from a review of commercial filter purchase prices from a range of manufacturers in North America. Filter installation, labour, and disposal prices, $\$_L$, were determined by Arnold et al. [74]. Filter constants and efficiencies in ASHRAE size bins 1-3 were determined from the comparison of commercially available filters and ASHRAE 52.2 test results. All filter properties in Table A.2 are subject to considerable variation within a given MERV [89] and the values used are representative of the general trend of filter design.

Table A.1: Total concentration, geometric mean particle diameter ($d_{p,i}$), and log of geometric standard deviation ($\log \sigma_i$) for modes of lognormal distributions of urban ambient aerosol, floor loading, and indoor generation. Ambient particle distribution has been scaled from Jaenicke [198] to match PM concentrations reported in London. A similar scaling method has been used for other cites in the study when appropriate.

		Mode 1			Mode 2			Mode 3		
Parameter	Units	Total	$d_{p,i}$ (μm)	$\log \sigma_i$ (-)	Total	$d_{p,i}$ (μm)	$\log \sigma_i$ (-)	Total	$d_{p,i}$ (μm)	$\log \sigma_i$ (-)
Outdoor Particle Distribution	$\#/m^3$	1.09E+10	0.05	0.337	4.13E+08	0.014	0.666	$3.11\text{x}10^{10}$	0.013	0.245
Floor Loading	g/m^2	0.173	0.7	0.165	0.425	10.2	0.282	-	-	-
Generation	#/s	$3.19\text{x}10^{10}$	0.06	0.287	-	-	-	-	-	-

Table A.2: Air filter model properties for MERV 6 through MERV 16 filters

Parameter	Value										
MERV Rating	6	7	8	9	10	11	12	13	14	15	16
E_1 (-)	0.04	0.08	0.13	0.16	0.20	0.27	0.49	0.66	0.79	0.88	0.88
E_2 (-)	0.39	0.45	0.52	0.57	0.62	0.79	0.86	0.94	0.96	0.98	0.99
E_3 (-)	0.48	0.61	0.76	0.88	0.95	0.97	0.98	0.99	0.99	0.99	1.00
Filter Constant, a	35	40	51	68	86	103	121	139	156	174	191
Filter Constant, b	0.010	0.010	0.009	0.008	0.007	0.006	0.006	0.005	0.004	0.003	0.002
Filter Constant, d	1.58	1.57	1.55	1.54	1.52	1.51	1.49	1.48	1.46	1.45	1.43
Filter Price, $\$_F$ (USD/filter)	5.89	6.63	7.46	8.40	9.46	63.18	73.68	85.69	99.42	115.12	133.08
Labour Price, $\$_L$ (USD/filter)	2.21	2.21	2.21	2.21	2.21	4.30	4.30	4.30	4.30	4.30	4.30

Note: For MERV 10 and lower it is assumed the filter is 2" thick, for MERV 11 and higher it is assumed that the filter is 12" thick. Prices are for North America.

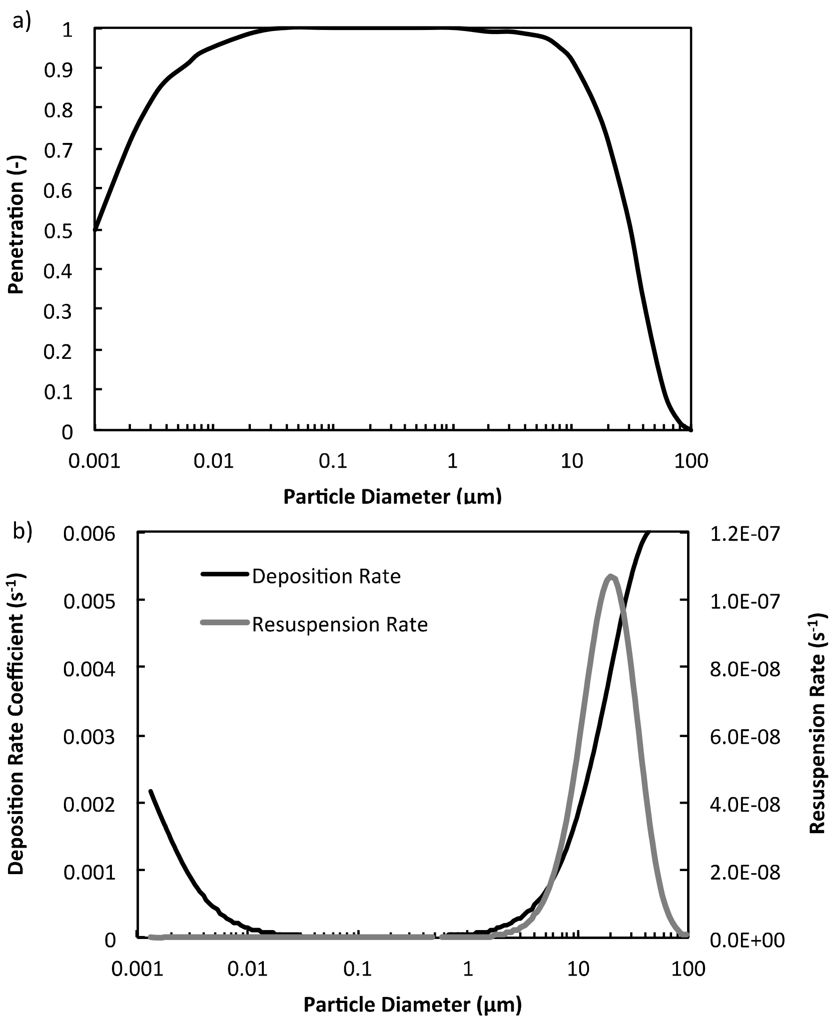

Figure A.1: Size resolved particle deposition rate coefficient, λ_d, resuspension rate, R, (a), and building penetration factor, P_{Bldg} (b).

Occupant Health Model Parameters

The baseline mortality rate was determined following the approach of Bekö et al. [92] and Sultan [91]. The population data from the US census [200] and compressed mortality data from the Center for Disease Control and Prevention [201] is used. The population weighted average mortality rate per 100 people was determined to be 0.3375 for the age range 20-64. A limiting assumption of this approach is that the building occupants are representative of the population in that age range.

The mortality effect estimate used is equivalent to that used by the USEPA [90]: 1.06% per 1μg/m^3 of $PM_{2.5}$. The USEPA estimate was itself determined by comparing epidemiological studies of Laden et al. [7] and Pope et al. [9]. A recent study by Crouse et al. [6] found a Hazard Ratio of 1.15 per 10μg/m^3 of $PM_{2.5}$ for all cause non-accidental mortality using census data for Canadians 24-60 years old, and satellite and ground based monitoring of PM concentration. This results in an effect estimate slightly higher than the mean value used by the USEPA [90] but is within the distribution investigated therein. The value from the USEPA [90] has been used for this study as it provides a more conservative estimate. The effect estimates from these studies have been determined based on studies of populations in North America exposed to annual average $PM_{2.5}$ concentrations of less than 40μg/m^3. Other studies have begun to produce similar C-R functions for exposure of populations in other cities and countries [202,203]. The ideal comparison would utilize C-R functions specific to the city being investigated but this detail is not available for all locations and so the C-R functions detailed by the USEPA [90] have been used for all cities. The extrapolation of these estimates to other locations and higher $PM_{2.5}$ concentrations is subject to an unknown level of error but remains the best available source of data.

The monetary value of an avoided case of mortality is determined by multiplying the years of lost life per death attributable to air pollution – which was determined to be 5.4 [92] using data from the WHO Air Quality Database [204] for the sub-region including the U.S., Canada, and Cuba – with the value of a statistical life year (VSLY) determined using the willingness to pay (WTP) method as detailed by the USEPA converted to 2010 dollars and a 2010 income level (426,750 USD/yr) assuming a 3% discount rate.

Indoor air quality has also been shown to have an impact on the productivity of building occupants. The available information utilizes self-reported productivity or productivity measured by reading and typing speed for varying levels of ventilation but does not provide quantifiable relations between productivity of typical office workers and indoor PM concentrations [5,205]. Increased productivity could be seen as an additional benefit of improved filtration but is not included in this study due to insufficient availability of a means of quantifying and monetizing productivity changes.

Converting to Different Regions

Filter cost data is most readily available for the North American market. The air filter purchase price in North America is used to convert to an equivalent purchase price in other locations using the Price Level Index (PLI). The PLI is a means of comparing prices of a certain basket of goods between countries. Air filters are not part of this fixed basket of goods, which will lead to model error by using the PLI for comparing filters between countries. It has been assumed that the PLI will provide an adequate estimate for this conversion in view of the absence of another means. An estimate of the purchase price of filters in USD for different countries can be made using the PLI by:

$$\$_{f,j} = \$_{f,US} \frac{PLI_j}{PLI_{US}} \qquad \text{Equation A.1}$$

where $\$_{f,j}$ is the filter price in city j (USD/filter), $\$_{f,US}$ is the filter price in the USA (USD/filter), PLI_j is the Price Level Index of the country for city j, and PLI_{US} is the Price Level Index in the USA.

Another factor to consider is variations in installation and disposal prices between cities. This conversion is modeled on variations in costs of health endpoints between various cities [91,206] which accounts for differences in wages based on Gross National Income (GNI). The relation for converting installation and disposal prices is:

$$\$_{L,j} = \$_{L,USA} \left(\frac{GNI_j}{GNI_{USA}}\right)^{e} \qquad \text{Equation A.2}$$

where $\$_{L,j}$ is the filter installation and disposal price in the country of city j (USD/filter); $\$_{L,USA}$ is the filter installation and disposal price in the USA (USD/filter); GNI_j is the Gross National Income per capita in the country of city j (USD/year); GNI_{USA} is the Gross National Income per capita in the USA (USD/year); and e is the income elasticity assumed to be 0.32 [91].

Another major factor to consider is variations in unit costs of morbidity and mortality endpoints between regions. This has been addressed previously for air quality related calculations by Sultan [91] and Quah & Boon [206] to convert between UK and Singapore figures. A similar approach will be used where:

$$\$_{i,j} = \$_{i,USA}\left(\frac{GNI_j}{GNI_{USA}}\right)^{e} \qquad \text{Equation A.3}$$

where $\$_{i,j}$ is the unit cost of morbidity/mortality endpoint *i* in the country of city *j* (USD/incident); $\$_{i,USA}$ is the unit cost of morbidity/mortality endpoint in the USA (USD/incident); and the other variables are defined in equation 5.

Results

Return Air Systems

Comparison of increased outdoor air or return air flow

Figure A.2 compares the net benefits of increased outdoor air and return airflow for a building operating with indoor generation. When there is an indoor source of particle generation within the building small increases in outdoor airflow rate increase the net benefit of the system. The positive effect of increased dilution air has an upper limit as seen by the maxima of the net benefit curves in Figure A.2 when the added outdoor airflow is approximately equal to the base ventilation rate. Beyond this point additional ventilation air reduces the net benefit of the system operation. The initial increase in net benefits with increased dilution is greater than that of increased return air for low filter efficiencies (see MERV 7 in Figure A.2). This is due to the relatively small impact that increasing airflow through low efficiency filters has on particle concentration. The relative superior performance of increasing outdoor airflow rate is limited to the initial increases before the cost of conditioning the air reduces the benefits and a return air system with identical total flow becomes more economically feasible.

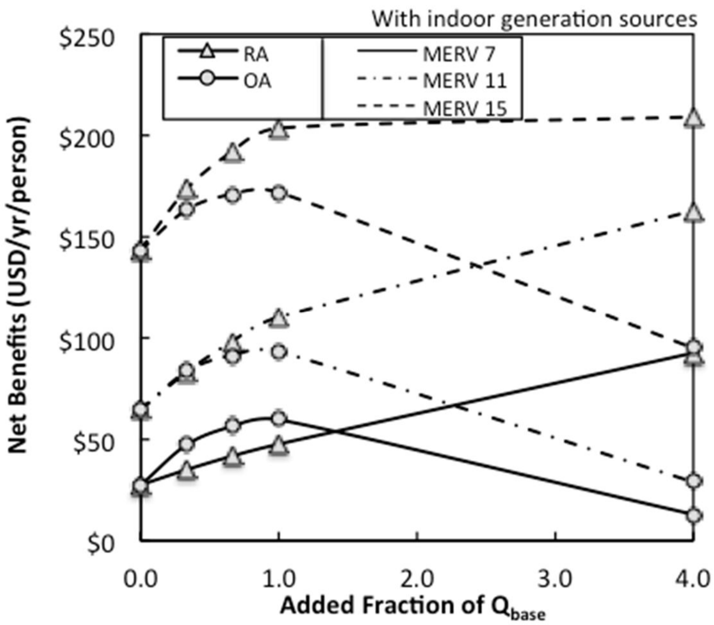

Figure A.2: Comparison of the effect of increasing flow rate in the return air or outdoor air stream on net benefits for a range of MERV with indoor generation for operation in London. Each symbol type denotes the airstream in which the flow is increased above the base case outdoor airflow only. The different line types denote the MERV rating of filters installed in the supply air stream.

The net benefits of increased return airflow rate with indoor generation shows similar trends as when indoor generation is absent. Initial increases in net benefits are associated with increased airflow rates but the trend shows diminishing returns as the indoor particle concentration is reduced by the added flow. A limit to the positive relation between increased return air flowrate also exists when there is an indoor generation source but is not within the range of flow presented in Figure A.2. The change in net benefits when increasing the return air flowrate is greater for buildings with indoor generation.

Impact of increased Filter Efficiency

Figure A.3 shows the benefits to costs of modifying the supply air MERV rating or return air flowrate for a building operating in London with indoor generation sources. The general trends are similar for systems operating with indoor generation sources as they are for systems without indoor generation sources, though the magnitude of potential benefits are greater. Depending on system operations there exists the potential to achieve improved benefits and reduced costs by improving filter efficiency while simultaneously reducing the return air flowrate.

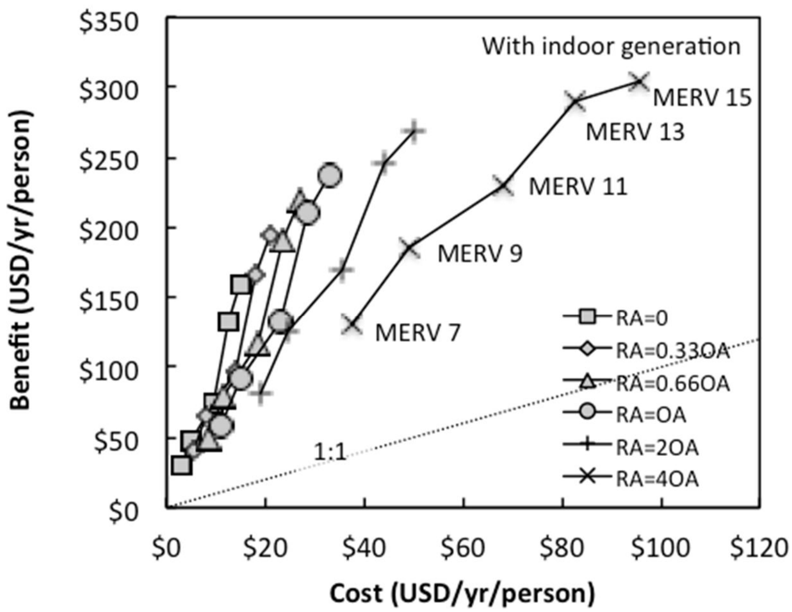

Figure A.3: Comparison of the benefits and costs of installing SA filters with increased efficiency in systems with varying return air flowrates for the model building operating in London with indoor particle generation. Each symbol type denotes a different return air flow rate. The sequence of points for a particular return air flowrate denotes different SA filter MERV ratings (from left to right: MERV 7, 9, 11, 13, 15)

Recirculation Air Systems

Impact of Airflow and Filter Efficiency

Figure A.4 compares the net benefits of increasing the recirculated airstream filter efficiency or flow rate for the theoretical building in London with outdoor airflow to meet baseline ventilation and MERV 7 or 15 filters with indoor generation. The slope of the curves is always positive indicating that it is beneficial to improve the efficiency of recirculation air filters. The increases in net benefits with improved recirculated air filters are greater in all cases when indoor generation is present. This is due to the higher concentration of particles in the incident airstream.

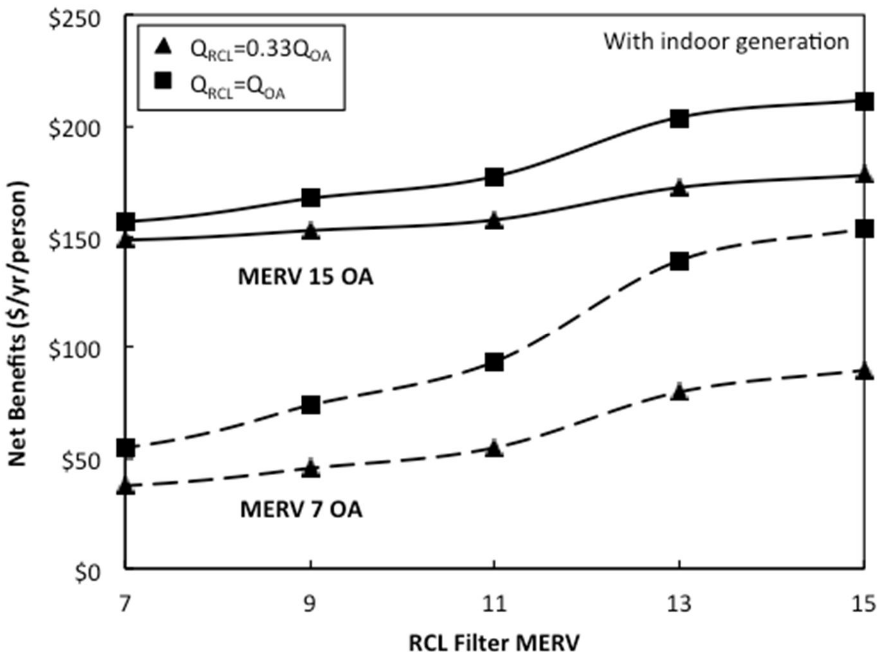

Figure A.4: Net benefits of increasing recirculated filter efficiency for the theoretical building with indoor generation operating in London with MERV 7 or 15 filters installed in the outdoor air stream. Open symbols represent scenarios *without* indoor particle generation. Closed symbols represent scenarios *with* indoor particle generation. Triangles represent a system where Q_{RCL}=0.33Q_{OA}. Squares represent a system where Q_{RCL}=Q_{OA}.

Figure A.5 compares the benefits and costs of filter selection in 100% outdoor air systems with varying levels of recirculated air for the model building located in London. The effect of varying outdoor air and recirculated air filter MERV rating and recirculated air flow rate is studied with indoor generation. Similar gains are possible for buildings with indoor generation sources as those without though the margins for improvement are smaller.

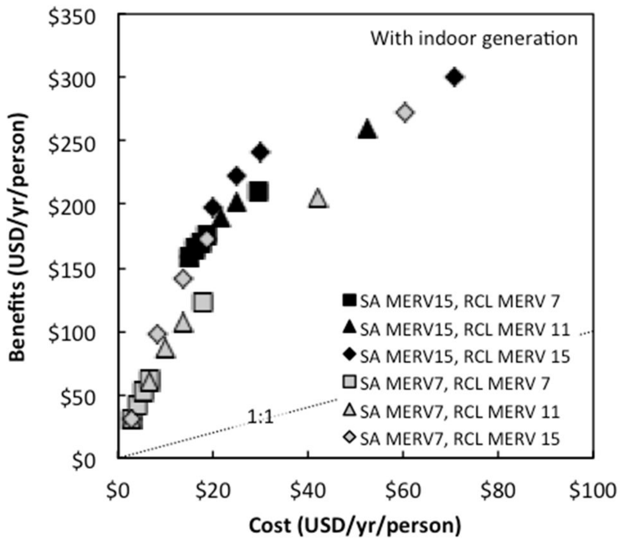

Figure A.5: Comparison of the benefits and costs of installing different combinations of outdoor air and recirculated air filters in a 100% outdoor air system operating with indoor generation for a building in London. Each symbol type denotes a different recirculated air filter MERV and each colour indicates a different supply air MERV rating. The subsequent points in each series denote airflow increases in recirculated airflow rate (from left to right: Q_{RCL}=0, Q_{RCL}=0.33Q_{OA}, Q_{RCL}=0.66Q_{OA}, Q_{RCL}=Q_{OA}, Q_{RCL}=4Q_{OA}).

Impact of Recirculation Air Filters in a Return Air System

Figure A.6 compares the benefits of utilizing recirculation airflow and filtration in a building that incorporates return air. The comparison has been performed for return air flow rates from Q_{RA}=0.33Q_{OA} to Q_{RA}=4Q_{OA} and recirculated airflow rates of Q_{RCL}=0.33Q_{OA} (a and c) and Q_{RCL}=Q_{OA} (b and d). Combinations of filter efficiencies tested include supply air filters of MERV 7 and 15, and recirculated air filters of MERV 7, 11, or 15. The simulated building is located in London and operates without (a and b) or with (c and d) indoor particle generation.

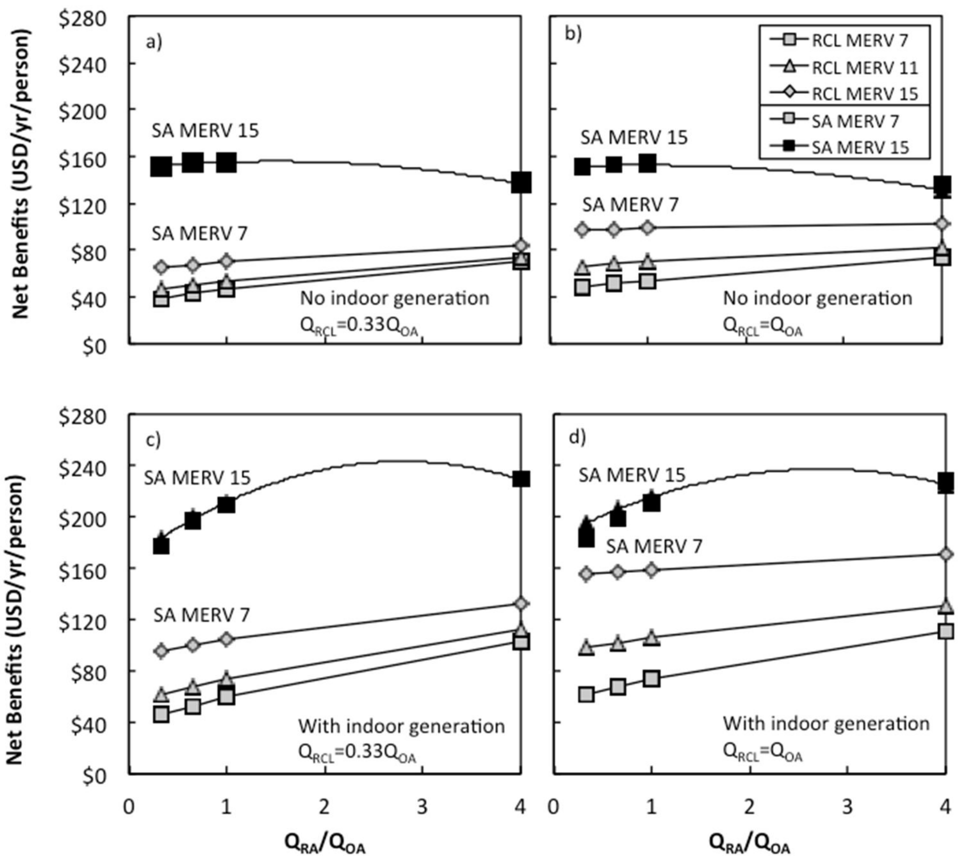

Figure A.6: Net benefits of systems with recirculated air filters and varying levels of return air for the theoretical building operating in London with MERV 7 (grey) or MERV 15 (black) supply air filters. The comparison is performed without (a and b) and with (c and d) indoor generation sources for recirculated air flow rates of $Q_{RCL}=0.33Q_{OA}$ (a and c) and $Q_{RCL}=Q_{OA}$ (b and d).

The comparison of systems with high efficiency MERV 15 filters (black symbols) and low efficiency MERV 7 filters (grey symbols) installed in the supply air stream shows two distinct variations. When MERV 15 filters are installed in the supply air stream all recirculation air filter options fall approximately on the same curve indicating that recirculation airflow does not substantially improve the indoor air quality. When MERV 7 filters are installed in the supply air stream the provision of recirculated air with increasing filter efficiency shows improvements in the net benefits of the system. The greatest increases in net benefits are seen when high efficiency (MERV 15) filters are added to a system with MERV 7 supply air filters. In all cases investigated the use of high efficiency filters in the supply air stream leads to higher net benefits than a combination of low efficiency supply air filters and high efficiency recirculated air filters.

Increasing the volume of recirculated air in the system has little impact on the net benefits as seen from a comparison between Figure A.6 a and b or Figure A.6 c and d. Increases in the amount of return airflow in the building increases the system net benefits but further reduces the relative benefits of installing high efficiency recirculation air filters. When high efficiency filters are installed in the supply air stream initial increases in net benefits with increased return air flow eventually taper and lead to reductions in benefits beyond a certain threshold. When MERV 15 filters are installed in the model building the limit is approximately Q_{RA}=1.3Q_{OA} when no generation is present (a and b) and Q_{RA}=2.7Q_{OA} with indoor generation for the levels of recirculated airflow and filter efficiency investigated in this study.